Thermodynamics of Singly Charged Particles

Areez Mody

A Thesis presented for the degree of
Doctor of Philosophy

Department of Physics
Harvard University
May 2004

Contents

List of Figures

Chapter 1

Introduction

1.1 The Experiment

For the last 20 years, Professor Gerald Gabrielse has led an effort to make the first anti-matter atoms. Cooling and trapping anti-electrons (positrons or e^+) and anti-protons ($\bar{p}$) nearby in the same trap was experimentally realized after years of work. Fig. (1.1) shows schematically the trapping apparatus. All lengths are labeled in units of microns (10^{-4}cm). Nine copper rings are stacked on top of each other and serve as electrodes, each of which is held at a constant electrostatic potential. Shown alongside is one typical choice of a sequence of potential values that the electrodes are held at. The resulting electrostatic potential viewed along the central trap axis is just a smoothed version of this step function sequence. The e^+ are confined at the potential minimum and the $\bar{p}$, being negatively charged, are confined at the electrostatic potential maximum. However, since it is impossible for an electrostatic potential to be simultaneously confining in all directions, both the e^+ and $\bar{p}$, feel an electric force pushing them transversely out of the trap. To combat this, a uniform magnetic field of 5.5 Tesla is applied along the trap axis. This succeeds in confining the particles transversely also. The superconducting magnets and entire apparatus is cooled to a temperature of ~ 4 Kelvin by liquid helium.

The particles are held in the trap for many seconds at a time. This is sufficiently long for the e^+ to thermalize with radiation from the electrode walls. The $\bar{p}$, however, cannot be radiatively cooled this way, because they radiate much too slowly owing to their large mass. Instead, they are pre-cooled in a separate stage by thermalizing them with ordinary electrons which are then removed. Understanding the equilibrium of the individual clouds and predicting their shapes and densities is crucial for the experiment and one of our main goals in the following chapters.

In Chapter (2) we point out that in addition to the temperature τ there is another parameter ω, with dimensions of frequency, which characterizes the equilibrium of the cloud. It owes its origin to the fact that the cloud is confined

c.g.s. Units where q=1, m(e+)=1, Length = 10^(−4) cm

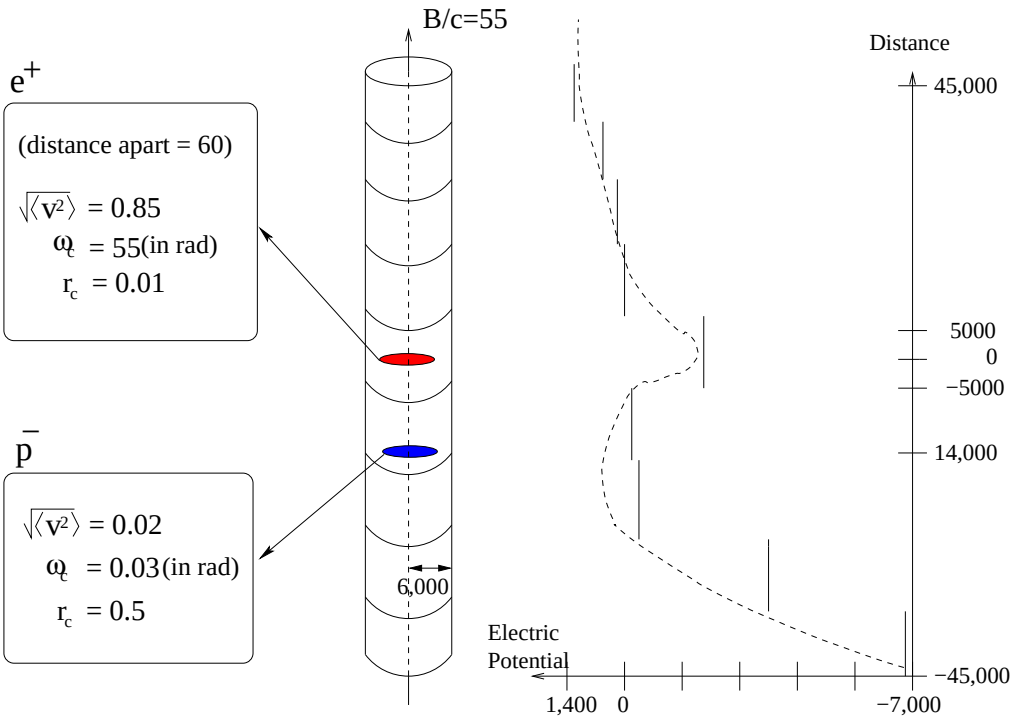

Plancks hbar = .0073
thermal energy kT = 0.23
light speed c =19,000

near z=0 $E_z(0,0,z) = -5.0\,10^{-5}z$

Figure 1.1: Schematic of Trap showing approximate values of important physical quantities in c.g.s. units defined in the figure heading.

in a cylindrically symmetric environment and is linked to the conservation of the cloud's (generalized) angular momentum. Chapter (2) explores the reasons for this in a general context, while also pointing out some general points of theoretical interest.

Chapter (3) then deals explicitly with the physical implications of ω. Over here we explicitly find the N particle equilibrium distribution and are able to simulate this for many particles using the Monte Carlo method described in Chapter (4). We wish to emphasize that for a given trapping field, temperature τ, and ω, this provides a complete solution to finding all equilibrium properties of a single species cloud. It would be quite feasible, if necessary to simulate this for even as many particles as in the experiment itself ($\sim 10^6$).

While the temperature τ is determined by the apparatus temperature (4 Kelvin), it appears that ω is a free parameter linked to the initial angular momentum possessed by the cloud. Chapter (3) demonstrates that this parameter is not quite arbitrary but spontaneously (but slowly) moves towards the value 0 as the angular momentum L_z adjusts itself to minimize the free energy. This implicitly assumes that L_z is only a quasi-conserved quantity over long times. This is because the cloud is continually radiating and absorbing microwave radiation. It may perhaps also be due to small asymetries in the trapping potential. For the unconfining trap potential of the experiment this implies that the trapping is thermodynamically unstable, so that all the particles will eventually escape. However, this evidently happens on a slow enough time scale once ω is near 0, since the clouds are experimentally observed to be trapped for many seconds. We would like to address the issue of this time scale in the future.

Imposing w

The understanding acquired from Chapter (3) leads us to suggest here the possibility of "imposing" an ω onto the cloud using time dependent trap potentials. It seems to us that this could easily be achieved experimentally by dividing the one electrode surrounding the plasma, into four quadrants, and superposing a "rotating potential" on the static potential it is already held at. For this particular experiment values of ω are typically in the MHz range. The required switching times of microseconds, on the 4 electrodes would be well within the range of conventional electronics which can achieve switching speeds of nanoseconds. This is not discussed further in this thesis.

Dynamics

Chapter (5) derives the algorithmic details of numerical code that allows us to follow the classical dynamics of the plasma cloud in time. In addition to independently confirming the equilibrium predictions of Chapters (3) and (4), this provides useful insight which is otherwise difficult to visualise. This is due to the facility we provided of viewing the dynamics in full three dimensions on a computer screen in real time. The computation and graphics code was written

by us from scratch, and the integration algorithms developed have at least a few improvements over many standard implementations.

The working code is already adapted to deal with close collisions of oppositely charged particles. We would like to exploit this in the future to look at both species of clouds simultaneously, and perhaps the atom formation itself.

Aside

Our numerical code holds the advantage of not being enslaved to the particular parameters of this experiment. In exploratory mode, we observed solid-like, liquid-like, and gas-like behavior of the plasma cloud in very different regimes of the parameters τ and ω. What implication, if any, this has for this particular experiment is unclear and would require further investigation. Hence we do not further discuss this in this thesis.

1.2 Synopsis of Anti-Hydrogen Paper

Last year, both the ATRAP (led by Gabrielse) and ATHENA collaborations observed anti-hydrogen atoms for the first time. A collaborative paper discussing the nature of these highly excited states in a strong magnetic field was published. Fig. (1.2) shows a typical trajectory of the relative coordinate for an atom. The relative coordinate moves in an effective potential (and magnetic field) whose contours on a particular plane are shown transparently in the figure. The effective potential posseses a saddle point which is shifted upwards due to an ionizing electric field in the z direction. Analyzing the energy and location of this saddle point allowed us to deduce the sizes of the atoms from the strength of the ionizing fields.

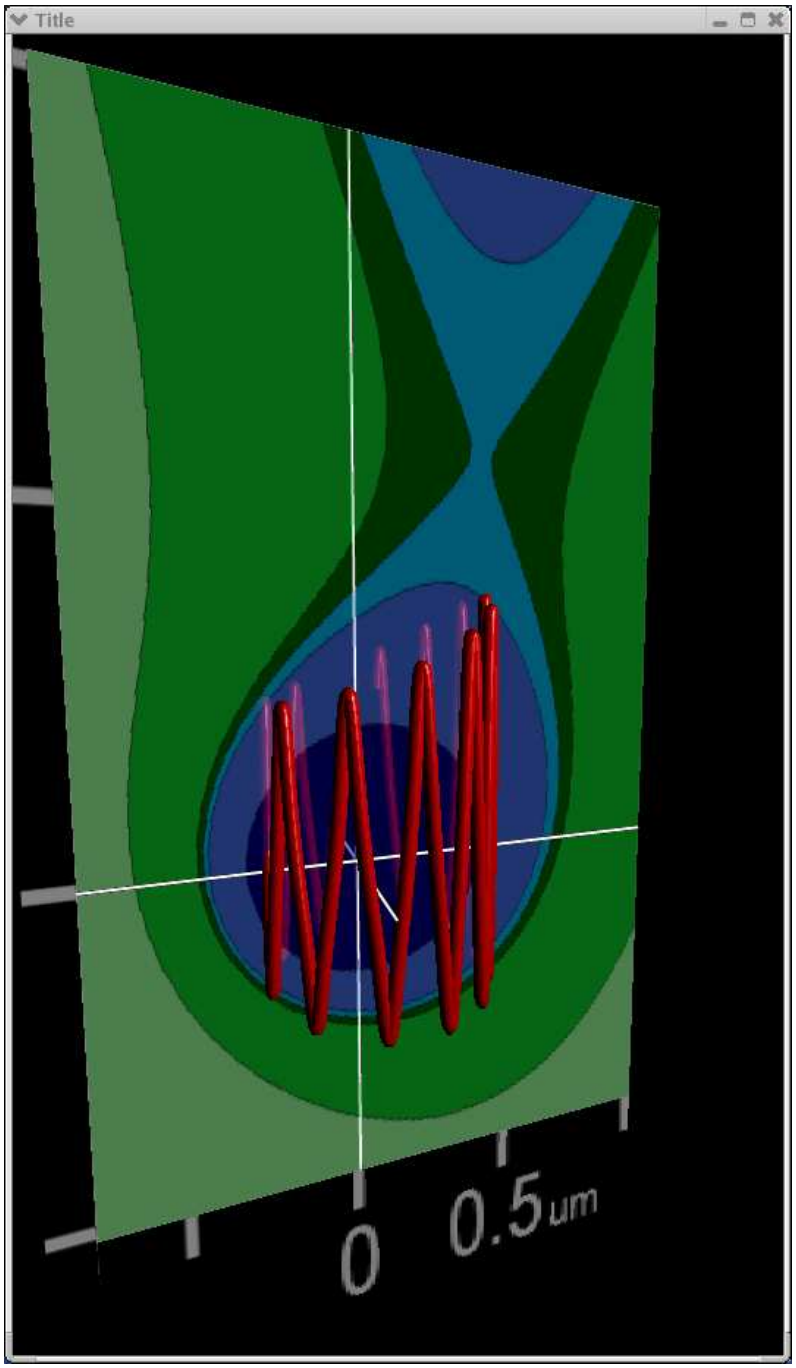

Figure 1.2: Trajectory of the relative coordinate in an effective potential and strong magnetic field. The thickness of the trajectory represents the cyclotron radius. The saddle point, already present in the effective potential is shifted upwards by the axial component of an ionizing electric field.

Chapter 2

Equilibrium

2.1 Equilibrium Ensembles

Consider a composite system, with internal degrees of freedom $\Gamma \equiv (\vec{r}_1 \cdots \vec{p}_N)$, such as a molecule, a star, or coulomb interacting particles, moving in a cylindrically symmetric (around $\hat{z}$ axis) trapping potential. If the system is completely isolated, then both the total energy E(Γ) and total $\hat{z}$ angular momentum $L_z(\Gamma)$ of the system will be conserved. For such a system it is natural to use the ensemble distribution given by

$$P(\Gamma) \propto \delta\left(E(\Gamma) - E_0\right) \times \delta\left(L_z(\Gamma) - L_{z0}\right), \tag{2.1}$$

in computing averages of macroscopic observables over long times after the system has reached internal equilibrium. If instead the system is placed in contact with a heat bath, the ensemble distribution given by

$$P(\Gamma) \propto \exp\left[-\beta E(\Gamma)\right], \tag{2.2}$$

is the appropriate one to use in computing observable averages. In this case it is the total energy of system+bath which is strictly conserved. Now consider a system-bath interaction such that the

1) total energy of system+bath is strictly conserved,

and

2) total $\hat{z}$ angular momentum of system+bath is strictly conserved.

Here the bath acts not only as a traditional heat bath, which enforces a temperature τ, but also as an angular momentum bath, which enforces a "rotation frequency" ω. In such a case, we will argue that the appropriate ensemble distribution to use is a generalization of Eq. (2.2) given by

$$P(\Gamma) \propto \exp\left[-\beta\{E(\Gamma) - \omega L_z(\Gamma)\}\right] \tag{2.3}$$

The δ distribution of Eq. (2.1) corresponds physically to the time averaged dynamical distribution of the system when it is isolated whereas the Boltzman

distributions of Eq. (2.2) and Eq. (2.3) correspond physically to the time averaged dynamical distribution of the system when it is placed in contact with a bath. When the system is in contact with a bath we must use Eq. (2.2) if the total energy is the only conserved quantity for the system+bath, and Eq. (2.3) if the total $\hat{z}$ angular momentum of system+bath is also conserved.

2.1.1 Ensemble Equivalence for Large N

For a system where the number of degrees of freedom N is large, it is physically reasonable to expect that it will be difficult to tell from an observation of its macroscopic properties alone, whether it is isolated or in contact with a bath. This is tantamount to saying that both distributions of Eqs. (2.1) and (2.3) are equivalent for use in computing averages of macroscopic variables. Thus even for an isolated system where $E(\Gamma)$ and $L_z(\Gamma)$ are fixed at E_0 and L_{z0}, one may use the distribution of Eq. (2.3) even though it does not adhere explicitly to the requirement that the observables $E(\Gamma)$ and $L_z(\Gamma)$ have their values both be exactly conserved. Rather, β and ω are tuned so as to make the distributions of $E(\Gamma)$ and $L_z(\Gamma)$ be sharply peaked at E_0 and L_{z0}, so that it is the mean of the random variables $E(\Gamma)$ and $L_z(\Gamma)$ which have their values fixed at E_0 and L_{z_0}.

2.2 Boltzmann Distribution

The distribution of Eq. (2.1) is justified since it is the only stationary distribution with energy and angular momentum strictly fixed which does not assume anything more about the specifics of the Hamiltonian. In this section we will justify the use of the distribution of Eq. (2.3) in the case where the sytem is in contact with a bath s.t. the system bath dynamics satisfies both conditions 1) and 2) described in the section above. We emphasize that for a system with very few degrees of freedom (in contact with such a bath) Eq. (2.3) (not Eq. (2.2)) is the *only* correct possibility. It is only for large N that either ensemble may be used.

Our starting point is similar to conventional treatments, but we will continue beyond to derive many other results not usually viewed from such a perspective. First, imagine a large collection of N_{ens} identical copies of our system I, II, III,$\cdots$, which are weakly interacting with each other. One may, if one wishes, imagine all members of this ensemble to simultaneously occupy the same region of physical space so long as particles in one system of the ensemble interact very weakly with particles in another, and the interaction strength goes to zero as $N_{ens} \to \infty$, so that one may unambiguously speak of the energy of any given ensemble member. Clearly, the total energy and total $\hat{z}$ angular momentum of this collection of interacting ensembles is strictly conserved.

This supersystem of interacting ensembles is only a clever device that facilitates the analysis. One particular member of this ensemble may be taken to be our system, with the remaining members collectively forming a special kind of

energy bath and $\hat{z}$ angular momentum bath. Since general physical (thermodynamic) considerations lead us to believe that ultimately it cannot matter what the bath exactly consists of, any result derived for this particular setup must be generally true. The next two sections give the discrete and contiuous versions of the same argument aimed at justifying Eq. (2.3)

2.2.1 Discrete Version

Divide the $\Gamma \equiv (\vec{r}_1 \cdots \vec{p}_N)$ phase space into discrete cells indexed $i = 1 \cdots c$, of volume

$$d\Gamma = d^3 r_1 \cdots d^3 p_N,$$

centered around equally spaced phase space points $\Gamma_i \equiv (\vec{r}_{1i} \cdots \vec{p}_{Ni})$. Then every state of our supersystem will induce a certain sequence $\{n_1, n_2, \ldots n_c\}$ where n_i is the number of ensemble members whose state belongs to the region enclosed by cell i. For example,

$$\begin{array}{ll} I, III, VII & \text{in cell 1} \\ V, IV & \text{in cell 2} \\ \cdots & \cdots \end{array} \tag{2.4}$$

and

$$\begin{array}{ll} II, IV, VI & \text{in cell 1} \\ III, V & \text{in cell 2} \\ \cdots & \cdots \end{array} \tag{2.5}$$

will both induce the same sequence $\{n_1 = 3, n_2 = 2, \ldots\}$, where $\{n_i\}$ will always satisfy the linear constraints of

$$\begin{array}{lcl} n_i > 0 \; \forall i & & \\ n_1 + n_2 + \cdots n_c & = & N_{ens} \\ n_1 E(\Gamma_1) + n_2 E(\Gamma_2) + \cdots n_c E(\Gamma_c) & = & N_{ens} \times E_0 \\ n_1 L_z(\Gamma_1) + n_2 L_z(\Gamma_2) + \cdots n_c L_z(\Gamma_c) & = & N_{ens} \times L_{z0} \end{array} \tag{2.6}$$

where

$$E(\Gamma_i) \equiv E(\vec{r}_{1i} \cdots \vec{p}_{Ni})$$

and

$$L_z(\Gamma_i) \equiv L_z(\vec{r}_{1i} \cdots \vec{p}_{Ni})$$

are the energy and $\hat{z}$ angular momentum of a state belonging to cell i. The total particle number, energy, and $\hat{z}$ angular momentum of the supersystem are all scaled as N_{ens}, so that the respective quantity per ensemble member remains fixed. Now both superstates of Eq. (2.4) and Eq. (2.5) correspond to two distinct pieces of superstate phase space with volume $(d\Gamma)^{N_{ens}}$. In fact, there will be $N_{ens}!/(n_1! n_2! \cdots n_c!)$ such distinct pieces of superstate phase space volume all inducing the same sequence $\{n_1, n_2, \ldots n_c\}$. Let $P[\{n_1 \cdots n_c\}]$ be the probability of observing a sequence $\{n_1, n_2, \ldots n_c\}$. If we then assume that

all states in superstate phase space satisfying the constraints of Eq. (2.6) are equally likely, we obtain using $n! \sim n \log n$ that

$$\log(P[\{n_1 \cdots n_c\}]) \propto \begin{cases} N_{ens} \log N_{ens} - N_{ens} \\ -(n_1 \log n_1 - n_1 + \cdots n_c \log n_c - n_c) \end{cases}, \tag{2.7}$$

for $\{n_i\}$ satisfying the constraints of Eq. (2.6) and

$$\log(P[\{n_1 \cdots n_c\}]) \propto \{ \ 0,$$

otherwise. Note $\sum_{i=1}^{c} n_i$ cancels N_{ens} in Eq. (2.7). The probability $P[\{n_1 \cdots n_c\}]$ or its logarithm is maximized for that sequence for which we can find Lagrange multipliers α, β, γ s.t.

$$\begin{array}{l} N_{ens} \log N_{ens} \\ -(n_1 \log n_1 + \cdots n_c \log n_c) \\ -\alpha(n_1 + \cdots n_c) \\ -\beta(n_1 E(\Gamma_1) + \cdots n_c E(\Gamma_1)) \\ -\gamma(n_1 L_z(\Gamma_1) + \cdots n_c L_z(\Gamma_c)) \end{array}$$

is an *unconstrained* maximum on the constraint surface. Setting the change due to an independent variation in each n_i equal to 0 we must solve

$$1 + \log n_i + \alpha + \beta E(\Gamma_i) + \gamma L_z(\Gamma_i) = 0 \qquad i = 1 \cdots c$$

simultaneously with the constraints of Eq. (2.6). Absorbing 1 with the α allows us to immediately obtain the functional form for the maximizing sequence $\{n_i^*\}$,

$$n_i^* = \exp(-\alpha - \beta E(\Gamma_i) - \gamma L_z(\Gamma_i)) \qquad i = 1 \cdots c \tag{2.8}$$

where the α, β, γ may be found in principle from substituting Eq. (2.8) into the three constraint equations of Eq. (2.6).

2.2.2 Continuous Version

Notice that the sequence $\{\frac{n_i}{N_{ens}}\}$ is nothing but a discretized version of a smooth normalized density distribution $\rho(\Gamma)$ describing the probability of finding the system (or an ensemble member) in a region $d\Gamma$ around the point Γ. Thus, dividing each of Eqs. (2.6) by N_{ens} and taking $d\Gamma \to 0$ (with N_{ens} and the number of cells c both going to ∞) we may reinterpret all of the above as having to find the constrained maximum of the *functional*

$$\sigma[\rho(\Gamma)] \equiv -\int d\Gamma \, \rho(\Gamma) \, \log(\rho(\Gamma)), \tag{2.9}$$

subject to the constraints

$$\begin{array}{lcl} \rho(\Gamma) & > & 0 \\ \int d\Gamma \rho(\Gamma) & = & 1 \\ \int d\Gamma E(\Gamma) \rho(\Gamma) & = & E_0 \\ \int d\Gamma L_z(\Gamma) \rho(\Gamma) & = & L_{z0}. \end{array} \tag{2.10}$$

This is maximixed for that distribution ρ satisfying Eq. (2.10) for which we can find Lagrange multipliers α, β, γ s.t. the functional

$$\sigma[\rho(\Gamma)] - \alpha \int d\Gamma \rho(\Gamma) - \beta \int d\Gamma\, E(\Gamma)\rho(\Gamma) - \gamma \int d\Gamma\, L_z(\Gamma)\rho(\Gamma) \tag{2.11}$$

is an *unconstrained* maxima. As in the discrete case setting the change due to an arbitrary variation $\delta\rho(\Gamma)$ in $\rho(\Gamma)$ equal to 0, we obtain that the functional form for the maximizing distribution $\rho = \rho^*$ is

$$\rho^*(\Gamma) = \exp(-\alpha - \beta E(\Gamma) - \gamma L_z(\Gamma)). \tag{2.12}$$

2.3 Partial Derivatives of the Entropy

While maximizing the functional of Eq. (2.11) we are free to impose the normalization constraint in Eq. (2.10) by manually constraining the search space rather than through introducing the undetermined Lagrange multiplier α. Then the very same $\rho = \rho^*$ of the previous section is also the maximizing distribution that maximizes the functional

$$F[\rho] \equiv \sigma[\rho] - \beta E[\rho] - \gamma L_z[\rho] \tag{2.13}$$

subject to variations $\delta\rho$ in ρ that keep ρ normalized. That is, the variations $\delta\rho(\Gamma)$ must satisfy

$$\int d\Gamma\, \delta\rho(\Gamma) = 0. \tag{2.14}$$

To make explicit the functional dependence of Eq. (2.13) on ρ we have defined

$$E[\rho] \equiv \langle E \rangle \equiv \int d\Gamma\, E(\Gamma)\rho(\Gamma)$$

and

$$L_z[\rho] \equiv \langle L_z \rangle \equiv \int d\Gamma\, L_z(\Gamma)\rho(\Gamma).$$

Now evaluate Eq. (2.11) at the maximizing $\rho = \rho^*$. Defining $F[\rho^*]$ as F^* and $\sigma[\rho^*]$ as σ^* we have

$$F^*_{(\beta,\gamma)} = \sigma^*_{(E_0, L_{z0})} - \beta E_0 - \gamma L_{z0} \tag{2.15}$$

because $\langle E \rangle = E_0$ and $\langle L_z \rangle = L_{z0}$ are the constraints of Eq. (2.10) that ρ^* must satisfy.

Now instead of specifying the values of the constraints E_0 and L_{z0} in Eq. (2.10), one may alternatively specify the Lagrange multipliers β and γ and ask what E_0 and L_{z0} these would correspond to. Mathematically, it is enough to specify either pair if the correspondence $(\beta, \gamma) \leftrightarrow (E_0, L_{z0})$ is one to one. (Untrue at a phase transition.) Then, if σ and F are both always evaluated at the maximizing ρ^* they become mere functions of either pair of parameters

(β,γ) or (E_0, L_{z0}). σ^* is naturally considered to be a function of E_0 and L_{z0}, whereas F^* is naturally considered as a function of β and γ. This choice is motivated by the fact that

$$\begin{array}{rcl} \frac{\partial \sigma^*_{(E_0,L_{z0})}}{\partial E_0} & = & \beta \\ \frac{\partial \sigma^*_{(E_0,L_{z0})}}{\partial L_{z0}} & = & \gamma \end{array} \tag{2.16}$$

and

$$\begin{array}{rcl} \frac{\partial F^*_{(\beta,\gamma)}}{\partial \beta} & = & -E_0 \\ \frac{\partial F^*_{(\beta,\gamma)}}{\partial \gamma} & = & -L_{z0}. \end{array} \tag{2.17}$$

To prove Eq. (2.16) remember that σ^* acquires its dependence on E_0 and L_{z0} through its functional argument ρ^* which depends on the constraint values E_0 and L_{z0}. Let us consider a small change ΔE_0 in the constraint E_0 keeping the constraint L_{z0} fixed. This induces ρ^* to undergo a variation $\delta\rho^*$. This $\delta\rho^*$ is nothing but a *particular* variation $\delta\rho$ (satisfying Eq. (2.14)) of ρ around ρ^* that causes changes of

$$\begin{array}{lll} \Delta\sigma & \text{in} & \sigma[\rho] \\ \Delta E & \text{in} & E[\rho] \\ \Delta L_z = 0 & \text{in} & L_z[\rho]. \end{array}$$

The corresponding variation ΔF of the functional $F[\rho]$ around $F[\rho^*]$ is

$$\Delta F = \Delta\sigma - \beta\Delta E = 0 \tag{2.18}$$

But any variation $\delta\rho$ around $\rho = \rho^*$ must keep F stationary.

$$\therefore \left.\frac{\partial \sigma^*_{(E_0,L_{z0})}}{\partial E_0}\right)_{L_z} = \beta.$$

It might appear that we have forgotten the terms $(\Delta\gamma)L_z$ and $(\Delta\beta)E$ in Eq.(2.18) which would have been produced by taking the differential of each term in Eq. (2.15). This is not so, however, because even though it is true that a change $(\Delta E_0, \Delta L_{z0} = 0)$ will cause both β and γ to change, $F[\rho]$ is claimed to be stationary to variations $\delta\rho$ for the *fixed* held values of β and γ corresponding to $\rho = \rho^*$. An identical argument proves the second partial of Eq.(2.16). Clearly then, F^* in Eq. (2.15) is the so-called Legendre transform of σ^* so that Eq. (2.17) follows from the well known Legendre transform property.

2.4 Free Energy

We pointed out above that rather than specify the constraints $E(\Gamma) = E_0$ and $L_z(\Gamma) = L_{z_0}$ it would be perfectly legitimate to specify the Lagrange multipliers (β,γ) instead. The corresponding values of the constraints could be retrieved by maximizing the functional $F[\rho]$ in Eq. (2.13) over all normalized ρ at $\rho = \rho^*$,

and then computing $E[\rho^*]$ and $L_z[\rho^*]$ as E_0 and L_{z_0}. But this is nothing but the familiar free energy *minimization* since

$$\begin{aligned} F^*_{(\beta,\gamma)} &= -\beta(E_0 - \omega L_{z_0} - \tau\sigma^*_{(E_0,L_{z0})}) \\ &\equiv -\beta A^*_{(\tau,\omega)}. \end{aligned} \tag{2.19}$$

where $\beta = 1/\tau$ is fixed. The natural variables of the free energy $A^*_{(\tau,\omega)}$, are taken as τ and ω since it may be easily verified that

$$\frac{\partial}{\partial\tau}\Big)_{\omega} A^*_{(\tau,\omega)} = -\sigma^*$$

and

$$\frac{\partial}{\partial\omega}\Big)_{\tau} A^*_{(\tau,\omega)} = -L_{z0}$$

2.4.1 Partition Function

Nowhere in the above did we use the explicit exponential form for ρ^* found in Eq. (2.12). We will now do so by first reexpressing Eq. (2.12) as

$$\rho^*(\Gamma) = \frac{\exp(-\beta E(\Gamma) - \gamma L_z(\Gamma))}{Z}.$$

Since $\rho^*(\Gamma)$ is necessarily normalized,

$$Z(\beta,\gamma) \equiv \int d\Gamma \exp(-\beta E(\Gamma) - \gamma L_z(\Gamma))$$

is the normalization. Substituting this explicit functional form for ρ^* into the definition $\sigma[\rho] \equiv -\int d\Gamma\rho(\Gamma)\log\rho(\Gamma)$ we have

$$\begin{aligned} \sigma^*_{(E_0,L_{z0})} \equiv \sigma[\rho^*] &= -\int d\Gamma\rho^*(\Gamma)\{-\beta E(\Gamma) - \gamma L_z(\Gamma) - \log Z\} \\ &= \log Z + \beta E_0 + \gamma L_{z_0} \end{aligned}$$

so that Eq. (2.15) simplifies as

$$\begin{aligned} F^*_{(\beta,\gamma)} &\equiv \sigma^* - \beta E_0 - \gamma L_{z_0} \\ &= \log Z(\beta,\gamma). \end{aligned} \tag{2.20}$$

This identification of F^* with $\log Z$ immediately leads to an alternate and direct proof of Eq. (2.17) in the usual manner by differentiating the integral expression for $Z(\beta,\gamma)$ under the integral sign. Finally putting Eq. (2.20) together with our definition for $A^*_{(\tau,\omega)}$ in Eq. (2.19) shows that

$$A^*_{(\tau,\omega)} = -\tau\log Z(\beta,\gamma),$$

thereby confirming the equivalence of our definitions with the usual ones.

2.5 Entropy

We have just confirmed that what we have been calling σ^* all along in the above sections, is the familiar thermodynamic entropy. Nevertheless, the functional $\sigma[\rho]$ is defined for any arbitrary distribution $\rho(\Gamma)$.

2.5.1 Shannon Entropy

In an entirely different context, Shannon introduced this quantity as a measure of the uncertainty or randomness in any probabilty distribution. Thus, the Boltzmann distribution $\rho^*(\Gamma)$ is interpreted as being that unique distribution which is the "most random" while satisfying the constraints that the mean values (over the distribution) of the random variables $E(\Gamma)$ and $L_z(\Gamma)$ are E_0 and L_{z0}.

It is illuminating to revisit the derivation of Section (2.2) in this light. In effect what we showed over there was that for a given distribution $\rho(\Gamma)$, the quantity $-\int d\Gamma \rho(\Gamma) \log \rho(\Gamma)$ measured the "number of distict ensembles" that could be picked from this distribution. In fact we will argue below that

$$\log(\text{"number of distinct ensembles"}) \backsimeq N_{\text{ens}} \left[-\int d\Gamma \rho(\Gamma) \log \rho(\Gamma) \right],$$

for large N_{ens}. To see this, we revert back to discretizing the phase space of the system into small cells of size $d\Gamma$. Now for a large ensemble of N_{ens} members drawn from a distribution $\rho(\Gamma)$, the number of members n_i belonging to cell i, will approximately satisfy

$$n_i \simeq N_{\text{ens}} \left[d\Gamma \rho(\Gamma_i) \right]. \tag{2.21}$$

Another sequence $\{n_i\}$, satisfying only $\sum_i n_i = N_{\text{ens}}$, but very different from Eq. (2.21) could also in principle result from an ensemble drawn from the distribution $\rho(\Gamma)$, but clearly such a sequence would occur only very rarely. This means that by considering only those ensembles inducing a sequence close to that of Eq. (2.21), we will have accounted for the majority of distinct possible ensembles. The log of the number of distinct ensembles histograming precisely to this binning sequence $\{n_i\}$ in phase space is

$$\begin{aligned}
\log\left(\frac{N_{\text{ens}}}{n_1! \cdots n_c!}\right) &= N_{\text{ens}} \log N_{\text{ens}} - \sum_i N_{\text{ens}}\, d\Gamma \rho(\Gamma_i)\, \log\left[N_{\text{ens}}\, d\Gamma \rho(\Gamma_i)\right] \\
&= N_{\text{ens}} \log N_{\text{ens}} - N_{\text{ens}} \sum_i d\Gamma \rho(\Gamma_i) \left[\log N_{\text{ens}} + \log \rho(\Gamma_i) + \log d\Gamma\right] \\
&\simeq N_{\text{ens}} \left[\left\{ -\sum_i d\Gamma \rho(\Gamma_i) \log \rho(\Gamma_i) \right\} + \log d\Gamma \right] \\
&= N_{\text{ens}} \left[\left\{ -\int d\Gamma \rho(\Gamma) \log \rho(\Gamma) \right\} \quad + \log d\Gamma \right],
\end{aligned}$$

as claimed. The additive term $\log d\Gamma$ is independent of the distribution $\rho(\Gamma)$.

2.5.2 Grand Ensemble

The two ensembles of Eqs. (2.1) and (2.3) defined for a system of N_0 particles were distributions defined on a $6N_0$ dimensional phase space. In order to enable us to be most general in what follows, we will first introduce a third ensemble which is defined on the union of all such $6N_0$ dimensional phase spaces for $N_0 = 0, 1, 2, \cdots$.

We assume without much discussion the well known result that the probability density in such an ensemble of being in a N-particle state $\Gamma_N = (\vec{r}_1 \cdots \vec{p}_N)$ is given by

$$P(\Gamma_N) \quad \propto \quad \frac{1}{h^{3N} N!} \exp\left[-\frac{1}{\tau_0}\left\{E(\Gamma_N) - \omega_0 L_z(\Gamma_N) - \mu_0 N\right\}\right]$$

The full N dependence has been carefully included in the r.h.s. Gibbs pointed out the necessity for the $N!$, and the $(h^3)^N$ enables us to compare volumes $d\Gamma_N$ and $d\Gamma_{N'}$ belonging to different dimensional phase spaces, by ensuring that they are both measured in their naturally appropriate dimensionless units. Note that as a matter of notation, we will sometimes put a subscript 0 on a parameter to indicate its *particular* value, so as to reserve the unsubscripted symbol for the generic random variable (an observable defined on phase space) itself.

Now consider finding the normalization of the probability density $P(\Gamma'_{N'})$ by performing

$$\sum_{N'=0}^{\infty} \int d\Gamma'_{N'} \frac{1}{h^{3N'} N'!} \exp\left[-\frac{1}{\tau_0}\left\{E'(\Gamma'_{N'}) - \omega_0 L'_z(\Gamma'_{N'}) - \mu_0 N'\right\}\right]. \qquad (2.22)$$

Now,

$$1 = \sum_{N=0}^{\infty} \int dE \int dL_z \; \delta_{NN'} \delta(E - E'(\Gamma'_{N'})) \delta(L_z - L'_z(\Gamma'_{N'})) \qquad (2.23)$$

for any fixed $\Gamma'_{N'}$ (and N') provided that the range of integration for E and L_z includes all the possible values that the observables $E'(\Gamma'_{N'})$ and $L'_z(\Gamma'_{N'})$ can assume. Inserting this expression for unity in Eq. (2.23) into the integrand of Eq. (2.22) and then reversing the order of summation/integration for the prime and unprimed variables, we immediately obtain that Eq. (2.22) which sums up all the relative probabilities may be cast as

$$\sum_{N=0}^{\infty} \int dE \int dL_z \underbrace{\frac{W(E, L_z, N)}{h^{3N} N!} \exp\left[-\frac{1}{\tau_0}\left\{E - \omega_0 L_z - \mu_0 N\right\}\right]}$$

where

$$W(E, L_z, N) \equiv \int d\Gamma_N \; \delta(E - E(\Gamma_N)) \delta(L_z - L_z(\Gamma_N)),$$

is the density of states. The probabilitiy density as a function of E, L_z, N is obviously then exactly proportional to the above bracketed integrand.

$$P(E, L_z, N) \propto \frac{W(E, L_z, N)}{h^{3N} N!} \exp\left[-\frac{1}{\tau_0}\left\{E - \omega_0 L_z - \mu_0 N\right\}\right] \qquad (2.24)$$

2.5.3 Entropy and the Density of States

By defining

$$\sigma(E, L_z, N) = \log\left(\frac{W(E, L_z, N)}{h^{3N} N!}\right), \tag{2.25}$$

Eq. (2.24) is usefully expressed as

$$P(E, L_z, N) \propto \exp\left[\sigma(E, L_z, N) - \beta E - \gamma L_z - \alpha N\right]. \tag{2.26}$$

Now we repeat the argument of Section (2.1.1). For a system with a large number of degrees of freedom N, it is physically reasonable to conclude that it will be difficult to tell from an observation of its macroscopic observables (such as E_0 and $L_{z_0}$and N_0) whether it is in contact with a large reservoir bath or not. In other words, the distribution as a function of (E, L_z, N) will be uni-modal and sharply peaked at some point (E_0, L_{z_0}, N_0); otherwise we could tell. At this point of local maximum, the argument of the exponential must be stationary so that

$$\begin{aligned} \frac{\partial \sigma(E_0, L_{z_0}, N_0)}{\partial E} &= \beta_0, \\ \frac{\partial \sigma(E_0, L_{z_0}, N_0)}{\partial L_z} &= \gamma_0, \\ \frac{\partial \sigma(E_0, L_{z_0}, N_0)}{\partial N} &= \alpha_0. \end{aligned} \tag{2.27}$$

The partials are evaluated at the point at which the distribution is peaked. Comparing the partials in Eq. (2.27) with the partials in Eq. (2.16) confirms that the definition of entropy in Eq. (2.25) is equivalent to our previous definition.

Aside:

Sometimes, at certain special values of the intensive variables τ_0, ω_0, μ_0, or $\beta_0, \gamma_0, \alpha_0$ the distribution as a function of E, L_z, and N is not sharply peaked. Indeed, at such a point it would be quite easy to tell whether the bath is connected or not since with a bath connected every macroscopic variable will show large fluctuation. For a large but finite N, the distribution of any one of them becomes bi-modal as the intensive variables pass through one of these special points, while the system remains undecided about which value to remain sharply peaked around.

2.6 $(E_0, L_{z_0}, N_0) \leftrightarrow (\tau_0, \omega_0, N_0)$ Mapping

To obtain the parameters E_0, L_{z_0} of the δ-ensemble given the parameters τ_0, ω_0 of the Boltzmann ensemble we simply compute the means of $E(\Gamma)$ and $L_z(\Gamma)$ over the (τ_0, ω_0, N_0) -Boltzmann distribution by using the metropolis algorithm to make repeated draws from that distribution. In principle, one could imagine

inverting this procedure to obtain τ_0, ω_0 given E_0, L_{z_0} by performing a root search. Practically, these are obtained differently. In the Boltzmann ensemble, a so-called estimator for the temperature parameter τ is easily shown to be

$$\tau = \frac{2}{3N} \sum_{i=1}^{N} \frac{p_i^2}{2m}.$$

That is, τ is a random variable whose mean over the Boltzmann distribution is analytically shown to be τ_0. But since τ is a macroscopic observable we expect that its mean over the δ-distribution of Eq. (2.1) should also give the same value. Thus computing the mean of τ over long time equilibrium dynamics with E_0 and L_{z_0} fixed, gives us a practical way to compute τ_0.

However, it is at least of theoretical interest that it *is* possible to explicitly exhibit random variables whose mean over the δ-distribution is exactly τ_0 and $-\omega_0/\tau_0$ as defined by

$$\frac{1}{\tau_0} \equiv \frac{\partial \sigma(E_0, L_{z_0}, N_0)}{\partial E} = \frac{\frac{\partial W(E_0, L_{z_0}, N_0)}{\partial E_0}}{W(E_0, L_{z_0}, N_0)}$$

and

$$\frac{-\omega_0}{\tau_0} = \frac{\partial \sigma(E_0, L_{z_0}, N_0)}{\partial L_{z0}} = \frac{\frac{\partial W(E_0, L_{z_0}, N_0)}{\partial L_{z0}}}{W(E_0, L_{z_0}, N_0)},$$

thereby providing us with an alternate way to extract the parameters τ_0 and ω_0. First, a lemma.

2.6.1 Lemma: Volume Change Under Flow

Consider a volume V in phase space that evolves under the flow of a vector field $\vec{u}(\Gamma)$. That is, each point Γ evolves in "time" according to the o.d.e.

$$\frac{d\Gamma_s}{ds} = \vec{u}(\Gamma_s).$$

In general, s will have dimensions different from time.

Lemma

The volume V itself evolves according to

$$\frac{dV_s}{ds} = \int_{V_s} d\Gamma \, \vec{\nabla} \cdot \vec{u}(\Gamma), \tag{2.28}$$

Eq. (2.28) has its more common version when the volume is an infinitesimal piece v_s flowing with the point Γ_s. Then

$$\frac{d\,(v_s)}{ds} = \vec{\nabla} \cdot \vec{u}(\Gamma)\ \ (v_s)\,.$$

Proof

Consider an oriented patch of area $dA\,\hat{n}$ on the surface $\Sigma(V)$ bounding the volume V. Under the flow for a "time" ds, this patch will sweep out a volume

$$dA\,\hat{n}\cdot\hat{u}\,ds.$$

The sign of $\hat{n}\cdot\hat{u}$ reflects whether the patch moves inside or outside the region V_s. Summing over all these signed increments of volume then gives the total increment of volume dV_s in V_s by

$$dV_s = \left(\int\limits_{\Sigma(V)} dA\,\hat{n}\cdot\hat{u}\right) ds.$$

Dividing by ds and using the divergence theorem gives Eq. (2.28) as claimed.

2.6.2 τ and ω as Dynamical Observables

Let

$$\vec{u}(\Gamma) \text{ and } \vec{\omega}(\Gamma)$$

be two vector fields that correspond to taking the partials

$$\frac{\partial}{\partial E}\Big)_{L_z,\cdots} \text{ and } \frac{\partial}{\partial L_z}\Big)_{E,---}, \tag{2.29}$$

in $6N_0$ dimensional phase space. The "$\cdots$" and "$---$" stand for the values at which the remaining $6N_0-2$ independent coordinates are to be held fixed. These will be different for each of the two partials. Thus for example, taking the partial w.r.t. E of any scalar function $f(\Gamma)$ holding L_z fixed is equivalent to the fisherman's derivative of f along the flow $\vec{u}$. The advantage of thinking in terms of the vector fields is that we are freed of having to explicitly specify the remaining the $6N_0-2$ independent coordinates. Since in any case we have to integrate over these to find the density of states, their exact choice will not affect this answer. Let $\Delta\epsilon$ and Δl_z to be very small intervals of energy and angular momentum. The volume of the region of phase space satisfying

$$E < E(\Gamma) < E+\Delta\epsilon \qquad \text{and} \qquad L_z < L_z(\Gamma) < L_z + \Delta l_z$$

is $W(E,L_z,N)\Delta\epsilon\Delta l_z$. Now apply our lemma to this volume moving along the flow induced by $\vec{u}$. We get

$$\frac{\partial}{\partial E}\Big)_{L_z}[W(E,L_z,N)\Delta\epsilon\Delta l_z] = \int\limits_{\substack{E<E(\Gamma)<E+\Delta\epsilon \\ L_z<L_z(\Gamma)<L_z+\Delta l_z}} \vec{\nabla}\cdot\vec{u}$$

Dividing by $\Delta\epsilon\Delta l_z$, we get

$$\frac{\partial}{\partial E}\Big)_{L_z} W(E, L_z, N) = \int d\Gamma \delta(E - E(\Gamma))\delta(L_z - L_z(\Gamma))\vec{\nabla}\cdot\vec{u}.$$

Then dividing both sides by $W(E, L_z, N)$ gives

$$\frac{\frac{\partial}{\partial E}\big)_{L_z} W(E, L_z, N)}{W(E, L_z, N)} = \frac{\int d\Gamma \delta(E - E(\Gamma))\delta(L_z - L_z(\Gamma))\vec{\nabla}\cdot\vec{u}}{\int d\Gamma \delta(E - E(\Gamma))\delta(L_z - L_z(\Gamma))}$$

which is

$$\frac{\partial\sigma(E, L_z, N)}{\partial E} = \langle\vec{\nabla}\cdot\vec{u}\rangle \tag{2.30}$$

where the mean is manifestly to be taken over the δ distribution. In identical fashion we proove

$$\frac{\partial\sigma(E, L_z, N)}{\partial L_z} = \langle\vec{\nabla}\cdot\vec{w}\rangle \tag{2.31}$$

2.6.3 Constructing $\vec{u}$ and $\vec{v}$

Requiring that $\vec{u}$ and $\vec{v}$ be interpretable as the partials in Eq. (2.29) is tantamount to the following. For each and every Γ, flowing for a "time" s along $\vec{u}$ should change the value of $E(\Gamma)$ by s keeping the value of $L_z(\Gamma)$ unchanged, and flowing for a "time" r along $\vec{v}$ should change $L_z(\Gamma)$ by r keeping the value of $E(\Gamma)$ unchanged. The two flows need not commute since "$\cdots$" and "$- - -$" are not the same in Eq. (2.29). Now it is clear that one may construct a $\vec{u}'$ and $\vec{v}'$ satisfying

$$\vec{u}'\cdot\vec{\nabla}L_z = 0 \tag{2.32}$$

and

$$\vec{w}'\cdot\vec{\nabla}E = 0, \tag{2.33}$$

by applying a simple Gram-Schmidt-like procedure to any two independent and non-zero vector fields. Then the fields

$$\vec{u} \equiv \frac{\vec{u}'}{\vec{u}'\cdot\vec{\nabla}E} \qquad \text{and} \qquad \vec{w} \equiv \frac{\vec{w}'}{\vec{w}'\cdot\vec{\nabla}L_z},$$

satisfy our requirements because the rates of change of $E(\Gamma)$ and $L_z(\Gamma)$ along the flow induced by $\vec{u}$ are

$$\begin{aligned}
\frac{\partial E_s}{\partial s} &= \vec{\nabla}E(\Gamma)\cdot\frac{\partial\Gamma}{\partial s} \\
&= \vec{\nabla}E(\Gamma)\cdot\vec{u}(\Gamma) \\
&= \vec{\nabla}E\cdot\frac{\vec{u}'}{\vec{u}'\cdot\vec{\nabla}E} \\
&= 1,
\end{aligned}$$

and

$$\begin{aligned}\frac{\partial L_{z_s}}{\partial s} &= \vec{\nabla} L_z(\Gamma) \cdot \frac{\partial \Gamma}{\partial s} \\ &= \vec{\nabla} L_z(\Gamma) \cdot \vec{u}(\Gamma) \\ &= \vec{\nabla} L_z \cdot \frac{\vec{u}'}{\vec{u}' \cdot \vec{\nabla} E} \\ &= 0,\end{aligned}$$

where the last equality uses Eq. (2.32). The rates of change of E and L_z along $\vec{w}$ are similarly confirmed.

2.6.4 Example

Consider N non-interacting particles moving in a rectangular box. The total energy E is the only conserved quantity. Define

$$\vec{u}'(\Gamma) = (\vec{p}_1, \vec{0}, \vec{p}_2, \vec{0}, \cdots). \tag{2.34}$$

where the position components are 0. Then

$$\begin{aligned}\vec{u}(\Gamma) = \frac{\vec{u}'}{\vec{u}' \cdot \vec{\nabla} E} &= \frac{(\vec{p}_1, \vec{0}, \vec{p}_2, \vec{0}, \cdots)}{(\vec{p}_1, \vec{0}, \vec{p}_2, \vec{0}, \cdots) \cdot (\frac{\vec{p}_1}{m}, \vec{0}, \frac{\vec{p}_2}{m}, \vec{0}, \cdots)} \\ &= \frac{m(\vec{p}_1, \vec{0}, \vec{p}_2, \vec{0}, \cdots)}{p^2}\end{aligned} \tag{2.35}$$

where

$$p^2 \equiv \vec{p}_1^{\,2} + \vec{p}_2^{\,2} + \cdots \vec{p}_N^{\,2}.$$

Notice that taking $\vec{u}'(\Gamma) = (\vec{p}_1, \vec{0}, 0, \vec{0}, \cdots)$ in Eq. (2.34) would have been unacceptable since the denominator $\vec{u}' \cdot \vec{\nabla} E$ of Eq. (2.35) would be zero at some points on the energy shell over which we have to compute the mean divergence

$$\vec{\nabla} \cdot \vec{u} = \frac{m}{p^2}(3N - 2).$$

Now using formula (2.30) gives us

$$\begin{aligned}\beta_0 &= \langle \vec{\nabla} \cdot \vec{u} \rangle \\ &= \frac{1}{E_0}\left(\frac{3N}{2} - 1\right)\end{aligned} \tag{2.36}$$

This is claimed to be exactly $\frac{\partial \sigma(E_0)}{\partial E}$, where $\sigma(E) = \log W(E)$. For this simple example we can also confirm this directly. The volume of phase space in an energy range dE around E is

$$\propto V^{3N} \times p^{3N-1} dp$$

where

$$2p\,dp = 2m\,dE.$$

Therefore

$$\sigma(E) = \log W(E) = \log\left(V^{3N} p^{3N-1} \frac{m}{p}\right).$$

So

$$\frac{\partial\sigma(E)}{\partial E} \quad = \quad (3N-2)\frac{1}{p}\frac{\partial p}{\partial E}$$

or

$$\frac{\partial\sigma(E_0)}{\partial E} \quad = \quad (3N-2)\frac{1}{2E_0}$$

in agreement with Eq. (2.36). Compare this to the relation between the parameter τ_0 in the Boltzmann distribution and the mean value E_0 of the energy $E(\Gamma)$ in that distribution.

$$\tau_0 = \frac{1}{E_0}\frac{3N}{2}.$$

Chapter 3

Single Species Equilibrium

Our system consists of N Coulomb interacting particles moving in a cylindrically symmetric trapping potential, in the presence of a uniform axial magnetic field. By substituting $\vec{B} = 0$ in any result we may read off the answer for the case when there is no B field. Nevertheless, we will often treat the $\vec{B} = 0$ case separately in its own right, because somewhat surprisingly the converse is also true: Appendix (B.1) shows why, in a literal sense, the $\vec{B} = 0$ case completely subsumes the $\vec{B} \neq 0$ case. Moreover, we find that thinking in the rotating frame is a useful source of insight.

3.1 Equilibrium Ensemble

From our discussion in Chapter (**??**) it follows that we may legitimately choose to describe the equilibrium of the system with the Boltzmann ensemble of Eq. (2.3) which is generically proportional to

$$e^{-\frac{1}{\tau}\{E-\omega L_z\}}. \tag{3.1}$$

The exponential form in Eq. (3.1) is mathematically more convenient than Eq. (2.1) since $E(\Gamma)$ and $L_z(\Gamma)$ appear additively in the exponent. This choice is one of convenience only and has no bearing on whether the experimental system is truly isolated or in contact with a bath. For the case of an isolated system, the value of τ and ω in Eq. (3.1) is determined spontaneously by the initial energy E and angular momentum L_z possessed respectively by the system, before it reaches equilibrium. If the system is in contact with a bath which itself is characterized by a temperature τ and rotation frequncy ω, then it is *these* values that are imposed upon the system as it reaches equlibrium.

To express Eq. (3.1) explicitly let us first choose appropriate coordinates for the N-particle phase space.

3.1.1 Phase space coordinates

It is implicitly understood that Eq. (3.1) expresses the ensemble distribution density in canonical coordinates in which phase space volume is conserved with time evolution. That is, both E and L_z in Eq. (3.1) are to be expressed as functions of a canonical set of coordinates. In the absence of a B field, these may be simply taken as $\Gamma = (\vec{r}_1 \cdots \vec{r}_N, \vec{p}_1 \cdots \vec{p}_N)$ where $\vec{p}_i = m_i \vec{v}_i$. In the presence of a B field we must use the coordinates $(\vec{r}_1 \cdots \vec{r}_N, \vec{s}_1 \cdots \vec{s}_N)$ where the canonical momentum $\vec{s}_i$ defined in Eq. (B.2.7) is some combination of $\vec{r}_i$ and $\vec{p}_i$. For the case of a uniform magnetic field this combination is just the linear combination

$$\vec{s}_i \equiv m\vec{v}_i + \frac{e_i B}{2c}\rho_i \hat{\phi}(\vec{r}),$$

as shown in Eq. (B.2.8) in the Appendix. Consequently the Jacobian for the change of coordinates from $(\vec{r}_1 \cdots \vec{r}_N, \vec{p}_1 \cdots \vec{p}_N)$ to $(\vec{r}_1 \cdots \vec{r}_N, \vec{s}_1 \cdots \vec{s}_N)$ is 1, as shown in Appendix (B.3). This means we may continue to use the coordinates $(\vec{r}_1 \cdots \vec{r}_N, \vec{p}_1 \cdots \vec{p}_N)$ in order to express the density in Eq. (3.1) without any modification arising from a Jacobian factor, even in the case of a B field. Thus, the very same form

$$P(\Gamma) \quad \propto \quad \exp\left[-\frac{1}{\tau}\left\{E(\Gamma) - \omega L_z(\Gamma)\right\}\right] \tag{3.2}$$

with $\Gamma \equiv (\vec{r}_1 \cdots \vec{r}_N, \vec{p}_1 \cdots \vec{p}_N)$ where $\vec{p}_i = m_i \vec{v}_i$, correctly describes the equilibrium ditribution both with and without a B field even though rhe dynamics of the particles in each case is very different. $E(\Gamma)$ in Eq. (3.2) is the usual kinetic plus potential energy and $L_z(\Gamma)$ is the appropriate conserved quantity arising due to cylindrical symmetry.

Cylindrical coordinates

Let (ρ_i, ϕ_i, z_i) be the cylindrical coordinates of the ith particle and $(p_{\rho_i}, p_{t_i}, p_{z_i}) \equiv m(v_{\rho_i}, v_{t_i}, v_{z_i})$ be the momentum along $\hat{\rho}, \hat{\phi}$, and $\hat{z}$. See Fig. (3.1). Note that p_{t_i} is not the canonical ϕ-momentum but simply the tangential component of the momentum.

3.1.2 $\vec{B} = 0$ Case

When $\vec{B} = 0$ the conserved quantity L_z is just the usual mechanical angular momentum

$$\begin{aligned} L_z &= L_z^{(\text{mech})} \\ &\equiv \sum_{i=1}^{N} \rho_i p_{t_i}. \end{aligned}$$

Expressing Eq. (3.2) in our cylindrical coordinates we get

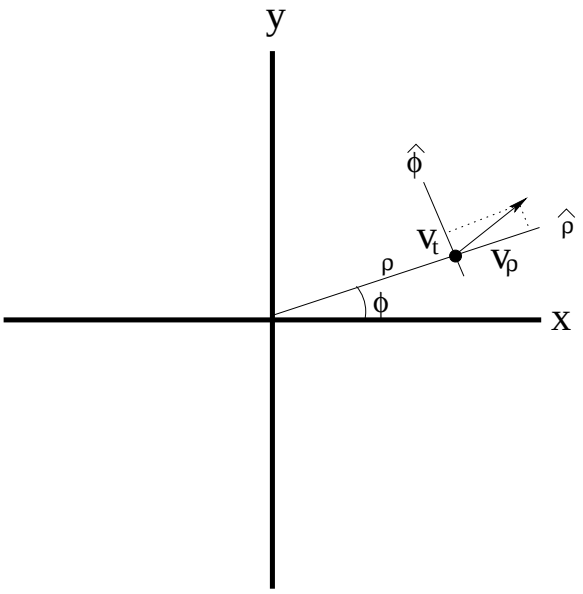

Figure 3.1: Cylindrical Coordinates

$$P(\Gamma) \propto \exp\left[-\frac{1}{\tau}\sum_{i=1}^{N}\left\{\frac{p_{\rho_i}^2}{2m}+\frac{p_{t_i}^2}{2m}+\frac{p_{z_i}^2}{2m}+V_T(\rho_i,z_i)-\omega p_{t_i}\rho_i\right\}+\sum_{i>j}^{N}V(\vec{r}_i,\vec{r}_j)\right]. \tag{3.3}$$

$V(\vec{r}_i,\vec{r}_j)$ is the interaction potential between particles i and j which is summed over all distinct particle pairs in the above equation. $V_T(\rho,z)$ is the cylindrically symmetric trapping potential felt equally by all the particles. Rewriting Eq. (3.3), by completing the square we may factor it as

$$\begin{aligned} P(\Gamma) \quad \propto \quad & \prod_{i=1}^{N}\left(\exp\left[\frac{-p_{\rho_i}^2}{2m\tau}\right]\exp\left[-\frac{(p_{t_i}-m\omega\rho_i)^2}{2m\tau}\right]\exp\left[\frac{-p_{z_i}^2}{2m\tau}\right]\right)\times \\ & \exp\left[-\frac{1}{\tau}\left\{\sum_{i=1}^{N}\left(V_T(\rho_i,z_i)-\frac{1}{2}m\omega^2\rho_i^2\right)+\sum_{i>j}^{N}V(\vec{r}_i,\vec{r}_j)\right\}\right]. \end{aligned} \tag{3.4}$$

Since the integral over the momenta is independent of the ρ_i, this allows (See Appendix (A.1)) the identifications

$$P(\vec{p}_1\cdots\vec{p}_N|\vec{r}_1\cdots\vec{r}_N) \propto \prod_{i=1}^{N}\left(\exp\left[\frac{-p_{\rho_i}^2}{2m\tau}\right]\exp\left[-\frac{(p_{t_i}-m\omega\rho_i)^2}{2m\tau}\right]\exp\left[\frac{-p_{z_i}^2}{2m\tau}\right]\right) \tag{3.5}$$

and

$$P(\vec{r}_1 \cdots \vec{r}_N) \propto \exp\left[-\frac{1}{\tau}\left\{\sum_{i=1}^{N}\left(V_T(\rho_i, z_i) - \frac{1}{2}m\omega^2\rho_i^2\right) + \sum_{i>j}^{N} V(\vec{r}_i, \vec{r}_j)\right\}\right]. \tag{3.6}$$

where $P(\vec{r}_1 \cdots \vec{r}_N)$ is the (marginal) distribution of the configuration coordinates with the momenta traced out and $P(\vec{p}_1 \cdots \vec{p}_N | \vec{r}_1 \cdots \vec{r}_N)$ is the conditional momentum distribution given a configuration. Thus, the equilibrium of the configurational coordinates is simply that of N interacting particles at temperature τ in an effective potential

$$V_w^{(\text{eff})}(\rho, z) = V_T(\rho, z) - \frac{1}{2}m\omega^2\rho^2.$$

3.1.3 $\vec{B} \neq 0$ Case

In the case of a uniform B field Appendix B shows that the conserved quantity L_z is the generalized angular momentum given by

$$\begin{aligned} L_z &= L_z^{(\text{mech})} + L_z^{(\text{field})} \\ &\equiv \sum_{i=1}^{N} \rho_i p_{t_i} + \frac{w_c}{2}\sum_{i=1}^{N} m_i\rho_i^2. \end{aligned}$$

By making the replacement

$$\omega\rho_i p_{t_i} \to \omega\left(\rho_i p_{t_i} + m_i\rho_i^2\frac{\omega_c}{2}\right),$$

for the term '$\omega\rho_i p_{t_i}$' occurring in Eq. (3.3) we may quickly deduce the form of Eq. (3.2) in the presence of a magnetic field. After making the replacement, it is convenient to group the extra resulting term $-\frac{1}{2}m_i\omega\omega_{c_i}\rho_i^2$ along with the potential term $V_T(\rho_i, z_i)$ in Eq. (3.3) so that the entire analysis following Eq. (3.3) goes through presicely as before. The final result is that the marginal configurational distribution is that of N interactering particles at temperature τ in an effective potential

$$\begin{aligned} V^{(\text{eff})}(\rho, z) &= V_T(\rho, z) - \frac{1}{2}m\omega\omega_c\rho^2 + \frac{1}{2}m\omega^2\rho^2 \\ &= V_T(\rho, z) - \frac{1}{2}m\omega(\omega + \omega_c)\rho^2. \end{aligned} \tag{3.7}$$

That is, the marginal distribution of the configuration coordinates is

$$P(\vec{r}_1 \cdots \vec{r}_N) \propto \exp\left[-\frac{1}{\tau}\left\{\sum_{i=1}^{N} V^{(\text{eff})}(\rho_i, z_i) + \sum_{i>j}^{N} V(\vec{r}_i, \vec{r}_j)\right\}\right]. \tag{3.8}$$

The conditional distribution of the momentum coordinates remains the same and is given by Eq. (3.5) as before.

3.2 The Effective Potential

Given the equilibrium parameters τ and ω of the cloud, the effective potential of Eq. (3.7) completely determines equlibrium properties of the cloud such as shape and density.

3.2.1 $w_c = 0$

With $w_c = 0$ in Eq. (3.7), the ω dependent extra piece

$$-\frac{1}{2}m\omega^2\rho^2,$$

in the effective potential is quite intuitive since it is just the repulsive centrifugal potential that causes the cloud to bulge at the equator due to the fact that the cloud is characterized by a "rotation frequency" ω. This bulge increases as $|\omega|$ increases. Indeed, in the absence of a $\vec{B}$ field, it is necessary that the confinement due to the trap potential be stronger than the unconfining effect of the centrifugal potential for there to be equilibrium at all. Otherwise the particles would all eventually escape.

3.2.2 $w_c \neq 0$

When $w_c \neq 0$ in Eq. (3.7), we find that it *is* possible to have the overall effective potential be confining even when the bare electrostatic trap potential is not. For example, let us pick an electrostatic potential which is unconfining in the transverse direction, such as

$$V_T(x, y, z) = \frac{m\omega_t^2}{2}(-x^2 - y^2 + 2z^2). \tag{3.9}$$

Even in such a trap potential, a uniform B field along $\hat{z}$ will suffice to completely confine coulomb interacting particles provided that

$$\frac{\omega_c}{2} > \omega_t, \tag{3.10}$$

since there is always *some* value of the rotation frequency ω for which the effective potential $V^{(\text{eff})}(\rho, z)$ in Eq. (3.7) is confining (provided that (3.10) holds).

3.2.3 Rotating frame

Consider the lab frame in which there is the magnetic field. Appendix B.1 shows that by transforming to a frame rotating at frequency $-w_c/2$ w.r.t this frame, one can completely rid oneself of the magnetic field and have it be replaced by a confining potential

$$\frac{1}{2}m\left(\frac{w_c}{2}\right)^2\rho^2,$$

which is to be added onto the trap potential already present. This then immediately makes clear why Eq. (3.10) is the appropriate condition for confinement.

Thinking in terms of the rotating frame is often a quick way to deduce the answer for many situations since the dynamics in this frame lacks the complication of a B field. However, a few caveats are in order.

a) Obviously the trick is only applicable if the B field is uniform and the trap potential in the lab frame is cyclindrically symmetric.

b) Even if the conditions in a) hold it is necessary that there be only one type of charge. This is because the direction of rotation of the rotating frame depends on the sign of the charge.

c) Finally it is important that we do not attempt to visualize even the tiniest dissipative force acting on the particles in the lab frame, because such forces transform somewhat unintuitively into the rotating frame causing qualititive effects very different from those one would typically expect of a dissipative force.

3.3 The "Rotation Frequency" ω

A glance at Eqs. (3.7,3.8,3.5) shows that the parameter ω affects the equilibrium state in two ways. We noted above that ω determines the effective potential and hence the equilibrium shape and density of the cloud. Of equal importance is the appearance of ω in the conditional distribution for the momenta. For a given configuration the momentum of each particle is assigned independently by drawing its velocity components v_ρ, v_t and v_z from independent gaussians of width$=\sqrt{\text{variance}}=\sqrt{\tau/m}$. The gaussian distributions for v_ρ and v_z are centered around 0, but the gaussian from which we draw the tangential component v_t is centered around $m\omega\rho$ where ρ is the cylindrical distance of the particle from the trap axis. Thus the momentum of each particle is correlated with its position in this simple way. It is important to realize that this correlation persists at all times during the equilibrium dynamics of the system. This is simply the mathematical truth that the distribution of Eq. (3.2) is rigorously stationary under time evolution of the sytem. Even at the risk of belabouring this point we will spell it out concretely. Suppose we pick an initial condition of the system, say Γ_0, by drawing from the distribution of Eq. (3.8). Now imagine following the dynamics of this state for any arbitrary time t to obtain the time evolved state $\Gamma_0(t)$. The claim is that $\Gamma_0(t)$ is drawn exactly from the same distribution as Γ_0 is. That is, if someone were to repeat this experiment many times over for independent choices of Γ_0 (drawn from (3.8)), and were to hand us the time evolved states $\Gamma_0(t)$, it would be impossible for us to statistically distinguish these from the states Γ_0 themselves. There would be no way to tell whether we were being handed the states Γ_0 or the states $\Gamma_0(t)$.

3.3.1 ω and Rigid Body Motion

From Eq. (3.5) it is clear that in equilibrium, the expected value of the velocity of each particle is precisely that which it would have if part of a rigid body spinning at the frequency ω. In spite of this fact, the actual dynamics of the system may in general be nothing like that of a rigid body motion. To resolve the apparently contradictory nature of these last two statements let us consider an example. To illustrate the point we will take $\vec{B} = 0$, even though the case with a magnetic field is qualitatively different. So take $\vec{B} = 0$ and a spherically symmetric trapping potential given by

$$\phi_T(r) = \frac{1}{2} m w_T r^2.$$

For a particular choice for the values of the parameters ω_T and the temperature τ, the equilibrium density of the coulomb interacting particles can be made to be so dilute that the particles interact very weakly with each other and collisions are rare. It is clear then that each particle will move in an independent trajectory of an elliptical shape, and at a frequency ω_T. Notice that the trajectory is not circular as in a rigid body and its frequency of motion has absolutely nothing to do with the parameter ω. It is only the collection of particles as a whole which shows a tendency to be rotating around more in one direrction than in the other and ω is a measure of the degree to which this bias exists.

Notwithstanding the fact that ω is not neccessarily related to a rigid body spin of the system with that frequency, it is satisfying to find that it is possible to find an interpretation of ω which does capture this intuitive feeling.

3.3.2 ω and Mechanical Angular Momentum

3.3.2.1 $\rho - p_t$ Correlation

We begin by computing the correlation between p_{t_i} and ρ_i for any one particle. It is useful to make the change of variables

$$\begin{aligned} \bar{p}_{t_i} &= p_{t_i} - m\omega\rho_i \\ \rho_i &= \rho_i \end{aligned}$$

with Jacobian equal to 1. $\bar{p}_{t_i}$ is the residual tangential component of thermal momentum of a particle after having subtracted away its rotatory component from p_{t_i} and is easily seen to be a random variable distributed independently from all the other degrees of freedom. Then the covariance

$$\begin{aligned} \mathrm{cov}(p_{t_i}, \rho_i) &= \mathrm{cov}(m\omega\rho_i + \bar{p}_{t_i}, \rho_i) \\ &= \mathrm{cov}(m\omega\rho_i, \rho_i) + \mathrm{cov}(\bar{p}_{t_i}, \rho_i) \\ &= m\omega\sigma^2_{\rho_i} \qquad\quad + 0, \end{aligned}$$

so that

$$\omega = \frac{1}{m}\frac{\mathrm{cov}(p_{t_i}, \rho_i)}{\mathrm{cov}(\rho_i, \rho_i)} = \frac{1}{m}\frac{\mathrm{cov}(p_{t_i}, \rho_i)}{\sigma^2_{\rho_i}}. \tag{3.11}$$

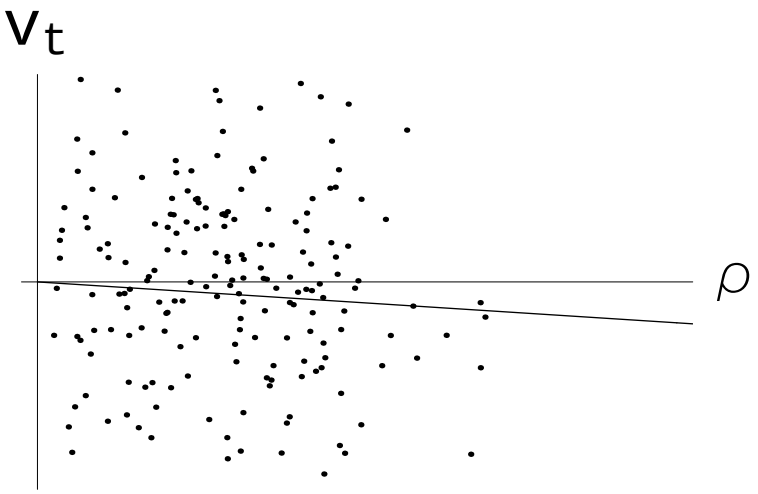

Figure 3.2: Scatter plot resulting from an equilibrium state of noninteracting particles. The slope of the line gives a statistical estimate of the parameter ω appearing in Eq. (3.12). Notice that even though ω is -ve there are many particles circulating in the opposite +ve direction.

For completeness we also compute the correlation $r(p_{t_i}, \rho_i)$, but this formula seems less useful. Since

$$\sigma^2_{p_{t_i}} = \sigma^2_{m\omega\rho_i} + \sigma^2_{\bar{p}_{t_i}} = (m\omega\sigma_{\rho_i})^2 + \sigma^2_{\bar{p}_{t_i}},$$

the correlation $r(p_{t_i}, \rho_i) \equiv \mathrm{cov}(p_{t_i}, \rho_i)/(\sigma_{p_{t_i}}\sigma_{\rho_i})$ is

$$r(p_{t_i}, \rho_i) = \frac{\mathrm{sign}(\omega)}{\sqrt{1 + \left(\frac{\sigma_{p_{t_i}}}{m\omega\sigma_{\rho_i}}\right)^2}}.$$

$\sigma^2_{p_{t_i}} = \sqrt{m\tau}$. σ_{ρ_i} depends on the equilibrium distribution resulting from Eq. (3.6).

3.3.2.2 Extracting w

Eq. (3.11) suggests a natural procedure to extract ω given a particular equilibrium state of the system. Plot the v_{t_i} and ρ_i coordinates of each particle in the $\rho - v_t$ plane. See Figure (3.2). This gives us a scatter plot to which we may fit a straight line through the origin. The slope of this line is ω. Applying the standard procedure of finding a least squares fit we find ourselves computing ω as

$$\omega = \frac{\langle v_t \rho \rangle}{\langle \rho\rho \rangle} \quad = \quad \frac{(v_{t_1}, \cdots v_{t_N}) \,.\, (\rho_1, \cdots \rho_N)}{(\rho_1, \cdots \rho_N) \cdot (\rho_1, \cdots \rho_N)}$$

which is nothing but

$$w = \frac{L_z^{(\mathrm{mech})}}{I_z} \tag{3.12}$$

where I_z is the moment of inertia. The derivation of Eq. (3.12) is quite general. It is valid both with or without a B field. The numerator in Eq. (3.12) however, is always the mechanical angular momentum.

To shed some light on Eq. (3.12) imagine a thought experiment in which the cloud is at equilibrium and is moving in some frictionless and massless fluid which is suddenly frozen at some instant. Having frozen into this solid form the whole assembly is now forced to rotate as a rigid body at some frequency. Eq. (3.12) makes the reasonable claim that this frequency is identical to the parameter ω even though the motion of the particle dynamics prior to "solidification" may be nothing like that in a rigid body.

3.3.2.3 Cyclotron and Drift Angular Momentum

We now take a closer look at the mechanical $\hat{z}$ angular momentum possesed by the sytem. A single particle possesses a certain mechanical $\hat{z}$ angular momentum around the trap axis as it moves under the joint influence of the electric fields due to the trap and the other particles. (It also feels the uniform B field). To the extent that the influence of all the other particles can be accounted for by a mean electric field, the mechanical angular momentum of a single particle can be thought of as arising due to two different contributions: 1) due to its cyclotron motion, and 2) due to its drift motion. See Fig. (3.3). This is analogous to the usual spin plus orbital contributions of electronic angular momentum in an atom except that our decomposition depends crucially on the validity of describing each and every particle's motion within the guiding center approximation.

To illustrate this decomposition, we will pick the case of a particle moving in a harmonic trap in the presence of a uniform B field, for which the equations of motion are linear and exactly soluble in terms of sines and cosines. The resulting motion, is a sum of two rotating vectors, one rotating slowly

$$\vec{R}(t) = \rho_s \left(\cos(\omega_s t), -\sin(\omega_s t)\right), \tag{3.13}$$

and one rotating fast

$$\vec{r}(t) = \rho_f \left(\cos(\omega_f t), -\sin(\omega_f t)\right). \tag{3.14}$$

See Figure (3.3). For a strong magnetic field, typically $\omega_s \ll \omega_f$ and $\rho_s \gg \rho_f$. Fig. (3.3) shows the path traced out in the $x-y$ plane for such conditions for a positive charge. ω_f is very nearly, but not quite, equal to the cyclotron frequency which is a positive number for a positive charge. w_s can be of either sign depending on the electric field which determines the drift velocity via

$$\vec{v}_{\mathrm{drift}} = c\frac{\vec{E}\times\vec{B}}{B^2}.$$

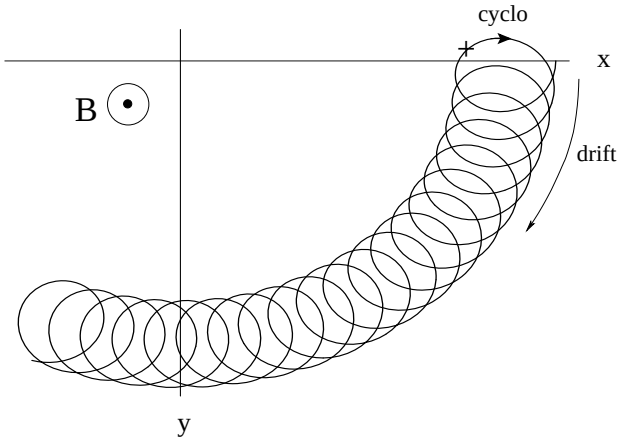

Figure 3.3: Angular momentum of a + charge moving in a strong magnetic field (and electric field) may be decomposed as the sum of the cyclotron angular momentum ("spin") and the drift angular momentum ("orbit").

If we now average the mechanical angular momentum of the motion

$$\vec{R}(t) + \vec{r}(t),$$

over a period

$$\frac{2\pi}{\omega_f + \omega_s} \sim \frac{2\pi}{\omega_f} \tag{3.15}$$

and denote this average as $\langle l_z^{(\mathrm{mech})} \rangle$ we have the exact result

$$\langle l_z^{(\mathrm{mech})} \rangle = -m\rho_f^2\omega_f + m\rho_s^2\omega_s, \tag{3.16}$$

for a single particle. Provided one is able to approximate the motion of each particle as a sum of the motions of Eqs. (3.13) and (3.14), then summing over the separate contributions of each particle to the terms in Eq. (3.16) , yields the decomposition

$$L_z^{(\mathrm{mech})} = L_z^{(\mathrm{cyclo})} + L_z^{(\mathrm{drift})}. \tag{3.17}$$

It is worth pointing out that in the actual experiment the averaging over the small period in Eq. (3.15) is automatically done for us, so to speak, by quantum mechanics. The actual experimental temperature is cold enough so that almost all the particles are in the first quantum mechanical ground state and so equally spread out over their cyclotron orbits making them more like a spinning ring.

3.4 Thermodynamically Unstable Equilibrium

The electrostatic potential typically generated by the trap electrodes is designed to confine the cloud in the axial direction. This potential being a solution to Laplaces equation is then necessarily unconfining in all transverse directions, such as for example the potential of Eq. (3.9). Nevertheless, we found above that a magnetic field would suffice to indefinitely confine the particles and bring them to thermal equilibrium. A careful look at the arguments concluding this will reveal the essential role played by the conservation of $\hat{z}$ angular momentum in reaching this conclusion. One might say that it is the strict conservation of angular momentum that makes the confinement and thermal equilibrium possible.

We will now show that this equilibrium is unstable in the sense that the slightest breaking of the cylindrical symmetry (with the concomitant *non*-conservation of angular momentum) will cause the particles to eventually make their way down the transverse repulsive hill of the trapping potential and escape to infinity. This could in principle be caused by

1) small cylindrically *a*symmetric fluctuations in the trap potential, or by

2) putting the whole assembly in a rectanguar box small enough that there are occassional collisions of the particles with the wall, or by

3) radiation friction that causes angular momentum to be no longer strictly conserved.

The last of these, most pertaining to the experiment, seems at first quite reasonable from a dynamical point of view. If there is radiation, then the energy radiated away can only make the particle roll downhill. However, this is not the whole story, since electromagnetic energy is also continully absorbed due to an ambient radiation bath. It is a thermodynamic agrument that makes clear how and why the equilibrium is unstable.

3.4.1 Minimizing the Free Energy

If L_z is really only a quasi-conserved quantity, then the equilibrium we have been speaking of thus far is really only a quasi-equilibrium. The role of L_z is now shifted to that of a freed internal thermodynamical constraint and the question that immediately arises is "What value of L_z does the system spontaneously desire to move towards?" Thermodynamically, this is answered by finding that value of L_z which minimizes the free energy A . Equivalently, we will maximize

$$-\beta A = \sigma(E, L_z) - \beta E. \tag{3.18}$$

$\sigma(E, L_z)$ in the equation above is identical the $\sigma^*_{(E,L_z)}$ we introduced in Chapter (**??**) so that we may apply all our results from there. Now let $\delta E, \delta L_z$ be a small variation in the equilibrium state of the system at constant temperature. The resulting variation in the quantity in $-\beta A$ of Eq. (3.18) is

$$\frac{\partial \sigma(E, L_z)}{\partial E}\delta E + \frac{\partial \sigma(E, L_z)}{\partial L_z}\delta L_z - \beta \delta E$$

$$= \frac{\partial \sigma(E, L_z)}{\partial L_z} \delta L_z,$$

because the first and third terms cancel. β is fixed. For this to be a stationary point (a maximum), then we must have

$$\frac{\partial}{\partial L_z}\Big)_E \sigma(E, L_z) = \frac{-\omega}{\tau} = 0 \tag{3.19}$$

or

$$\omega = 0.$$

Eq. (3.19) may also be arrived at more directly. If L_z desires to change - when freed from its constraint - it will do so whether the system is in contact with a bath or is kept isolated. But in an isolated system it is the entropy that is maximized for a fixed energy. Eq. (3.19) merely expresses this fact.

3.4.2 Analogy

Fig. (3.4) shows the (p, τ) parameter space for a gas at temperature τ in analogy with the (ω, τ) parameter space for the confined plasma. Shown alongside are the respective so-called "extensive" parameters of each system. By keeping the clamp locked in place and constraining the piston, we may constrain the volume

$$V_g = \text{area } h$$

of the gas to have any arbitrarily fixed value of our choosing. Obviously with the clamp in place the mass m is of no consequence and plays no role. The pressure p is automatically determined as the gas equilibrates at this fixed volume V_g. For the confined plasma, the analog of having the clamp in place is that we do not allow any radiation or asymmetry in the confining potential thereby keeping any arbitrary initial value of L_z fixed. The rotation frequency ω is automatically determined as the cloud equilibrates at this fixed value of L_z. Allowing radiation or any asymmetry would be like removing the clamp and allowing the volume V_g of the gas to spontaneously change. "What value of V_g does the gas spontaneously desire to move towards?" In exact analogy with Eq. (3.18) this is answered by maximizing

$$\sigma(E_g, V_g) - \beta(E_g + m\, g\, h), \tag{3.20}$$

w.r.t. V_g. Eq. (3.20) is nothing but $-\beta$ times the free energy of the gas+weight system except that since the weight is treated as a single degree of freedom of the system, its energy $m\, g\, h$ contributes negligibly to the system's gas+weight entropy.

Now let δE_g and δV_g be a variation in the equilibrium state of the system at constant temperature. The variation of Eq. (3.20) is

$$\frac{\partial \sigma(E_g, V_g)}{\partial E_g} \delta E_g + \frac{\partial \sigma(E_g, V_g)}{\partial V_g} \delta V_g - \beta \delta E_g - \beta m g \frac{\delta V_g}{\text{area}}$$

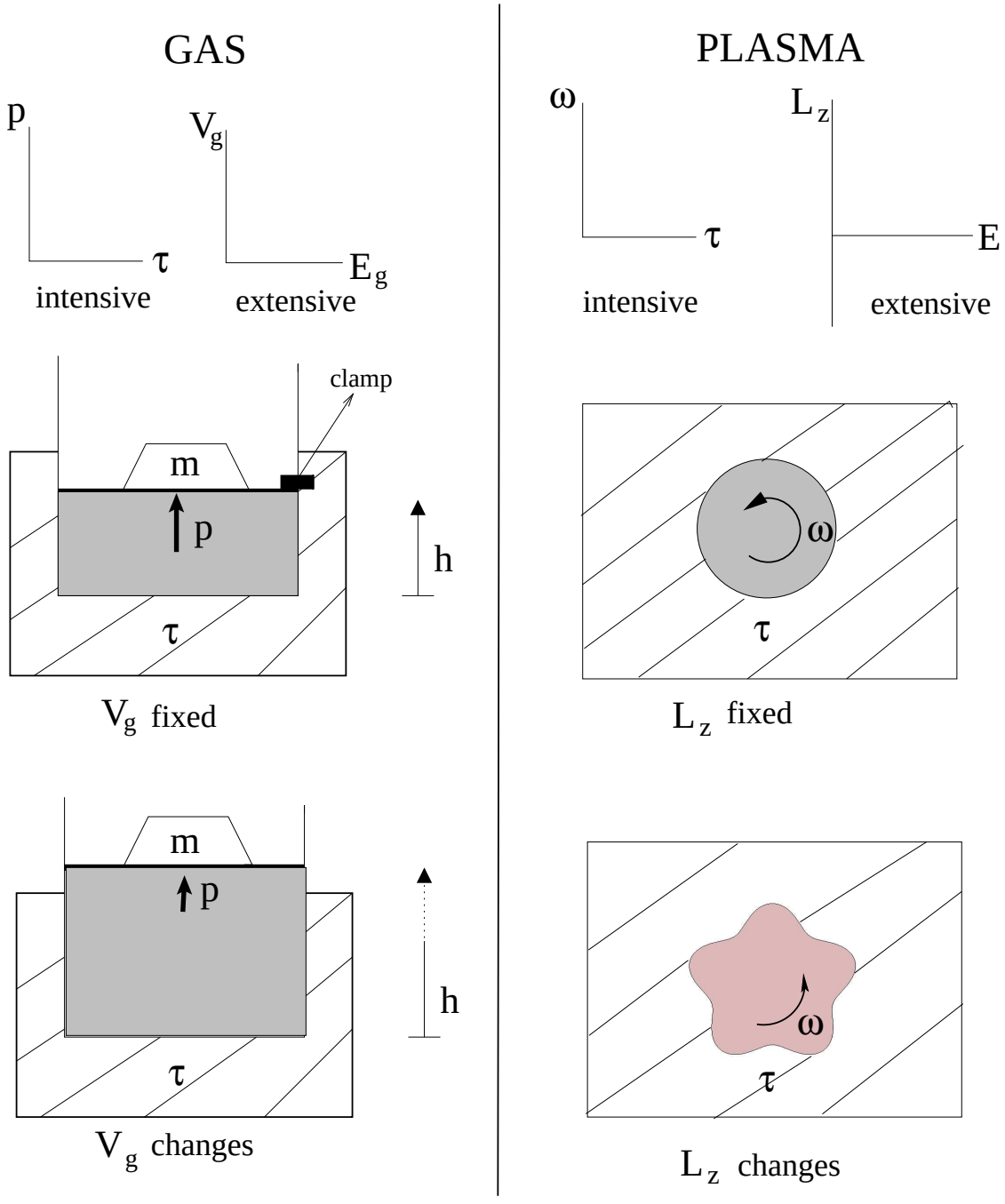

Figure 3.4: L_z being strictly conserved in the plasma cloud is analogous to V_g, the volume of a gas, being constrained to a fixed value. Analogous to the intensive variable ω of the plasma is the pressure p of the gas.

$$= \frac{\partial \sigma(E_g, V_g)}{\partial V_g}\delta V_g - \beta mg\frac{\delta V_g}{\text{area}}$$

$$= \frac{p}{\tau}\delta V_g - \beta mg\frac{\delta V_g}{\text{area}}$$

where we used the familiar result that $\frac{p}{\tau} = \frac{\partial \sigma(E_g, V_g)}{\partial V_g}$ for a gas. This is zero when

$$p = \frac{mg}{\text{area}}. \tag{3.21}$$

Eq. (3.21) is exactly analogous to Eq. (3.19) except that Eq. (3.19) has no analogous term on its r.h.s. This is because while the gas has a weight that imposes a value of the pressure p on it, there is no agency in our setup that plays the role of an angular momentum bath that imposes a value of the rotation frequency ω on the cloud. This is not to say that there could not be such an agency. But as it stands, the cloud if left to itself will gradually move towards the equilibrium state with rotation frequency $\omega = 0$, in order to minimize its free energy. This is what Eq. (3.19) predicts.

However, it is easy to show (Section 3.4.3) that it is impossible to support an equilibrium with rotation frequency $\omega = 0$ if the trapping potential is unconfining in the transverse direction. See Fig. (3.5). Thus equilibrium in the unconfining trap potential of the experiment is necessarily unstable.

3.4.3 Restricted Range of ω

The thick arrows in Fig. (3.5) show the range of possible values that the rotation frequency ω can have in an equilibrium state for which L_z is strictly conserved. The figure plots

$$-\frac{1}{2}m\omega(\omega + \omega_c),$$

vs. ω. This is the strength of the centrifugal term in the effective potential that depends on w. In the figure we have chosen $w_c > 0$, as for positively charged particles. The range of ω is determined simply by the criterion that the overall effective potential be confining. As one may expect, this range of ω increases as the trapping potential provides a stronger and stronger confinement. Notice that the strength of the piece $(1/2)mw(w + w_c)\rho^2$, and hence the overall transverse strength of $V_\omega^{(\text{eff})}$, is symmetric not around $\omega = 0$ but rather around $-\omega_c/2$. It is strongest at $-\omega_c/2$. The physical consequence of this is reflected in the Figure by schematically showing the equilibrium cloud shapes corresponding to three different values of ω arranged symmetrically around $-\omega_c/2$, for the case when the bare trap potential is transversely unconfining.

In Section 3.4.1 we showed how relaxing the constraint of conserving L_z makes the value of w want to relax towards 0. For positively charged particles ($\omega_c > 0$) this approach takes place from the negative side without ever quite being able to reach 0. For the transversely unconfining trap potential, the free energy can indefinitely decrease, as $L_z(\text{mechanical} + \text{field}) \to \infty$, and is never able to realize a minimium.

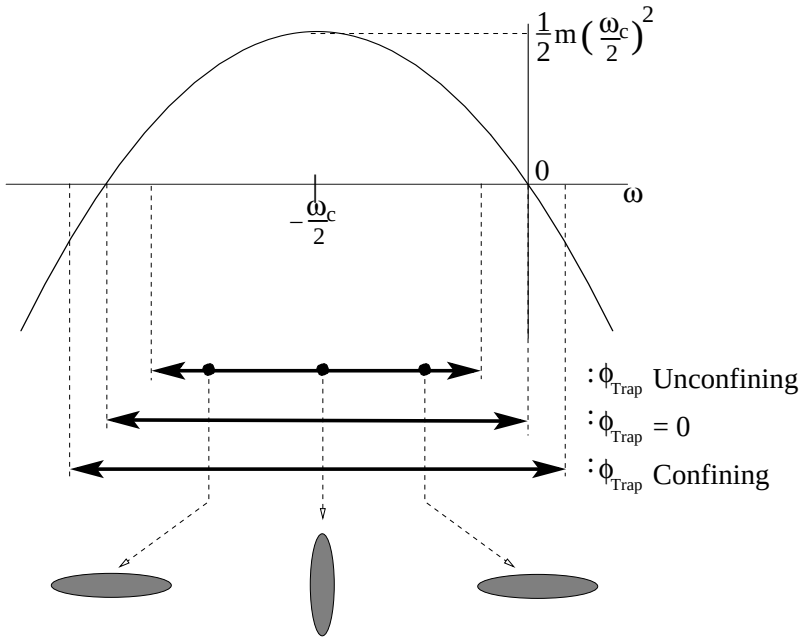

Figure 3.5: Plot of the strength of the centrifugal term in the effective potential vs. ω.

3.4.4 Dynamical Argument

We have seen that if the trapping potential is unconfining, then equilibrium with $\omega = 0$ is impossible. The equilibrium distribution of Eq. (3.8) along with the form of $V_\omega^{(\text{eff})}$ made that clear.

It is illuminating to also argue from purely dynamical considerations why equilibrium with a rotation frequency of $\omega = 0$ is impossible in a trap potential that is transversely unconfining. From Section 3.3.2.2 recall that

$$\omega = \frac{L_z^{(\text{mech})}}{I_z}.$$

Therefore, $\omega = 0$ implies that

$$L_z^{(\text{mech})} = 0.$$

But since $L_z^{(\text{mech})} = L_z^{(\text{cyclo})} + L_z^{(\text{drift})}$ we must have

$$L_z^{(\text{cyclo})} + L_z^{(\text{drift})} = 0. \tag{3.22}$$

The cyclotron contribution

$$L_z^{(\text{cyclo})} = -\sum_{i=1}^{N} m\rho_{c_i}^2 \omega_c$$

is manifestly negative since $\omega_c \equiv (eB/mc)$ is positive number for a positively charged particles. It is just the sum of the angular momentum contributions of each particle due to its clockwise cyclotron motion. Therefore by Eq. (3.22) $L_z^{(\text{drift})}$ must be sufficiently positive to exactly cancel this negative contribution. A simple consideration using

$$\vec{v}_{\text{drift}} = c\frac{\vec{E} \times \vec{B}}{B^2}$$

then shows that the mean electric field felt by a particle must point inwards if its drift angular momentum is to be positive. But this is only posible if the trap potential is confining. (The field of the space charge itself points outward and can be of no help.) Thus it is impossible for the total mechanical angular momentum to be 0 in equilibrium, when the trap is transversley unconfining.

3.5 Bohr Van-Leeuven Theorem

One may view the clockwise cyclotron motion of an individual charged particle as its diamagnetic response to the applied B field. The fact that the drift angular momentum must cancel the cyclotron angular momentum in stable thermal

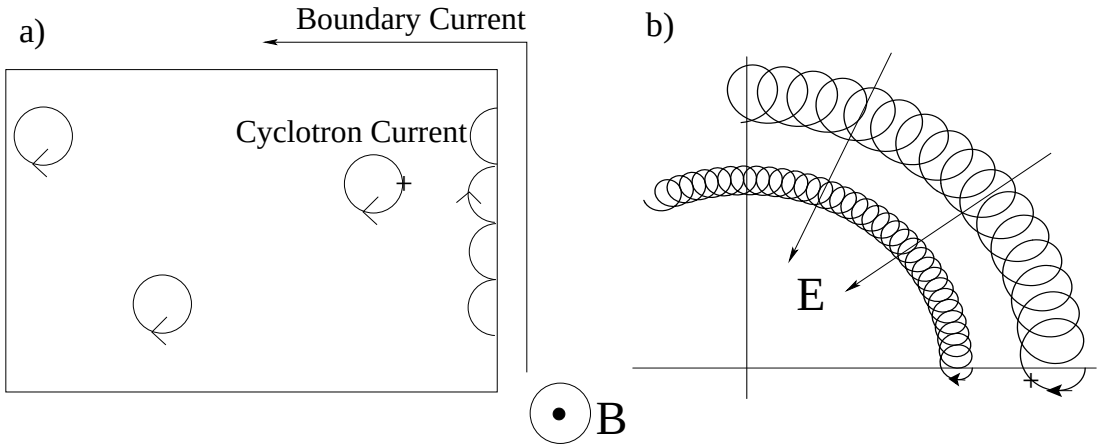

Figure 3.6: a) shows particles in a box. b) shows particles in a smooth confining potential. In both cases there is a uniform B field pointing out of the board.

equilbrium may then be viewed as the statement that the overall diamagnetic response of the plasma cloud must be 0.

This is very reminiscent of the Bohr Van-Leeuven theorem which states that diamagnetism in a classical system is impossible. By considering charged particles in a magnetic field confined to a rectangular box, Bohr pointed out the crucial role of the boundary walls. Particles bouncing off the wall in "edge states" (see Fig. (3.6 a)) set up a current circulating in a direction opposite to that of the current loops due to unobstructed cyclotron motion. Bohr argued that the magnetic moments due to these two current sources would have to cancel exactly in thermal equilibrium making the total induced magnetic moment 0. Fig. (3.6 b) shows the plasma system. Here in effect we have every particle participating in an edge-like state due to its drift motion resulting from the smoother confinement. Notice that this is dynamically possible only if the overall electric field is transversely confining as in the figure.

Finally we point out that the (quasi-)equilibrium states realized explicitly in the unconfining transverse potential of the experiment, provide a *counterexample* to the Bohr-Van Leeuven theorem, because of the extra (quasi-)conserved quantity L_z which obviously they did not consider. These equilibrium states do indeed endow the cloud with an overall magnetic moment since $L_z^{(\text{cyclo})}$ and $L_z^{(\text{drift})}$ are of the same sign.

Chapter 4

Metropolis Algorithm

Given any N-body probability distribution

$$P(\vec{r}_1 \cdots \vec{p}_N) \propto f(\vec{r}_1 \cdots \vec{p}_N) \tag{4.1}$$

the Metropolis algorithm allows us to draw a state $\Gamma = (\vec{r}_1 \cdots \vec{p}_N)$ from this distribution. It is not necessary to know the exact $P(\Gamma)$, but only to be able to evaluate the relative densities $f(\Gamma)$ in Eq.(4.1) for any arbitrary function f. The idea is to construct a particular Markov Green's function $G(\Gamma, \Gamma')$ with the properties described below.

4.1 Markov Process

A Markov Green's function is defined as follows: if the system is certainly in state Γ' then the probability $P([\Gamma, \Gamma + d\Gamma] \leftarrow \Gamma')$ of making a transition to a state in a region $d\Gamma$ around Γ is

$$P([\Gamma, \Gamma + d\Gamma] \leftarrow \Gamma') = d\Gamma G(\Gamma, \Gamma').$$

Thus, state Γ_{n+1} is obtained from Γ_n by drawing a random Γ from the distribution $G(\Gamma, \Gamma_n)$. Clearly

$$G(\Gamma, \Gamma') > 0, \tag{4.2}$$

and

$$\int d\Gamma G(\Gamma, \Gamma') = 1. \tag{4.3}$$

That is, G is positive and each column is sum-normalized, i.e. sums to 1. Now an ensemble of systems distributed as $\rho_n(\Gamma)$ becomes distributed as

$$\rho_{n+1}(\Gamma) = \int d\Gamma' G(\Gamma, \Gamma') \rho_n(\Gamma') \tag{4.4}$$

after one Markov step in which each system of the ensemble has undergone one transition. While the distribution of the ensemble as a whole changes in the

well determined manner of Eq.(4.4), the trajectory $\Gamma_0, \Gamma_1, \cdots \Gamma_n$ of a particular ensemble member is stochastic. Γ_n is obviously distributed as $\rho_n(\Gamma)$. The goal is to construct $G(\Gamma, \Gamma')$ such that for any arbitrary initial $\rho_0(\Gamma)$,

$$\rho_{n\to\infty}(\Gamma) = P(\Gamma),$$

where $P(\Gamma)$ is the desired distribution of Eq. (4.1). In particular, this implies that $P(\Gamma)$ is a stationary distribution of this Markov process. That is,

$$P(\Gamma) = \int d\Gamma' G(\Gamma, \Gamma') P(\Gamma'). \tag{4.5}$$

A sufficient condition for Eq.(4.5) to hold is

$$G(\Gamma_1, \Gamma_2) P(\Gamma_2) = G(\Gamma_2, \Gamma_1) P(\Gamma_1). \tag{4.6}$$

Algebraically, this is seen by integrating both sides of Eq. (4.6) $\int d\Gamma_1$whereby we immediately obtain Eq. (4.5) using Eq. (4.3). Rewriting Eq. (4.6) as

$$d\Gamma_1 G(\Gamma_1, \Gamma_2) \left[P(\Gamma_2) d\Gamma_2 N_{ens}\right] = d\Gamma_2 G(\Gamma_2, \Gamma_1) \left[P(\Gamma_1) d\Gamma_1 N_{ens}\right] \tag{4.7}$$

gives it a simple physical interpretation. Start with a large number N_{ens} of ensemble members distributed according to the initial distribution $P(\Gamma)$, and then allow each member of the ensenble to undergo one transition according to the Markov Greens function $G(\Gamma, \Gamma')$. Eq. (4.7) says that the number of ensemble members making a transition from the region $d\Gamma_2$ to $d\Gamma_1$ (l.h.s.) is equal, on average, to the number of members making a transition from $d\Gamma_1$ to $d\Gamma_2$.(r.h.s.) That is, *every* two regions of phase space have the fluxes between them being in a "detailed balance". It is then evident, without any algebra, that the condition of Eq. (4.7) will make the total flux in or out of any phase space region be equal to 0 for an initial distribution $P(\Gamma)$.

We note in passing that Eq. (4.6) is sufficient for making Eq. (4.5) be true but is certainly not necessary. For example, let $P(\Gamma)$ be any distribution depending only on $E(\Gamma)$, and let $G(\Gamma, \Gamma')$ be the time evolution map for the system for any finite fixed time. Then, since time evolution a) preserves the 6N dimensional volume element $d\Gamma$, and b) maps a state to another state having the same E, it follows that the time evolved distribution is identical in form to the initial distribution $P(\Gamma)$. Yet, obviously there is no reason for Eq. (4.6) to hold.

In what follows we will restrict ourselves to requiring "detailed balance".

4.2 Constructing $G(\Gamma, \Gamma')$

We desire a Greens function under which it is easy to map forward a single trajectory. Choosing

$$G(\Gamma, \Gamma') = P(\Gamma)$$

independently of Γ' would certainly satisfy all our requirements except that in attempting to step forward a given trajectory we would find ourselves back to square one since $P(\Gamma)$ is itself the "difficult" distribution which we are trying to simulate. Instead, we begin by choosing a trial Greens function $TG(\Gamma, \Gamma')$ satisfying Eqs. (4.2) and (4.3), with which it is easy to iterate a trajectory forward. To construct our desired $G(\Gamma, \Gamma')$ we modulate this trial Greens function by a factor $A(\Gamma, \Gamma')$ where

$$0 < A(\Gamma, \Gamma') < 1. \tag{4.8}$$

Then,

$$G(\Gamma, \Gamma') = \begin{cases} A(\Gamma, \Gamma') \times TG(\Gamma, \Gamma') & \Gamma \neq \Gamma' \\ r(\Gamma')\delta(\Gamma - \Gamma') & \Gamma = \Gamma' \end{cases} \tag{4.9}$$

where

$$r(\Gamma') \equiv 1 - \int d\Gamma A(\Gamma, \Gamma') TG(\Gamma, \Gamma'), \tag{4.10}$$

a positive number satisfying

$$0 < r(\Gamma') < 1,$$

is the required strength of the delta function in Eq. (4.9) so that $G(\Gamma, \Gamma')$ be properly normalized. Eq. (4.9) is simply

$$G(\Gamma, \Gamma') = r(\Gamma')\delta(\Gamma - \Gamma') + A(\Gamma, \Gamma')TG(\Gamma, \Gamma'). \tag{4.11}$$

In Sec. (4.3) we will show how to choose $A(\Gamma, \Gamma')$ so that the detailed balance condition of Eq. (4.6) is satisfied. The whole point now is that it is still easy to map forward a trajectory with this $G(\Gamma, \Gamma')$ thus constructed. To do so we simply accept a Γ drawn from $TG(\Gamma, \Gamma')$ with probability $A(\Gamma, \Gamma')$, and reject it otherwise. Thus, $A(\Gamma, \Gamma')$ is just an acceptance probability. Or to rephrase: the product $A(\Gamma, \Gamma') \times TG(\Gamma, \Gamma')$ in Eq. (4.9) or (4.11) is not a product of two distributions of Γ (for fixed Γ'). Rather, $TG(\Gamma, \Gamma')$ is a distribution and $A(\Gamma, \Gamma')$ is just a pure probability between 0 and 1. The delta function in equations (4.9) and (4.11) keeps $G(\Gamma, \Gamma')$ normalized and is of course essential in mapping forward a distribution using Eq. (4.4). However, it need not concern us in mapping forward a single trajectory. It is automatically implemented at every step by the very possibility of there being a rejection with probability $r(\Gamma')$, so that a trajectory will certainly possess contiguous, identical repeated states in the sequence $\Gamma_0, \Gamma_1, \cdots \Gamma_n$. Curiously, it is just this possibility that is essential to making $\Gamma_{n\to\infty}$ have the desired distribution. In the words of C.H. Bennett, "The road to success is through failure."

4.3 Choosing $A(\Gamma, \Gamma')$

It remains to show how to choose $A(\Gamma, \Gamma')$ such that the detailed balance condition in Eq. (4.6) is satisfied. Substituting Eq. (4.11) in Eq. (4.6) it follows

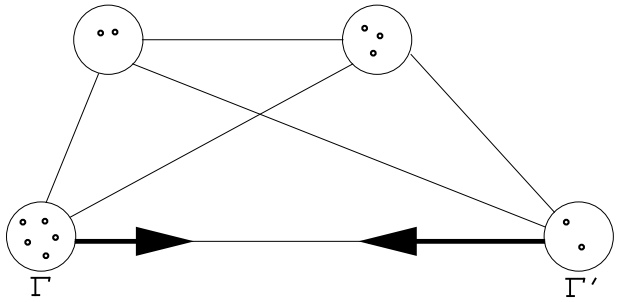

Figure 4.1: Each circle represents a region of phase space containing a number of ensemble numbers represented by the dots.

that for any pair Γ_1, Γ_2 not identically equal we must have

$$\frac{A(\Gamma_1, \Gamma_2)}{A(\Gamma_2, \Gamma_1)} = \frac{TG(\Gamma_2, \Gamma_1)P(\Gamma_1)}{TG(\Gamma_1, \Gamma_2)P(\Gamma_2)}.$$

Since the target $P(\Gamma)$ is known and $TG(\Gamma, \Gamma')$ is chosen by us, $A(\Gamma, \Gamma')$ is easily solved for in terms of these two known quantites as

$$\begin{array}{rcl} A(\Gamma_1, \Gamma_2) & = & c(\Gamma_1, \Gamma_2) \times \frac{TG(\Gamma_2, \Gamma_1)P(\Gamma_1)}{TG(\Gamma_2, \Gamma_1)P(\Gamma_1) + TG(\Gamma_1, \Gamma_2)P(\Gamma_2)} \\ A(\Gamma_2, \Gamma_1) & = & c(\Gamma_1, \Gamma_2) \times 1 \leftrightarrow 2 \end{array} . \tag{4.12}$$

Note that the pair of arguments (Γ_1, Γ_2) appear in the same order in the function c. For every pair (Γ_1, Γ_2), $c(\Gamma_1, \Gamma_2)$ can be set to any arbitrary positive number so long as both quantities above are < 1 in order that Eq. (4.8) holds. Now it is clearly of advantage to make the chance of a rejection as low as possible and hence to make $A(\Gamma, \Gamma')$ to be as large as possible. Therefore, $c(\Gamma_1, \Gamma_2)$ is chosen so as to make the larger of the two quantities in Eq. (4.12) be equal to 1. Having thus chosen $c(\Gamma, \Gamma')$ for each pair (Γ, Γ'), the resulting solution in Eq. (4.12) may be concisely, but somewhat obscurely, written as

$$A(\Gamma, \Gamma') = \min\left(1, \frac{TG(\Gamma', \Gamma)P(\Gamma)}{TG(\Gamma, \Gamma')P(\Gamma')}\right). \tag{4.13}$$

4.4 Analogy

It is helpful to now summarize the entire algorithm described above with the aid of a metaphor using the graph in figure (4.1). Figure (4.1) shows four countries (vertices) each with a given population (dots). Each year every citizen of a given country immigrates to another with probability

$$TG(\Gamma = \text{new country}, \Gamma' = \text{old country}).$$

$TG(\Gamma,\Gamma')$ may be thought of as a popularity measure for the country Γ as perceived by citizens of Γ'. (The probability to stay behind may be finite even though in the case of a continuous Γ this usually is most naturally 0 as $d\Gamma \to 0$ around Γ, even though it need not be if $TG(\Gamma,\Gamma')$ itself has a delta function *before* being modulated by $A(\Gamma,\Gamma')$.)

Now the total number of immigrants $\Gamma \to \Gamma'$ (from Γ to Γ') is the popularity of Γ' viewed from Γ, multiplied by the population $P(\Gamma)$ of Γ itself. The ratio

$$\frac{\text{people flow } \Gamma \to \Gamma'}{\text{people flow } \Gamma \leftarrow \Gamma'} = \frac{TG(\Gamma',\Gamma)P(\Gamma)}{TG(\Gamma,\Gamma')P(\Gamma')},$$

will in general not be equal to one. Suppose for example it is (5/4) as depicted in figure (4.1). This means that an unrestricted interaction between countries Γ and Γ' will tend to increase the population of Γ' and decrease the population of Γ. But this imbalance of flow is easily corrected by rejecting (4/5)ths of the applicants wanting to immigrate $\Gamma \to \Gamma'$ (i.e. $A(\Gamma \to \Gamma') \equiv A(\Gamma',\Gamma) = 4/5$) while unquestionably accepting *all* applicants wanting to immigrate $\Gamma \leftarrow \Gamma'$ (i.e. $A(\Gamma \leftarrow \Gamma') \equiv A(\Gamma,\Gamma') = 1$). This is the content of Eq. (4.13).

As noted at the end of Sec. (4.1), it is also evident from this analogy that the populations for each country can be balanced on the whole without requiring that there be a "detailed balancing" between every two countries.

4.5 Simulating the $\tau - \mu$ or $\tau - n$ Ensemble

The above discussion allows one to implement a simulation of any ensemble distribution for which the particle number is fixed. It is no harder to extend the method for the τ (temperature) - μ(chemical potential) ensemble in which the temperature and chemical potential are fixed allowing the energy and particle number to fluctuate. This distribution is written as

$$P(\Gamma_N) \propto \frac{(e^{\mu/\tau})^N}{N!\,(h^3)^N}\, e^{-\beta E(\vec{r}_1 \cdots \vec{p}_N)}.$$

If the energy

$$E(\vec{r}_1 \cdots \vec{p}_N) = \frac{\vec{p}_1{}^2}{2m} + \cdots \frac{\vec{p}_N{}^2}{2m} + V(\vec{r}_1 \cdots \vec{r}_N)$$

separates into a kinetic plus potential piece, then we can trace out the momenta to obtain

$$\begin{aligned} P(q_N) &\propto \frac{1}{N!}\left(\frac{e^{\mu/\tau}}{\lambda^3}\right)^N e^{-\beta V(q_N)} \\ &= \frac{n^N}{N!} e^{-\beta V(q_N)}. \end{aligned} \tag{4.14}$$

$\lambda \equiv \sqrt{h^2/(2\pi m\tau)}$ and $q_N = (\vec{r}_1 \cdots \vec{r}_N)$ is the N-particle configuration state of $3N$ coordinates and $n \equiv 1/(e^{-\mu/\tau}\lambda^3)$ is a parameter with units of a number density.

Tracing out the position coordinates from Eq. (4.14), the τ, n distribution for the particle number for interacting particles is

$$P(N) \propto \frac{n^N Q_N}{N!},$$

where

$$Q_N \equiv \int d^3r_1 \cdots d^3r_N e^{-\beta V(\vec{r}_1, \cdots \vec{r}_N)}, \tag{4.15}$$

is the so-called configurational partition function.

4.5.1 Constructing $G(q_N, q'_{N'})$

We begin by choosing a trial Greens function, defined piece-wise as

$$TG(q_n, q'_{N'}) = \begin{cases} (1/2) \times r_{q'_{N'}}(q_N) & N = N' - 1 \\ (1/2) \times i_{q'_{N'}}(q_N) & N = N' + 1 \\ 0 & \text{otherwise} \end{cases} . \tag{4.16}$$

It is non-zero for $N = N' - 1$ and $N = N' + 1$ and 0 for all other N including $N = N'$. (The boundary case of $N' = 0$ is dealt with separately at the end in Sec. (4.5.4)). Thus every Markov iteration either changes the particle number by at most ± 1, or leaves the entire state unchanged if the trial step is rejected. Given an initial configuration state $q'_{N'}$ the probability density function for removing one particle $r_{q'_{N'}}(q_N)$ is defined on the N-particle spaces only when $N = N' - 1$:

$$r_{q'_{N'}}(q_N) = \frac{1}{N'} \sum_{i=1}^{N'} \underbrace{\delta(\vec{r}_1 - \overrightarrow{ip_1})\delta(\vec{r}_2 - \overrightarrow{ip_2}) \cdots \delta(\vec{r}_N - \overrightarrow{ip_N})}_{\text{N } \delta \text{ functions}} . \tag{4.17}$$

In Eq. (4.17) $\sum_{i=1}^{N'}$ denotes a sum over all the N' possible assignments of $\overrightarrow{ip_1}, \overrightarrow{ip_2}, \cdots \overrightarrow{ip_N}$ by

$$(\overrightarrow{ip_1}, \overrightarrow{ip_2}, \cdots \overrightarrow{ip_N}) = (\vec{r}_1\,', \vec{r}_2\,' \cdots \widehat{\vec{r}_i\,'} \cdots \vec{r}_{N'}\,') \qquad \text{for each } i = 1 \cdots N' \tag{4.18}$$

where the hat on $\widehat{\vec{r}_i\,'}$ means that this term is to be omitted on the right hand side before making the assignment. Prefacing each "$\vec{p}$" with an "i" is just our notation that facilitates an indexing of the particlar assignment in Eq. (4.18) which is being spoken of. For future use we observe here that each term in the sum of Eq. (4.17) is a product of N delta functions. Once again to clarify Eq. (4.17): as we move through the ith product of delta functions, the subscript on $\vec{r}$ goes continuously from $1 \cdots N$ whereas the subscript on $\vec{r}\,'$ goes through $1, 2, \cdots \hat{i}, \cdots N$', skipping the value i. See section 4.5.2 for an example.

Similarly, given $q'_{N'}$ the probability density function for inserting one particle $i_{q'_{N'}}(q_N)$ is defined on the N-particle spaces only when $N = N' + 1$:

$$i_{q'_{N'}}(q_N) \quad = \frac{1}{N}\sum_{i=1}^{N} \underbrace{\delta(\overrightarrow{ip_1} - \vec{r}_1\,')\delta(\overrightarrow{ip_2} - \vec{r}_2\,')\cdots\delta(\overrightarrow{ip_N} - \vec{r}_{N'}\,')}_{\text{N' } \delta \text{ functions}} \cdot I(\vec{r}_i) \quad . \tag{4.19}$$

In equation Eq. (4.19) $\sum_{i=1}^{N}$ denotes a sum over all the N possible assignments of $\overrightarrow{ip_1}, \overrightarrow{ip_2}, \cdots \overrightarrow{ip_N}$ by

$$(\overrightarrow{ip_1}, \overrightarrow{ip_2}, \cdots \widehat{\overrightarrow{ip_i}} \cdots \overrightarrow{ip_N}) = (\vec{r}_1, \vec{r}_2 \cdots \widehat{\vec{r}_i} \cdots \vec{r}_N) \qquad \text{for each } i = 1 \cdots N$$

For future use we observe here that each term in the sum of Eq. (4.19) is a product of N' delta functions. To clarify Eq. (4.19): as we move through the ith product of delta functions, the subscript on $\vec{r}$ goes from $1, 2, \cdots \hat{i}, \cdots N$ skipping the integer i, whereas the subscript on $\vec{r}\,'$ goes continiuously from $1 \cdots N'$. Again, see section 4.5.2 for an example.

$I(\vec{r})$ is a normalized probability distribution from which the coordinates of the inserted particle is drawn. In Eq. (4.19) its argument is the coordinate of the particle with index name i, meaning simply that the particle being inserted is the ith one and all the other existing particles are renamed with the remaining indices $1, 2, \cdots \hat{i}, \cdots N$, where the hat on $\hat{i}$ means that the index i is omitted from the set. Notice how we are forced into explicitly renaming each particle (actually particle position) with a unique particle index every time an insertion or removal of a particle is made. This is necessary in order that the configuration state be uniquely specified, since classically each particle is distinguishable. Also note that we have chosen to do this renaming (where an index is assigned to every position coordinate) not in every one of $N'!$ possible ways (for an insertion) but rather only in a restricted set of N' ways which keep an identical ordering for the position coordinates occurring in the initial state. Any other choice would be valid also so long as $TG(q_{N_1}, q_{N_2}) \neq 0 \Leftrightarrow TG(q_{N_2}, q_{N_1}) \neq 0$ which obviously must be true before detailed balance can be enforced by choosing $A(q_{N_1}, q_{N_2})$ to balance the unbalanced fluxes that TG induces on the equilibrium distribution.

4.5.2 Figure

Figure (4.2A) shows a schematic of $TG(q_N, q_{N'=2})$ with $q_{N'=2} = (1, 3)$. (For simplicity, we replace the three coordinates of $\vec{r}_1\,'$ and $\vec{r}_2\,'$ by one, setting $\vec{r}_1\,' = 1$ and $\vec{r}_2\,' = 3$.) The two points in the $N = 1$ particle space and the three infinitesmally thin but long cuboids (extending from -5 to 5) in the $N = 3$ particle space show the regions to which there is a non-zero probability of making a trial transition. Similarly, Figure (4.2b) shows the schematic of $TG(q_N, q_{N'=3})$ with $q_{N'=3} = (1, 3, -2)$. The three points in the $N = 2$ particle space is the region to which there is a non-zero probability of making a trial transition. The region in the $N = 4$ particle space of the four infinitesmally thin but long cuboids is not shown.

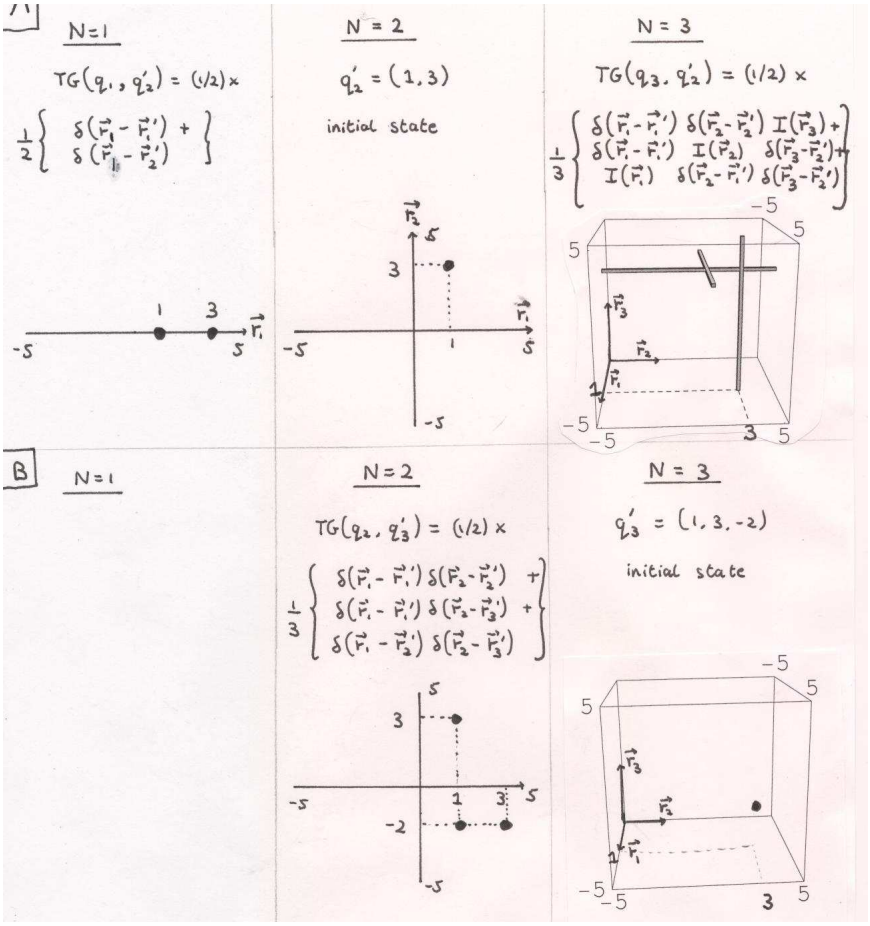

Figure 4.2: Schematic showing different N particle spaces and the Trial Greens function.

4.5.3 Choosing $A(q_N, q'_{N'})$

From Eq. (4.13)

$$A(q_{N_1}, q_{N_2}) = \min\left(1, \frac{TG(q_{N_2}, q_{N_1})P(q_{N_1})}{TG(q_{N_1}, q_{N_2})P(q_{N_2})}\right).$$

Simplifying when $N_1 = N_2 - 1$ (attempting a removal of one particle) we get

$$\frac{TG(q_{N_2}, q_{N_1})P(q_{N_1})}{TG(q_{N_1}, q_{N_2})P(q_{N_2})} = \frac{(1/2) \times \frac{1}{N_2}\text{product of } N_1 \text{ } \delta \text{ functions}}{(1/2) \times \frac{1}{N_2}\text{product of } N_1 \text{ } \delta \text{ functions}} \frac{I(\vec{r}_i)}{} \frac{P(q_{N_1})}{P(q_{N_2})}. \tag{4.20}$$

$i \in \{1, 2, \cdots N_2\}$ is the index of the particle we are attempting to remove at position $\vec{r}_i$. In the numerator, we pick up the ith term in the sum for $i_{q_{N_1}}(q_{N_2})$ and in the denominator we pick up the ith term in the sum of $r_{q_{N_2}}(q_{N_1})$. These delta functions are best thought of as being slightly "imperfect" (width $= \epsilon$, height $= 1/\epsilon$, $\epsilon \to 0$) so that we may legitimately cancel terms of the same order $(1/\epsilon)^{N_1}$ in ϵ.

The case $N_1 = N_2 + 1$ may be simplified easily by inverting Eq. (4.20) and interchanging $N_1 \leftrightarrow N_2$. Thus

$$A(q_{N_1}, q_{N_2}) = \begin{cases} \min\left(1, \frac{I(\vec{r}_i)\, P(q_{N_1})}{P(q_{N_2})}\right) & N_1 = N_2 - 1 \\ \min\left(1, \frac{P(q_{N_1})}{I(\vec{r}_i)\, P(q_{N_2})}\right) & N_1 = N_2 + 1 \end{cases},$$

is piecewise defined since TG was. Simplifying,

$$A(q_N, q_{N'}) = \begin{cases} \min\left(1, \frac{I(\vec{r}_i)\, N'}{n} e^{-\beta[V(q_N) - V(q_{N'})]}\right) & N = N' - 1 \\ \min\left(1, \frac{n}{I(\vec{r}_i) N} e^{-\beta[V(q_N) - V(q_{N'})]}\right) & N = N' + 1 \end{cases}.$$

4.5.4 Boundary Case $N = 0$

Since the particle number cannot be less than 0, we must deal separately with the case when either one of the initial or final states happens to be the 0 particle state. If q_0 is the 0 particle state, the trial greens function is

$$TG(q_1, q_0) = \begin{cases} I(\vec{r}_1) & N = 0 + 1 \end{cases},$$

which lacks the factor $1/2$ as in Eq. (4.16) since there is no possibility of removing a particle. $TG(q_0, q_1)$ is obtained from Eq. (4.16) as usual. Then,

$$A(q_0, q_1) = \min\left(1, 2I(\vec{r}_1) \cdot \frac{1}{n} \cdot e^{-\beta[0 - V(q_1)]}\right),$$

and

$$A(q_1, q_0) = \min\left(1, \frac{1}{2I(\vec{r}_1)} \cdot n \cdot e^{-\beta[V(q_1) - 0]}\right),$$

4.5.5 Example

In addition to illuminating the preceding discussion an example will make explicit some properties of a Markov Greens function which we thus far only implicitly alluded to. We take the case of non-interacting particles in a box of volume V. Then Q_N of Eq. (4.15) becomes $Q_N = V^N$, and the distribution for the particle number becomes the Poisson distribution

$$P(N) \propto \frac{n^N V^N}{N!} = \frac{3^N}{N!}$$

where nV is the mean number of particles, where for the purposes of this example, we have taken $nV = 3$. We will now construct the Greens function $G(N, N')$ satisfying Eq. (4.6) for this distribution. $I(\vec{r})$ the insertion probability is uniformly equal to $1/V$ for $\vec{r} \in V$ and 0 outside. The trial greens function from Eq. (4.16), and the relative probabilities are

$$TG = \begin{pmatrix} 0 & .5 & & & \\ 1 & 0 & .5 & & \\ & .5 & 0 & .5 & \\ & & .5 & 0 & \ddots \\ & & & \ddots & \ddots \end{pmatrix}, \qquad P = \begin{pmatrix} 1 \\ 3/1! \\ 3^2/2! \\ 3^3/3! \\ 3^4/4! \end{pmatrix}.$$

Note that the matrix and vector indices run from $0, 1 \cdots$. The matrix elements of A are solved for simultaneously in pairs of two by examining the corresponding two matrix elements of TG.

$$A = \begin{pmatrix} 0 & \frac{2}{3} & & & & \\ 1 & 0 & \frac{2}{3} & & & \\ & 1 & 0 & 1 & & \\ & & 1 & 0 & 1 & \\ & & & \frac{3}{4} & 0 & \ddots \\ & & & & \frac{3}{5} & \ddots \end{pmatrix}.$$

Then A modulates TG *pointwise* element by element. Eq. (4.10) then prescribes that we find the diagonal elements $r(N)$ by requiring each column to sum to 1. Then,

$$G = \begin{pmatrix} 0 & \frac{1}{3} & & & & \\ 1 & \frac{1}{6} & \frac{1}{3} & & & \\ & \frac{1}{2} & \frac{1}{6} & \frac{1}{2} & & \\ & & \frac{1}{2} & \frac{1}{8} & \frac{1}{2} & \\ & & & \frac{3}{8} & \frac{1}{5} & \frac{1}{2} \\ & & & & \ddots & \ddots \end{pmatrix}.$$

Fig. (4.3A) shows a density plot of G truncated at $N = 15$. This is tantamount to modifying the infinite matrix G by setting $G_{N+1,N} = 0$ and $G_{N,N+1} =$

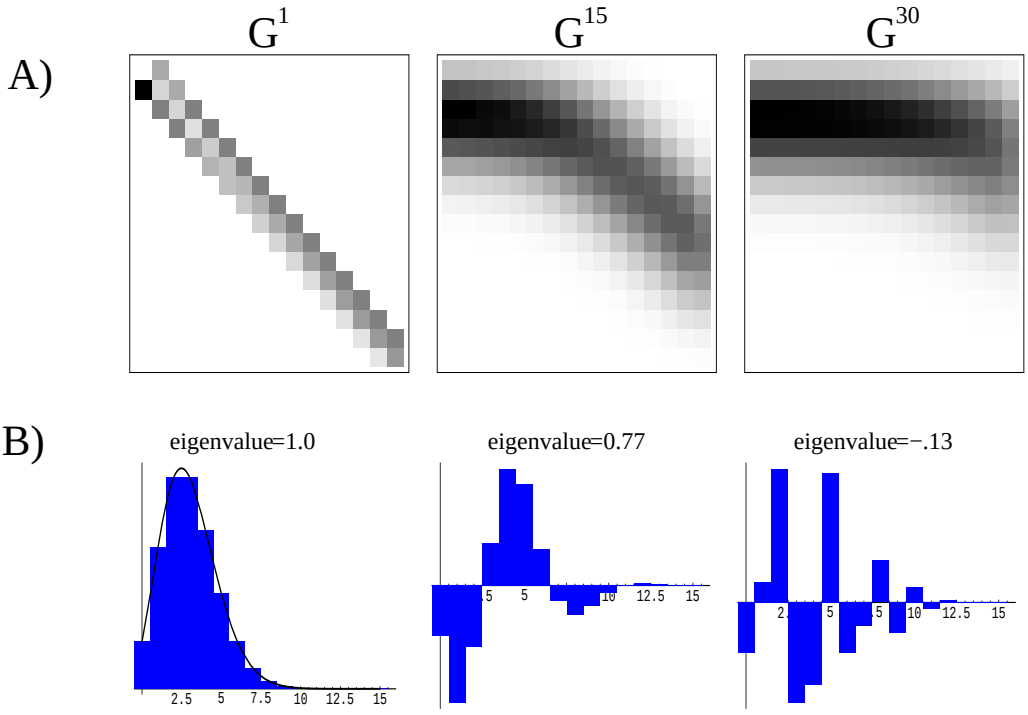

Figure 4.3: A) Powers of truncated Greens function. B) 3 selected eigenvectors of the Greens function.

0, because this clearly decouples the $(0, \cdots N)$ component subspace from the $(N+1, \cdots \infty)$ component subspace making these the invariant subspaces for this modified G. The truncated G in Fig. (A) then is just the action of the modified infinite matrix G on the first invariant subspace of components $(0, \cdots N)$. Physically $G_{N+1,N} = 0$, means we have forced a boundary condtion of creating a sink at N, whereby a Markov transition results in a certain fraction $(G_{N+1,N})$ of ensemble members disappearing and being lost forever. Similarly $G_{N,N+1} = 0$, means that there is no source at N. In principle this means that probability is lost, but in practise if the expected number of particles (for us $nV = 3$) is much less than the N at which we truncate, then we will never much feel the sink at N.

Fig.(4.3B) shows the four eigenvectors of G corresponding to the 0th, 3rd, 7th and 15th eigenvalues when arranged in descending order. All eigenvalues and eigenvectors are real in ths example. Having one eigenvalue be 1 (almost 1 due to truncation) is a immediate property of a Markov Greens function: Each column of G sums to $0 \Rightarrow$ Each column of $G - I$ sums to $0 \Rightarrow$ The vector sum of the rows of $G - I$ sum to $0 \Rightarrow G - I$ is singular. Furthermore all eigenvectors belonging to eigenvalues less than one must oscillate possesing both +ve and −ve entries which sum to 0. This is because a mapping under G must on the one hand scale this eigenvector by a factor not equal to one, and on the other hand must keep the sum of its elements fixed. Finally, information contained in any initial distribution is gradually lost, as its projections on all these eigenvectors damp out to 0 over long times leaving only its projection on the eigenvector with eigenvalue 1. This effect is apparent in the long time greens functions themselves in Fig4.3A) where each and every column converges onto the Poisson distribution.

Chapter 5

Simulating Many-Body Classical Dynamics

5.1 ODE Integration

We derive our method based on a reformulation and adaptation of the Predictor-Corrector method in which one stores the history of the trajectory (either values, derivatives, or both) at previous times. Instead, we store the Taylor coefficients of the trajectory at the present time. These may be obtained by finite differencing the history values stored in the Predictor-Corrector method. Changing the time step is then much faster and easier to implement. First we review the Predictor-Corrector method to solve the generic ode

$$y'(t) = f(t, y(t)) \tag{5.1}$$

5.1.1 Predictor-Corrector

The idea is to extrapolate the curve $f(t, y(t))$ a litttle ahead and then find the area under this newly extrapolated piece. This gives the increment in $y(t)$. (See Fig.(5.1.1)) If the exact value history of $y(t)$, $y_{-2} \equiv y(t_0 - 2h)$, $y_{-1} \equiv y(t_0 - h)$, and $y_0 \equiv y(t_0)$ is known, then by evaluating f of Eq.(5.1) at these points the exact derivative history of y

$$\begin{array}{lcll} f_{-2} & \equiv & f(t_0 - 2h, y_{-2}) & = & f(t_0) + (-2h)f'(t_0) + \frac{(-2h)^2}{2!}f''(t_0) + \cdots \\ f_{-1} & \equiv & f(t_0 - 1h, y_{-1}) & = & f(t_0) + (-1h)f'(t_0) + \frac{(-1h)^2}{2!}f''(t_0) + \cdots \\ f_0 & \equiv & f(t_0, y_0) & = & f(t_0), \end{array} \tag{5.2}$$

is also known. The most common Predictor-Corrector stores only

$$y_0 \text{ and } hf_0, hf_{-1}, hf_{-2}. \tag{5.3}$$

Given this data, the question is how to step ahead and compute the final approximations y_1 and f_1 to the functions $y(t)$ and $f(t, y(t))$ at $t_0 + h$. It might

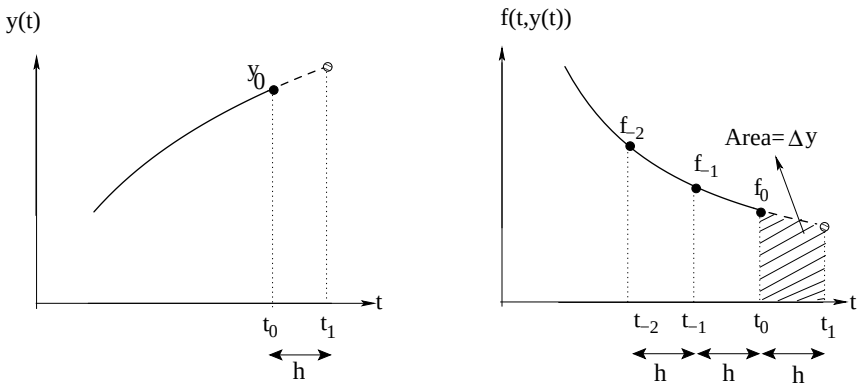

Figure 5.1: Predictor-Corrector Method

seem that we could use the data in Eq.(5.3) to simply extrapolate these values, but of course this would nowhere use the ode itself. Heuristically speaking, we also need to force the values y_1 and f_1 to be consistent with the ode itself, and so be related by

$$f_1 = f(t_0 + h, y_1). \tag{5.4}$$

This is conventionally achieved as follows.

5.1.1.1 Prediction

Remembering that $f^{(n)}(t_0)$ is just $y^{(n+1)}(t_0)$, we predict the value of y at $t_0 + h$ (call it y_{1p}) by extrapolation.

$$\begin{aligned} y_{1p} &\equiv y_0 + \overbrace{a_{-2}hf_{-2} + a_{-1}hf_{-1} + a_0 hf_0} \\ &= y(t_0) + hf(t_0) + \tfrac{h^2}{2!}f'(t_0) + \tfrac{h^3}{3!}f''(t_0) + O(h^4) \end{aligned} \tag{5.5}$$

where the predictor cofficients a_{-2}, a_{-1}, a_0 are chosen so as to make the second equality of Eq.(5.5) be true. Substituting Eq.(5.2) in Eq.(5.5) this requires us to solve

$$\begin{pmatrix} 1 & 1 & 1 \\ -2h & -h & 0 \\ \frac{(-2h)^2}{2!} & \frac{(-h)^2}{2!} & 0 \end{pmatrix} \begin{pmatrix} a_{-2} \\ a_{-1} \\ a_0 \end{pmatrix} = \begin{pmatrix} 1 \\ h/2! \\ h^2/3! \end{pmatrix}.$$

Notice that all h's cancel so that $(a_{-2}, a_{-1}, a_0) = (5/12, -4/3, 23/12)$ is independent of h.

5.1.1.2 Evaluation

$$f_1 \equiv f(t_0 + h, y_{1p}) \tag{5.6}$$

yielding f_1 the derivative at $t_0 + h$. This is where the ode gets used. Notice that we did not extrapolate to find f_1 here.

5.1.1.3 Correction

The bracketed increment in Eq.(5.5) added to y_0 to compute y_{1p} can be interpreted as the shaded area between t_0 and $t_1 = t_0 + h$ under the f curve of Fig(5.1.1), where this region of the f curve has been obtained by a simple extrapolation. However, with f_1 in hand, we are in a position to find the area of the *interpolated* f curve. Interpolation is always a safer operation than extrapolation. Thus, an improved corrected guess for y_1 is

$$\begin{aligned} y_{1c} &\equiv y_0 + \overbrace{A_{-2}hf_{-2} + A_{-1}hf_{-1} + A_0hf_0 + A_1hf_1} \\ &= y(t_0) + hf(t_0) + \tfrac{h^2}{2!}f'(t_0) + \tfrac{h^3}{3!}f''(t_0) + \tfrac{h^4}{4!}f'''(t_0) + O(h^5). \end{aligned} \tag{5.7}$$

Again, the bracketed term represents the shaded area of Fig.(5.1.1). The corrector cofficients $(A_{-2} \cdots A_1) = (1/24, -5/24, 19/24, 3/8)$ (independent of h) may be mechanically computed using the same method as in finding the predictor coefficients. More intuitively, they can be thought of as implementing a high order polynomial quadrature scheme for the shaded area in Fig.(5.1.1) by interpolating a third order polynomial $p(t)$ through the data f_{-2}, f_{-1}, f_0, f_1 and then computing $\int_{t_0}^{t_0+h} dt\, p(t)$.

5.1.1.4 Step Error Estimate

We wrap up by accepting

$$y_1 = y_{1c}$$

of Eq.(5.7) and

$$f_1 = f(t_0 + h, y_{1p})$$

of Eq.(5.6) as our final y_1 and f_1 values. The step error is computed as

$$\text{error}=y_{1c} - y_{1p} \sim \text{const} \times h^4 y^{(4)}(t_0) + O(h^5) \tag{5.8}$$

where the constant can be exactly found. Later we will use the fact that the error scales as h^4 in order to adapt the time step to control the local step error.

Remarks

Clearly, y_1 and f_1 as chosen do not exactly satisfy the consistency Eq.(5.4) which we proposed since f_1 was based on y_{1p} and not y_{1c}. This could be remedied by re-evaluating f as $f(t_0 + h, y_{1c})$, and taking this as our final value for f_1. But now, how to resist the temptation that our y_{1c} should be based on this improved f_1 and so on... Indeed, iterating this cycle to convergence is tantamount to finding y_1 or f_1 by locating the fixed point of the map

$$\bar{y} \to y_0 + A_{-2}hf_{-2} + A_{-1}hf_{-1} + A_0hf_0 + A_1hf(t_0 + h, \bar{y})$$

or

$$\bar{f} \to f(t_0 + h, A_{-2}hf_{-2} + A_{-1}hf_{-1} + A_0hf_0 + A_1h\bar{f})$$

respectively. For classical many body dynamics, all such improvements are out of question. Evaluation of f (the acceleration) is by far the most expensive numerical operation, and we must be content, if possible, with a single evaluation of it per time step.

5.1.2 Taylor Series Method

This is our own name. The method is different from other elementary methods found in texts that go by the same name. Similar methods in the literature are known as multivalue methods, ours being like and based on the so-called Norsdeik Method.

Associated with each time t the predictor-corrector stores the data consisting of the current value and derivative history of $y(t)$ as written in Eq.(5.3) for $t = t_0$.

5.1.3 History Data Set $\vec{u}$

Let us collect this set into a column vector $\vec{u}(t)$. Then

$$\vec{u}_0 \equiv \vec{u}(t_0) = (y_0, hf_0, hf_{-1}, hf_{-2})$$

and clearly

$$\vec{u}_1 \equiv \vec{u}(t_0 + h) = (y_1 = y_{1c}, hf_1, hf_0, hf_{-1}).$$

Using this notation, it is easily verified that the entire Predictor-Corrector step-forward algorithm may be written as

$$\begin{pmatrix} y_1 \\ hf_1 \\ hf_0 \\ hf_{-1} \end{pmatrix} = \begin{pmatrix} 1 & a_0 & a_{-1} & a_{-2} \\ 0 & \frac{-(A_0 - a_0)}{A_1} & \frac{-(A_{-1} - a_{-1})}{A_1} & \frac{-(A_{-2} - a_{-2})}{A_1} \\ 0 & 1 & 0 & 0 \\ 0 & 0 & 1 & 0 \end{pmatrix} \begin{pmatrix} y_0 \\ hf_0 \\ hf_{-1} \\ hf_{-2} \end{pmatrix} + (hf(t_0 + h, u_{1p,1}) - u_{1p,2}) \begin{pmatrix} A_1 \\ 1 \\ 0 \\ 0 \end{pmatrix}$$

or

$$\begin{aligned} \vec{u}_1 &= \mathbf{A}\vec{u}_0 + (hf(t_0 + h, u_{1p,1}) - u_{1p,2})\vec{d} \\ &= \mathbf{A}\vec{u}_0 + (hf_1 - u_{1p,2})\vec{d} \end{aligned} \tag{5.9}$$

where

$$\vec{u}_{1p} \equiv \mathbf{A}\vec{u}_0$$

with components $(u_{1p,1}, u_{1p,2}, u_{1p,3}, u_{1p,4})$ is the predicted value of $\vec{u}$ at $t_0 + h$. Since $u_{1p,1} = y_{1p}$ by Eq. (5.5), we have $f(t_0 + h, u_{1p,1}) = f_1$ by (5.6).

Claim

The matrix multiply of Eq. (5.9) implements an extrapolation to predict all the desired quantities on the l.h.s. accurate to $O(h^3)$. The correcting increment $(hf_1 - u_{1p,2})\vec{d}$ is an $O(h^4)$ quantity. Its role is *not* to improve the accuracy of the predicted quantity $\vec{u}_{1p}$ but rather to make the whole method stable and possible since it is the only place where the ode equation is used.

Proof of Claim

We already know that $u_{1,1} = y_1 = y_{1c}$ and $u_{1p,1} = y_{1p}$ differ to $O(h^4)$ by comparing Eqs. (5.5) and (5.7). It follows that the quantity $(hf_1 - u_{1p,2})$ must be an $O(h^4)$ quantity since A_1 is independent of h. Hence, $\vec{u}_{1p}$ must agree with

$\vec{u}_1$ to $O(h^3)$. As a byproduct, it is now clear that $u_{1p,2}$ is an $O(h^3)$ prediction of hf_1. It may be verified that the row 2 coefficients of the matrix $\mathbf{A}$ achieve this by a simple polynomial extrapolation of the values hf_{-2}, hf_{-1}, hf_0 to the time $t_0 + h$.

5.1.4 Taylor Data Set $\vec{w}$

Instead of storing the 4 components of $\vec{u}$ as our data set, we may equally well deal with any linear combination of them. Define

$$\vec{w}_n = \mathbf{C}\vec{u}_n,$$

where

$$\mathbf{C} = \begin{pmatrix} 1 & 0 & 0 & 0 \\ 0 & 1 & 0 & 0 \\ 0 & \frac{3}{4} & -1 & \frac{1}{4} \\ 0 & \frac{1}{6} & -\frac{1}{3} & \frac{1}{6} \end{pmatrix}. \tag{5.10}$$

How does one advance one time step in the $\vec{w}$ basis? Multiplying Eq. (5.9) by $\mathbf{C}$ and using $\vec{u}_0 = \mathbf{C}^{-1}\vec{w}_0$ we get

$$\mathbf{C}\vec{u}_1 = \mathbf{C}\mathbf{A}\mathbf{C}^{-1}\vec{w}_0 + (hf(t_0 + h, u_{1p,1}) - u_{1p,2})\mathbf{C}\vec{d}.$$

With

$$\mathbf{B} \equiv \mathbf{C}\mathbf{A}\mathbf{C}^{-1} = \begin{pmatrix} 1 & 1 & 1 & 1 \\ 0 & 1 & 2 & 3 \\ 0 & 0 & 1 & 3 \\ 0 & 0 & 0 & 1 \end{pmatrix}, \quad \vec{e} \equiv \mathbf{C}\vec{d} = \begin{pmatrix} \frac{3}{8} \\ 1 \\ \frac{3}{4} \\ \frac{1}{6} \end{pmatrix},$$

we get

$$\begin{aligned} \vec{w}_1 &= \mathbf{B}\vec{w}_0 + (hf(t_0 + h, w_{1p,1}) - w_{1p,2})\vec{e} \\ &= \mathbf{B}\vec{w}_0 + (hf_1 - w_{1p,2})\vec{e} \end{aligned} \tag{5.11}$$

where

$$\vec{w}_{1p} \equiv \mathbf{B}\vec{w}_0$$

with components $(w_{1p,1}, w_{1p,2}, w_{1p,3}, w_{1p,4})$ is the predicted value of $\vec{w}$ at $t_0 + h$. In simplifying to Eq.(5.11) we used that the first two components of $\vec{w}_{1p}$ and $\vec{u}_{1p}$ are identical. This follows by noticing that $\vec{w}_{1p} = \mathbf{C}\vec{u}_{1p}$ is generally true and then using the simple form of rows 1 and 2 of our particular $\mathbf{C}$ in Eq.(5.10). Rows 3 and 4 of $\mathbf{C}$ act on $\vec{u}_0$ to produce a finite difference estimate of $(h^2/2!)f''(t_0)$ and $(h^3/3!)f'''(t_0)$, both correct to $O(h^3)$ (including the explicit factors of h). Thus we see that the $\vec{w}$ data set at time t is just the first 4 Taylor Series terms for $y(t)$ around t. That is,

$$\begin{aligned} \vec{w}(t) &= (y(t), \quad hf(t), \quad \tfrac{h^2}{2!}f'(t), \quad \tfrac{h^3}{3!}f''(t)) \\ &= (y(t), \quad hy'(t), \quad \tfrac{h^2}{2!}y''(t), \quad \tfrac{h^3}{3!}y'''(t)). \end{aligned}$$

With this interpretation for the components of $\vec{w}$ it is easy to arrive at the same matrix $\mathbf{B}$ used to compute $\vec{w}_{1p}$ by the following independent argument. Write

$$y(t_0 + h) = y_0 + hf(t_0) + \frac{h^2}{2!}f'(t_0) + \frac{h^3}{3!}f''(t_0). \tag{5.12}$$

The Taylor Series of $y(t)$ around $t_0 + h$ is then easily read off by shifting the center of the taylor expansion to $t_0 + h$ or by repeatedly differentiating Eq. (5.12) w.r.t. h to compute the various taylor series terms at $h = h$. It was only to determine

$$\vec{e} = \begin{pmatrix} \frac{3}{8} \\ 1 \\ \frac{3}{4} \\ \frac{1}{6} \end{pmatrix}$$

in the correcting piece of Eq. (5.11) that we went through all this effort. It is precisely this correcting piece that makes the method stable since it inherits all of its properties from the well studied Predictor-Corrector method.

Advancing the $\vec{w}$ data set via Eq. (5.11) is exactly equivalent to advancing the $\vec{u}$ data set via Eq. (5.9). It is in changing the step size that the $\vec{w}$ data set proves far superior. This is because all the h dependence in the $\vec{w}$ data set is explicitly in the factors $1, h, h^2/2!, h^3/3!$. Thus, to take a different time step of k instead of h, we simply re-scale the components of $\vec{w}$ by $1, (k/h), (k/h)^2, (k/h)^3$ respectively.

An unexpected further benefit of the method is that the particular structure of $\mathbf{B}$ allows the operation $\vec{y} = \mathbf{B}\vec{x}$ to be performed very efficiently as follows. First, temporarily set $y_i = x_i$ for each $i = 1 \cdots 4$. Then perform the following sequence of operations column by column (left to right) where each column is traversed in the direction indicated by the arrow (bottom to top).

$$\uparrow \begin{pmatrix} y_1 = y_1 + y_2 \\ y_2 = y_2 + y_3 \\ y_3 = y_3 + y_4 \end{pmatrix} \qquad \uparrow \begin{pmatrix} \\ y_2 = y_2 + y_3 \\ y_3 = y_3 + y_4 \end{pmatrix} \qquad \uparrow \begin{pmatrix} \\ \\ y_3 = y_3 + y_4 \end{pmatrix}.$$

No multiplications are invloved.

5.2 Integrating Equations of Motion

To integrate the second order equations of motion for a particle, both the position x and velocity vx need to be updated. For simplicity, we ignore the y and z components. Then, y and f in Eq.(5.1) are vector-valued

$$\begin{aligned} \vec{y} &= (x, vx), \\ \vec{f}(t, \vec{y}(t)) &= (f_x(t, x, vx), \quad f_{vx}(t, x, vx)) \\ &= (vx, \quad a_x(t, x, vx)) \end{aligned}$$

The x component of the acceleration will involve the velocity if there is friction or a magnetic field. The taylor data set used to advance the quantities x and

vx we call $\overrightarrow{wx}(t)$ and $\overrightarrow{wvx}(t)$. At $t = t_0$ these are

$$\overrightarrow{wx}_0 = (x_0, hx'_0, \frac{h^2}{2!}x''_0, \frac{h^3}{3!}x'''_0)$$

and

$$\overrightarrow{wvx}_0 = (vx_0, hvx'_0, \frac{h^2}{2!}vx''_0, \frac{h^3}{3!}vx'''_0).$$

The corresponding history data sets $\overrightarrow{ux}(t)$ and $\overrightarrow{uvx}(t)$ at $t = t_0$ are $\overrightarrow{ux}_0$ and $\overrightarrow{uvx}_0$. These are related by

$$\begin{aligned} \overrightarrow{wx}_0 &= \mathbf{C}\overrightarrow{ux}_0 \\ \overrightarrow{wvx}_0 &= \mathbf{C}\overrightarrow{uvx}_0. \end{aligned}$$

Now it would certainly be possible to simultaneously carry forward both these data sets using Eq.(5.11). However, an obvious advantage of the $\vec{w}$ formulation can be exploited. The last three components of $\overrightarrow{wx}(t)$ and the first three components of $\overrightarrow{wvx}(t)$ are both $O(h^3)$ approximations to the same quantities (up to known multiplicative constants). Therefore, one could hope to carry forward just the one value $x(t)$ and the four values in $\overrightarrow{wvx}(t)$. In addition, we will argue that both the prediction and correction steps for $x(t)$ can be rolled into one.

Let us start by considering the original Predictor-Corrector recipe for advancing $x(t)$ from t_0 to $t_0 + h$. The final value for $x(t_0 + h)$ which we accept is

$$x_1 = x_{1c} \equiv x_0 + A_{-2}\, h\, vx_{-2} + A_{-1}\, h\, vx_{-1} + A_0\, h\, vx_0 + A_1\, h\, f_{x1}. \qquad (5.13)$$

This may be conveninetly rewritten as

$$\begin{aligned} x_1 &= x_0 + (0, A_0, A_{-1}, A_{-2}) \cdot \overrightarrow{ux}_0 + A_1\, h\, uvx_{1p,1} \quad \text{(a)} \\ &= x_0 + (0, A_0, A_{-1}, A_{-2}) \cdot \mathbf{C^{-1}}\overrightarrow{wx}_0 + A_1\, h\, wvx_{1p,1} \quad \text{(b)} \end{aligned} \qquad (5.14)$$

where $uvx_{1p,1}$ is the first component of $\overrightarrow{uvx_{1p}}$ and $wvx_{1p,1}$ is the first component of $\overrightarrow{wvx_{1p}}$. In going from equation (5.14a) to (5.14b) we shifted to using the taylor data sets in place of the history data sets. Still (5.14b) is exactly equivalent to the full corrector equation for x_1 we began with in Eq. (5.13) so long as $\overrightarrow{wx}_0$ and $\overrightarrow{wvx}_0$ are both independently and simultaneously stepped forward using Eq. (5.11). As it stands (5.14b) is a linear combination of the four components of $\overrightarrow{wx}_0$ and $\overrightarrow{wvx}_0$ (recall $\overrightarrow{wvx_{1p}} = \mathbf{B}.\overrightarrow{wvx}_0$). But, if as proposed above, we always obtain the last three components of $\overrightarrow{wx}_0$ from the first three components of $\overrightarrow{wvx}_0$, then the r.h.s. of Eq.(5.14b) is just a linear combination of x_0 and the four components of $\overrightarrow{wvx}_0$ alone. Since the replacement is $O(h^3)$ accurate, it follows that the r.h.s. of Eq. (5.14b) must be the taylor expansion for $x(t_0 + h)$ accurate to $O(h^3)$. This implies that Eq. (5.14b) must simplify as

$$x_1 = x_0 + h\, vx_0 + \frac{h^2}{2!}vx'_0 + \frac{h^3}{3!}vx''_0 + (?)\frac{h^4}{4!}vx'''_0. \qquad (5.15)$$

We verify this by an obvious direct computation which also gives us the (as yet unknown) coefficient of the last term. The second term of Eq. (5.14b) is

$$(0, A_0, A_{-1}, A_{-2}) \cdot \mathbf{C^{-1}} = \begin{pmatrix} 0 \\ 5/8 \\ 1/4 \\ -1/8 \end{pmatrix}$$

and

$$A_1\ h\ wvx_{1p,1} = \frac{3}{8}\, h\, \left(vx_0 + hvx_0' + \frac{h^2}{2!} vx_0'' + \frac{h^3}{3!} vx_0''' \right).$$

Thus we see how Eq. (5.14b) explicitly simplifies to Eq. (5.15), and also find the last coefficient of Eq. (5.15) to be 3/2. Hence the Taylor series data x_0 is advanced to its value at $t_0 + h$ by

$$x_1 = x_0 + h\, vx_0 + \frac{h^2}{2!} vx_0' + \frac{h^3}{3!} vx_0'' + (3/2)\frac{h^4}{4!} vx_0'''. \tag{5.16}$$

The last coefficient of 3/2 appears to be "wrong" but it is what the analysis leads us to. Numerical experiments showed that replacing it it by 1 was not a disaster, but using 3/2 almost always made things noticeably better.

$\overrightarrow{wvx}(t)$ is advanced as usual using Eq. (5.11) where $f_{vx,1}$ is computed as

$$\begin{aligned} f_{vx}(t_0 + h, x_{1p}, vx_{1p}) &= a_x(t_0 + h, x_{1p}, vx_{1p}) \\ &= a_x(t_0 + h, x_1,\ vx_{1p}) \end{aligned}$$

since we may as well use the fully corrected x_1 of Eq. (5.16) in place of x_{1p}. Summarizing, we advance x_0 and $\overrightarrow{wx_0}$ by

Step 1) $x_1 = x_0 + h\, wvx_{0,1} + \frac{h}{2}\, wvx_{0,2} + \frac{h}{3}\, wvx_{0,3} + \frac{3}{2} \cdot \frac{h}{4}\, wvx_{0,4}$

Step 2) $\overrightarrow{wvx_{1p}} = \mathbf{B} \cdot \overrightarrow{wvx_0}$

Step 3) $f_{vx,1} = a_x(t_0 + h, x_1, wvx_{1p,1})$

Step 4) $\overrightarrow{wvx_1} = \overrightarrow{wvx_{1p}} + (h\, f_{vx,1} - wx_{1p,2})\vec{e}$

5.3 Independent Time Step

Each particle is in general assigned its own time step which itself will possibly change from step to step. Below we will discuss how this time step is decided based on the step error. For now, we will assume that each particle indexed $i = 1 \cdots N$ exists with its data set at time t_i and is scheduled for an advance to time $t_i + \Delta t_i$. All the t_i and Δt_i will in general be different. The h in the data set of the ith particle will be equal to Δt_i. Now clearly the particle in need of immediate attention, so to speak, is the particle with the smallest value of $t_i + \Delta t_i$. Let us suppose this is true for the particle with index $i = 7$. To advance it to $t_7 + \Delta t_7$ we perform the following steps.

(i) Compute the next accepted value for x at time $t_7 + \Delta t_7$ as in Step 1) and predict $\overrightarrow{wvx_{1p}}$ as in Step 2).

(ii) Predict all other particle position coordinates to time $t_7 + \Delta t_7$ by simple extrapolation.

(iii) Correct $\overrightarrow{wvx_{1p}}$ and accept this as our next data set at $t_7 + \Delta t_7$.

(iv) Use the step error to decide upon the next appropriate value for Δt_7.

5.3.1 Priority Queue and a Tree Structure

Executing (i) above requires being able to repeatedly find the smallest amongst N real values $t_i + \Delta t_i$, replacing this with a new value and then finding the smallest again. In other words we need an efficient algorithm to

(a) Find the smallest among N real numbers (and do something with it),

(b) Replace this value with a new value and repeat step (a).

A brute force search among an unsorted list of these values is $O(N)$. Maintaining these numbers in a sorted array would make the search $O(\log N)$. However, insertion of the new value in step (b) would require shifting members of the array resulting in $O(N)$ copy operations. This insertion problem is itself solved by maintaining the values in a linked list as approached to a contiguous array. However, now making the $O(\log N)$ binary search in step (a) becomes impossible since a linked list is necessarily traversed sequentially. It turns out that it is possible to implement a binary tree structure in a way that simultaneously also solves the insertion difficulty of step (b) although it is not at all obvious how to do this.

Instead, this is more elegantly solved by using a tree structure known as a Heap by computer scientists. In fact, the reader may have recognized that what we are attempting to implement is a so-called priority queue.

Figure (5.2) shows a tree possessing the Heap property where each node has two children with a smaller priority than their parent node. There is no requirement between children at the same depth in the tree. For us, node A has a greater priority than node B if the value it contains is smaller.

The top node is clearly the node with the highest priority and the value it contains immediately solves step (a). After processesing this value and generating a new one, the old value is deleted from this node. Now both children of this node *and* the newly generated value compete for being promoted/inserted into the empty node. The one with the highest priority wins. If this happens to be one of the two children, we call this a promotion, and if it is a new value, we call this an insertion. A promotion always results in some node being left empty requiring a new competition between its children (for promotion) and the new value for insertion. The tree is finally completely updated when an insertion plugs the empty node. The number of steps involved for this is clearly at most equal to the depth of the tree which is $O(\log_2 N)$.

5.3.2 Adaptive Step Size

A measure of the accuracy of a single time step is the step error

$$\propto h^4 vx^{(4)}(t_0)$$

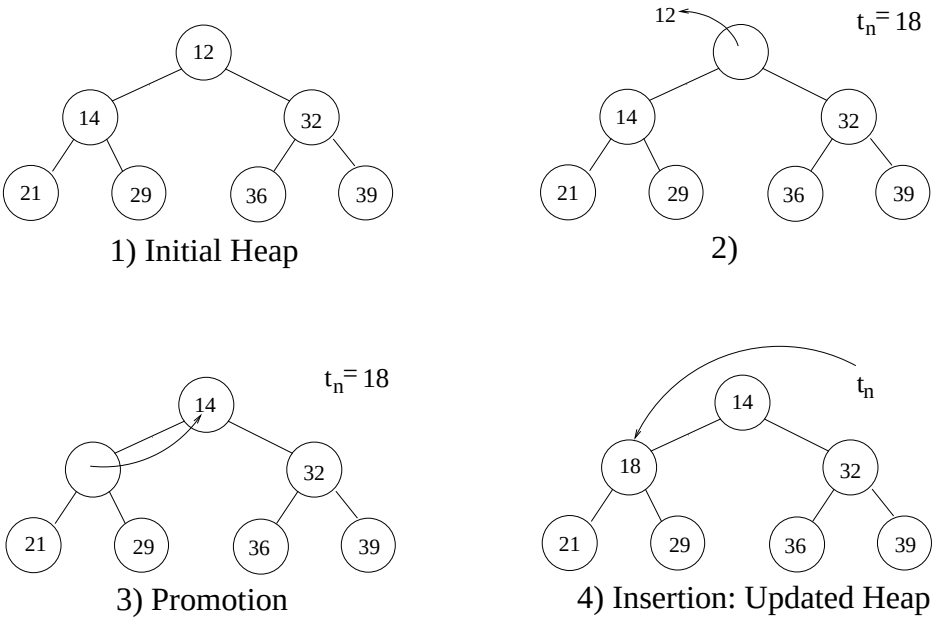

Figure 5.2: Implementing a priority queue

given in Eq. (5.8). We would like to take a time step of h so this quantity is constrained to remain below some value, say $\epsilon = 10^{-6}$, in absolute value. If the value of $vx^{(4)}(t_0)$ were known this would be easy. Under the assumption that $vx^{(4)}(t_0)$ incurs a small fractional change from one time step to the next this is achieved by choosing the next time step as

$$h = h_{-1} \left(\frac{\epsilon = 10^{-6}}{|err|} \right), ^{1/4}$$

where err is the known error in taking the last step of size h_{-1}. Further discussion to be filled in....

Chapter 6

The no-sticking effect in ultra-cold collisions

Abstract

We provide the theoretical basis for understanding the phenomenon in which an ultra cold atom incident on a possibly warm target will not stick, even in the large n limit where n is the number of internal degrees of freedom of the target. Our treatment is non-perturbative in which the full many-body problem is viewed as a scattering event purely within the context of scattering theory. The question of sticking is then simply and naturally identified with the formation of a long lived resonance. One crucial physical insight that emerges is that the many internal degrees of freedom serve to decohere the incident one body wavefunction, thus upsetting the delicate interference process necessary to form a resonance in the first place. This is the physical reason for not sticking.

6.1 Introduction

The problem of low energy sticking to surfaces has attracted much attention over the years[1, 2, 3, 4, 5]. The controversial question has been the ultralow energy limit of the incoming species, for either warm or cold surfaces. A battle has ensued between two countervailing effects, which we will call classical sticking and quantum reflection. The concept of quantum reflection is intimately tied into threshold laws, and was recognized in the 1930's by Lennard-Jones[1]. Essentially, flux is reflected from a purely attractive potential with a probability which goes as $1 - \alpha\sqrt{\epsilon}$, as $\epsilon \to 0$, where α is a constant and ϵ is the translational energy of the particle incident on the surface. Classically the transmission probability is unity. Reflection at long range prevents inelastic processes from occurring, but if the incoming particle should penetrate into the strongly attractive region, the ensuing acceleration and hard collision with the repulsive short

range part of the potential leads to a high probability of inelastic processes and sticking.

The blame for the quantum reflection can be laid at the feet of the WKB approximation, which breaks down in the long range attractive part of the potential at low energy. Very far out, the WKB is good even for low energy, because the potential is so nearly flat. Close in, the kinetic energy is high, because of the attractive potential, even if the asymptotic energy is very low, and again WKB is accurate. But in between there is a breakdown, which has been recognized and exploited by several groups[6, 7, 8, 9, 10, 11]. We show in the paper folling this one that the breakdown occurs in a region around $|V| \approx \epsilon$; i.e. aproximately where the kinetic and potential energies are equal.

It would seem that quantum reflection would settle the issues of sticking, since if the particle doesn't make it in close to the surface there is no sticking. (Fig 6.1) There is one caveat, however, which must be considered: quantum reflection can be defeated by the existence of a resonance in the internal region, i.e. a threshold resonance. (Fig 6.2)

The situation is very analogous to a high Q Fabry-Perot cavity, where using nearly 100% reflective, parallel mirrors gives near 100% reflection except at very specific wavelengths. At these specific energies a resonace buildup occurs in the interior of the cavity, permiting near 100% transmission. Such resonances are rare in a one dimensional world, but the huge number of degrees of freedom in a macroscopic solid particle makes resonance ubiquitous. Indeed, the act of colliding with the surface, creating a phonon and dropping into a local bound state of the attractive potential describes a Feshbach resonance. Thus, the resonances are just the sticking we are investigating, and we must not treat them lightly! Perhaps it is not obvious after all whether sticking occurs.

After the considerable burst of activity surrounding the sticking issue on the surface of liquid Helium[12, 13], and after a very well executed theoretical study by Clougherty and Kohn[4], the controversy has settled down, and the common wisdom has grown that sticking does not occur at sufficiently low energy. While we agree with this conclusion, we believe the theoretical foundation for it is not complete, nor stated in a wide enough domain of physical situations. For example, Ref. [4] treats only a harmonic slab with one or two phonon excitation. It is not clear whether the results apply to a warm surface. On the experimental side, even though quantum reflection was observed from a liquid Helium surface, that surface has a very low density of available states (essentially only the ripplons) which could be a special case with respect to sticking. Thus, the need for more rigorous and clear proof of non-sticking in general circumstances is evident. This paper gives such an analysis. In a following paper, application is made to specific atom-surface and slab combinations, and the rollover to the sticking regime as energy is increased (which can be treated essentially analytically) is given.

The strategy we use puts a very general and exact scattering formalism to work, providing a template into which to insert the properties of our target and scatterer. Then very general results emerge, such as the non-sticking theorem at zero energy. The usual procedure of defining model potentials and considering

one phonon processes etc. is not necessary. All such model potentials and Hamiltonians wind up as parameters in the R-matrix formalism. The details of a particular potential are of course important for quantitative results, but the range of possible results can be much more easily examined by inserting various parameters into the R-matrix formalism. All the possible choices of R-matrix parameters give the correct threshold laws. Certain trends are built into the R-matrix formalism which are essentially independent of the details of the potentials.

Before commencing with the R matrix treatment, we briefly consider the problem perturbatively in order to better elucidate the role played by quantum reflection. We emphasize that none of the perturbation section is actually necessary for our final conclusions.

In a perturbative treatment for our slab geometry, quantum reflection simply results in the entrance channels' wave function (at threshold) having its amplitude in the interaction region go to zero as $k_e \sim \sqrt{\epsilon}$ when normalized to have a fixed incoming flux. (k_e is the magnitude $|\vec{k}_e|$ of the incident wavevector of the incoming atom). The inelastic transition probabilities are proportional to the potential weighted overlap of the channel wavefunctions and this immediately leads to the conclusion that the inelastic probability itself vanishes as $k_e \sim \sqrt{\epsilon}$. As mentioned, this conclusion is shown to rigorously remain true using the R matrix. We show in this paper that in spite of the inherently many-body nature of the problem, in the ultra-cold limit we can correctly obtain the long-range form of the entrance channel's wavefunction by solving for the one-dimensional motion in the long-range surface-atom attraction (i.e. the diagonal element of the many-channel potential matrix). This allows quantitative predictions of the sticking probability, which we do in the following paper. There, we further exploit the perturbative point of view together with an analysis of WKB to predict a 'post-threshold' behavior as quantum reflection abates, when the incoming energy is increased.

6.2 Geometry and notation

The incident atom is treated as a point particle at position (x, y). To keep the notation simple we leave out the z-coordinate and confine our discussion to two spatial dimensions. Thus a cross-section will have dimensions of length etc. It will be quite obvious how and where z may be inserted in all that follows. Let u represent all the bound degrees of freedom of the scattering target, which we take to be a slab of crystalline or amorphous material. Let $\Omega_c(u)$, $c = 1, 2, \cdots$, be the manybody target wave functions in the absence of interactions with the incident particle, and having energy E_c^{target}. These are normalized as $\int_{\text{all u}} du\ |\Omega_c(u)|^2 = 1$. x is the distance of the scatterer (atom) from the face of the slab which is approximately (because the wall is rough) along the line $x = 0$. The internal constituents of the slab lie to the left of $x = 0$ and the scatterer is incident from the right with kinetic energy $\epsilon = \hbar^2 k_e^2/2m$.

Figure 6.1: The stationary state one body wavefunction of the incident atom moving in the y-independent mean potential felt by it. The amplitude inside the interaction region is supressed by $k_e \sim \sqrt{\epsilon}$. This is tantamount to the reflection of the atom.

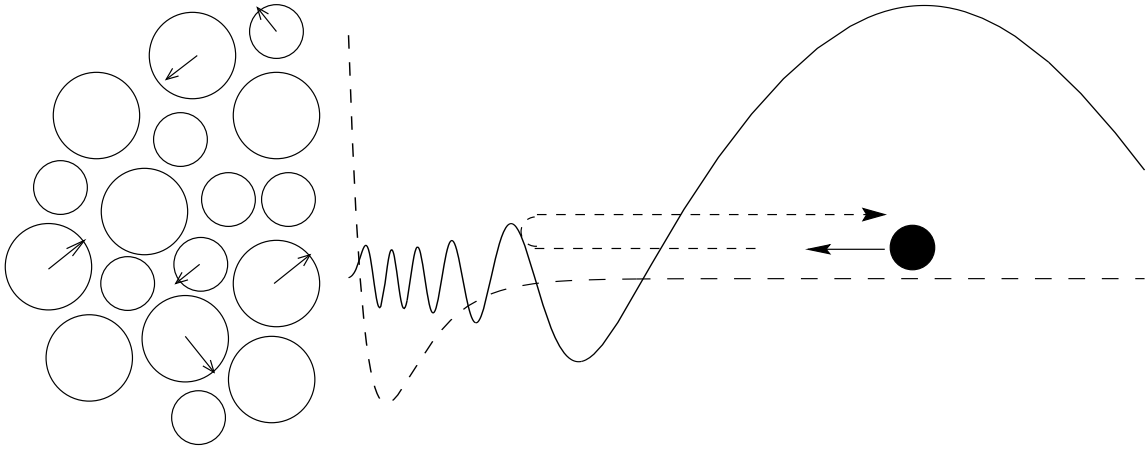

Figure 6.2: A schematic view of a Feshbach resonance wherein the incident atom forms a long lived quasi-bound state with the target. The many body wavefunction in this situation (not shown) has a large amplitude in the 'interior' region near the slab.

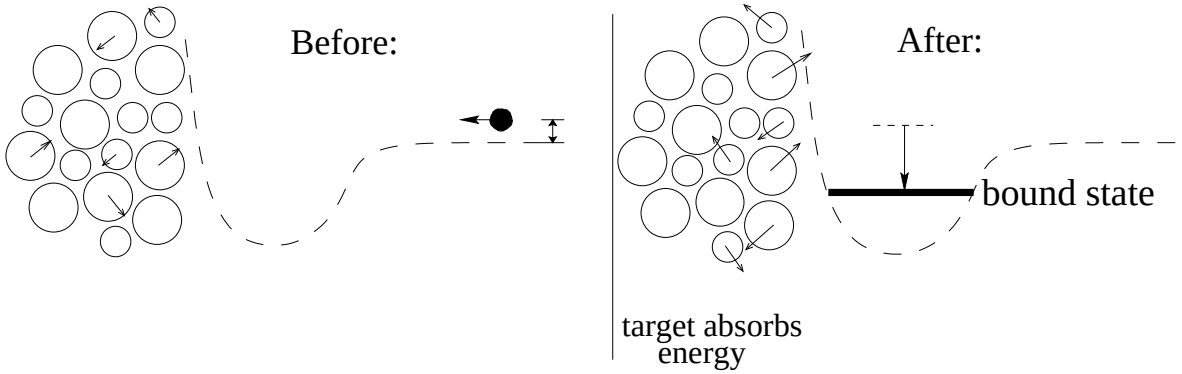

The total energy E of the system is

$$E = \epsilon + E_e^{\text{target}} \tag{6.1}$$

where $c = e$ is the index of the 'entrance channel' i.e. the initial internal state of the slab before the collision is $\Omega_e(u)$. Notice that we say nothing about the value of E_e^{target} itself. In particular the slab need not be cold. k_c is the magnitude of the wave vector $\vec{k}_c$ of the particle when it leaves the target in the state $\Omega_c(u)$ after the collision. Our interest focusses on $k_e \to 0$. k_e is the magnitude of the wavevector of the incoming particle. For the open channels $c = 1, \cdots n$ (this defines n) for which $E > E_c^{\text{target}}$

$$k_c \equiv \sqrt{\frac{2m(E - E_c^{\text{target}})}{\hbar^2}} \qquad (c \leq n) \ ; \tag{6.2}$$

whereas for the closed channels $(c > n)$, $E < E_c^{\text{target}}$ and

$$k_c \equiv i\sqrt{\frac{2m(E_c^{\text{target}} - E)}{\hbar^2}} \equiv i\kappa_c \qquad (c > n) \ . \tag{6.3}$$

$\kappa_c > 0$. We will use (k_{cx}, k_{cy}) as the x, y components of $\vec{k}_c$. Let $U_{\text{int}}(x, y, u) = (2m/\hbar^2)V_{\text{int}}(x, y, u)$, where $V_{\text{int}}(x, y, u)$ describes quite generally the interaction potential between the incident atom and all the internal degrees of freedom of the slab. For simplicity we assume for the moment that there is no interaction between slab and atom for $x > a$.

6.3 Preliminaries: Perturbation

As stated above, we excercise the perturbative treatment for insight only; our final conclusions are based on nonperturbative arguments.

We treat the interaction $U_{\text{int}}(x, y, u)$ between slab and atom by separating out a 'mean' potential felt by the atom that is independent of y and u; call it $U^{(0)}(x)$. The remainder $U^{(1)}(x, y, u) \equiv U_{\text{int}}(x, y, u) - U^{(0)}(x)$ is treated as a perturbation.

Now the incident beam is scattered by the entire length (say from $y = -L$ to $L = 2L$) of wall which it illuminates. If all measurements are made close to the wall so that its length $2L$ is the largest scale in the problem, then it is appropriate to speak of a cross-section per unit length of wall, a dimensionless probability. More specifically, we will assume that the matrix elements $U^{(1)}_{cc'}(x, y) \equiv \int_{\text{all u}} du\, \Omega_c^*(u) U^{(1)}(x, y, u) \Omega_{c'}(u)$ of the perturbation $U^{(1)}(x, y, u)$ in the $\Omega_c(u)$ basis are given by the simple form $U^{(1)}_{cc'}(x, y) = U^{(1)}_{cc'}(x) f(y)$ for $y \in [-L, L]$ and 0 elsewhere. $f(y)$ is a random persistent (does not die to 0 as

$|L| \to \infty$) function that models the random roughness of the slab and is characterized by its so-called spectral density function S, a smooth positive-valued non-random function, such that

$$\left| \int_{-L}^{L} dy\, e^{iky} f(y) \right|^2 \equiv 2LS(k) \qquad \forall k \tag{6.4}$$

as $L \to \infty$.

Now, applying either time-independent perturbation (equivalently the Born approximation for this geometry) or time-dependent perturbation theory via the Golden Rule, gives that the cross-section per unit length of wall for inelastic scattering to a final channel c is

$$P^{\text{in}}_{c \leftarrow e}(\theta) = \frac{2\pi}{k_e} \left(\int_{-\infty}^{a} dx' \phi(x'; k_{cx}) U^{(1)}_{ce}(x') \phi(x'; k_{ex}) \right)^2 S(k_{cy} - k_{ey}) \tag{6.5}$$

where $\phi(x; k_x)$ is the solution of the o.d.e.

$$\left(\frac{d^2}{dx^2} - U^{(0)}(x) + k_x^2 \right) \phi(x; k_x) = 0 \tag{6.6}$$

which is regular or goes to zero as $x \to -\infty$ inside the slab and is normalized as

$$\phi(x; k_x) \sim \sin(k_x x + \delta) \qquad \text{as} x \to \infty \tag{6.7}$$

Accepting for the moment that as $k_e \to 0$ the amplitude of $\phi(x; k_{ex})$ in the internal region $x < a$ goes to zero as $k_e \sim \sqrt{\epsilon}$, then the square of the overlap integral in Eq. (**??**) behaves as k_e^2, because by our proposition the amplitude of $\phi(x'; k_{ex}) \sim k_{ex} \sim k_e$. Together with the $1/k_e$ prefactor we get an overall behavior of k_e for the inelastic probability as claimed.

To show that indeed as $k_e \to 0$ the amplitude of $\phi(x; k_{ex})$ in the internal region $x < a$ goes to zero as $k_e \sim \sqrt{\epsilon}$, we temporarily disregard the required normalization of $\phi(x; k_x)$ of Eq. (6.7) and fix its initial conditions (slope and value) at some point inside the interaction region $x < a$ such that the regularity condition is ensured. We then integrate out to $x = a$. Let us denote this unnormalized solution with a prime, as $\phi'(x; k_x)$. The point is for k_x varying near 0, both v(the value) and s(the slope) that the solution emerges with at $x = a$, are independent of k_x and in fact the interior solution thus obtained is itself independent of k_x. This is because the local wave vector $k(x) = \sqrt{2m(\epsilon - U(x))/\hbar^2}$ essentially stays the same function of x for all ϵ near 0. Therefore for $x > a$ $\phi(x; k_x)$ continues onto

$$v \cos[k_x(x-a)] + \frac{s}{k_x} \sin[k_x(x-a)] \qquad x > a \tag{6.8}$$

This is a phase-shifted sine wave of amplitude $\sim 1/k_x$. We must enforce the normalization of Eq. (6.7) and get $\phi(x; k_x) \sim k_x \phi'(x; k_x)$. As a result, the

interior solution gets multiplied by k_x and we thereby have our result. $\phi(x;k_x)$ is the solution of a one-dimensional Schrodinger equation for the incoming particle in the one-dimensional long-range potential created by the slab. The suppression of its amplitude by $\sqrt{\epsilon}$ near the slab is due to the reflection it suffers where the interaction turns on. Within the perturbative set-up the non-sticking conclusion is then already foregone[1].

The problem is whether we can really accept this verdict of the one-dimensional unperturbed solution, when in fact we know that the turning on of the perturbation (many body interactions) causes a multitude of resonances to be created, internal resonances being exactly the situation in which the Proposition above is known to badly fail. It appears that the perturbation is in no sense a small physical effect. Therefore a nonpeturbative approach is needed. Here we use R-matrix theory in its general form to accomplish the task.

6.4 S-matrix and R-matrix

One point that the preceding section has made clear is that it is the energies (both initial and final) in the x-direction, perpendicular to the slab that are most relevant. In fact as regards the final form of our answers the motion of the y degree of freedom may as well have been the motion of another internal degree of freedom of the slab. In other words, mathematically speaking, the y degree of freedom may be subsumed by incorporating it as just another u. For example, we may imagine the incident atom being confined in the y-direction by the walls of a wave-guide at $y = -L \text{and} L$ that is large enough so that it could not possibly change the physics of sticking. Then we quite rigorously have a bound internal state of the form

$$\Omega_{c,n}(y,u) = \Omega_c(u) \sin \frac{n\pi y}{L} \tag{6.9}$$

x is now the only scattering degree of freedom. There will be no necessity in carrying along the extra index n and variable y as in Eq. (6.9), and we will simply continue to write $\Omega_c(u)$ instead. Thus with this understanding, the problem is essentially one-dimensional in the scattering degree of freedom.

We proceed to derive the expression for the **S** matrix in terms of the so-called **R** matrix, and derive the structure of the **R** matrix. For simplicity we continue to assume for the moment that there is no interaction for $x > a$. Then for $x > a$, the scattering wavefunction of the interacting system corresponding to the scattering particle coming in on one entrance channel, say $c = e$, with energy $\epsilon = \hbar^2 k_e^2/(2m)$ is

$$\psi(x,u) = \sum_{c=1}^{\infty} \left(\frac{e^{-ik_e x}}{\sqrt{k_e}} \delta_{ce} - \frac{e^{ik_c x}}{\sqrt{k_c}} S_{ce} \right) \Omega_c(u) \qquad x > a \tag{6.10}$$

where the sum must include all channels, even though the open channels are finite in number. The factors of $k_c^{-1/2}$ in Eq. (6.10) mean that the flux in each

channel is proportional only to the square of the coefficient and hence ensure the unitarity of $\mathbf{S}$. With this convention, the open-open part of the $\mathbf{S}$-matrix—the $n \times n$ submatrix $S_{cc'}$ with $c, c' = 1, 2, \ldots, n$—is unitary. $\sqrt{k_c} \equiv e^{i\pi/4}\sqrt{\kappa_c}$ may be arbitrarily chosen since it cannot affect the open-open part of $\mathbf{S}$.

$\mathbf{S}$ is found in analogy to the one-dimensional case by introducing the matrix version of the inverse logarithmic derivative at $x = a$ called $\mathbf{R}(E)$ the Wigner $\mathbf{R}$-matrix defined by

$$\vec{v} = \mathbf{R}(E)\ \vec{s} \tag{6.11}$$

where the components of $\vec{v}$ and $\vec{s}$ are the expansion coefficients of $\psi(x = a, u)$ and $\frac{\partial\psi(x=a,u)}{\partial x}$ respectively in the $\Omega_c(u)$ basis. Supposing $\frac{\partial\psi(x=a,u)}{\partial x}$ to be known, we will (like in electrostatics) use the Neumann Green's function $G_N(x, u; x', u')$ to construct $\psi(x, u)$ everywhere in the interior $x < a$. $\psi(x, u)$ satisfies the full Schrödinger equation with energy E. We need $\chi_\lambda(x, u)$ $\lambda = 1, 2, \cdots$, the normalized eigenfunctions of the full Schrödinger equation in the interior $x < a$ with energies E_λ, satisfying Neumann boundary conditions $\frac{\partial\chi(x=a,u)}{\partial x} = 0$. So

$$\left(\frac{-\hbar^2}{2m}\nabla^2 + V_{\text{int}}(x, u) - E\right)\psi(x, u) = 0 \tag{6.12}$$

$$\left(\frac{-\hbar^2}{2m}\nabla^2 + V_{\text{int}}(x, u) - E_\lambda\right)\chi_\lambda(x, u) = 0 \tag{6.13}$$

$$\left(\frac{-\hbar^2}{2m}\nabla^2 + V_{\text{int}}(x, u) - E\right)G_N(x, u; x', u') = \delta(x - x')\delta(u - u') \tag{6.14}$$

where $\nabla^2 \equiv \frac{\partial^2}{\partial x^2} + \frac{\partial^2}{\partial u^2}$ and

$$\frac{\partial G_N(x = a, u; x', u')}{\partial x} = 0 \qquad \text{and} \qquad \frac{\partial\chi(x = a, u)}{\partial x} = 0 \tag{6.15}$$

$$\Rightarrow G_N(x, u; x', u') = \sum_{\lambda=1}^{\infty} \frac{\chi_\lambda(x, u)\chi_\lambda(x', u')}{E_\lambda - E} \tag{6.16}$$

G_N is symmetric in the primed and unprimed variables. By Stokes' Theorem,

$$(-\hbar^2/2m) \int_{x'<a} dx' \int_{\text{all u'}} du' \left(\phi_1\nabla'^2\phi_2 - \phi_2\nabla'^2\phi_1\right) = (-\hbar^2/2m) \int_{\text{x'=a, all u'}} du' \left(\phi_1\nabla'_{\hat{n}}\phi_2 - \phi_2\nabla'_{\hat{n}}\phi_1\right) \tag{6.17}$$

where $\nabla'_{\hat{n}}(\cdot) \equiv \hat{x}'(\cdot) \cdot \nabla'$ with $\phi_1 = \psi(x', u')$ and $\phi_2 = G_N(x, u; x', u')$ gives

$$\psi(x, u) = \frac{\hbar^2}{2m} \int_{\text{all u'}} du'\ G_N(x, u; x', u')\frac{\partial\psi(x' = a, u')}{\partial x'} \qquad x < a \tag{6.18}$$

Put $x = a$ and it is deduced using Eqs. (6.11) and (**??**) together that

$$R_{cc'}(E) = \sum_{\lambda=1}^{\infty} \frac{\gamma_{\lambda c}\gamma_{\lambda c'}}{E_\lambda - E} \tag{6.19}$$

where $\gamma_{\lambda c} = \sqrt{\frac{\hbar^2}{2m}} \int_{\text{all u}} du\ \chi_\lambda(a, u)\Omega_c(u)$.

6.4.1 The S matrix

Now shifting attention to the outside ($x > a$), we see that we can compute both $\nabla_{\hat{n}}\psi(a,u)$ and $\psi(a,u)$ on the surface $x = a$ using the asymptotic form of Eq. (6.10) which automatically gives these expanded in the $\Omega_c(u)$ basis. Writing the matrix Eq. (6.11) is now simple. It is best to do it all in matrix notation, and thus be able to treat all possible independent asymptotic boundary conditions simultaneously.

Let e^{ikx}, $\sqrt{k}$ and $1/\sqrt{k}$ be diagonal matrices with diagonal elements $e^{ik_c x}$, $\sqrt{k_c}$ and $1/\sqrt{k_c}$. Then Eq. (6.11) reads

$$\frac{e^{-ika}}{\sqrt{k}} - \frac{e^{ika}}{\sqrt{k}}\mathbf{S} = i\mathbf{R}k\left(\frac{-e^{-ika}}{\sqrt{k}} - \frac{e^{ika}}{\sqrt{k}}\mathbf{S}\right) . \tag{6.20}$$

Each column $c = 1, \ldots, n$ of the matrix equation above is just Eq. (6.11) for the solution corresponding to an incoming wave only in channel c (For $c > n$ the wavefunctions blow up as $x \to \infty$). Remembering that non-diagonal matrices don't commute, we solve for $\mathbf{S}$ to get

$$\mathbf{S} = e^{-ika}\sqrt{k}\frac{1}{1 - i\mathbf{R}k}(1 + i\mathbf{R}k)\frac{1}{\sqrt{k}}e^{-ika} \tag{6.21}$$

or, with some simple matrix manipulation,

$$\mathbf{S} = e^{-ika}\frac{1}{1 - i\sqrt{k}\mathbf{R}\sqrt{k}}(1 + i\sqrt{k}\mathbf{R}\sqrt{k})e^{-ika} . \tag{6.22}$$

6.5 S matrix near a resonance

As discussed in the introduction, the resonances are a key to the sticking issue. Sticking is essentially a long lived Feshbach resonance in which energy has been supplied to surface and bulk degrees of freedom, temporarily dropping the scattering particle into a bound state of the attractive potential. Thus we must study resonances in various circumstances in the low incident translational energy regime. We derive the approximation for $\mathbf{S}(E)$ near $E = E_0$, a resonant energy of the compound system. E_0 is the total energy of the joined (resonant) system. Within the R-matrix approach, the $\chi_\lambda(x,u)$ of section 6.4 are bound, compound states with Neuman boundary conditions at $x = a$. R-matrix theory properly couples these bound state to the continuum, but some of the eigenstates are nonetheless weakly coupled to the continuum, as evidenced by small values of the $\gamma_{\lambda c}$'s of section 6.4; these are the measure of the strength of the continuum couplings. While every one of the $R-$matrix bound states will result in a pole E_λ in the R matrix expansion, only the weakly coupled ones are the true long lived Feshbach resonances of physical interest. It is also helpful to know that the values of these 'truly' resonant poles at E_λ are the most stable to changes in the position $x = a$ of the box. This in fact provides one unambiguous way to identify them. Our purpose here is to derive the resonant approximation

to the **S** matrix in the vicinity of one of these Feshbach resonances. We do so using the form of the **R**-matrix in Eq. (6.19}). Note that the energy density $\rho(E) = 1/D(E)$ of these Feshbach resonances will be large because of the large number of degrees of freedom of the target. $D(E)$ is the level spacing of the quasibound, resonant states.

6.5.1 Isolated Resonance

As mentioned, the point of view we will take is to identify a resonant energy with a particular pole E_λ in the **R** matrix expansion of Eq. (6.19). Those E_λ corresponding to resonances are a subsequence of the E_λ appearing in the expansion in Eq. (6.19). For E near a well isolated resonance at E_λ we separate the sum-over-poles expansion of the R-matrix into a single matrix term having elements $\frac{\gamma_{\lambda c}\gamma_{\lambda c'}}{E_\lambda - E}$, plus a sum over all the remaining terms, call it N. If the energy interval between E_λ and all the other poles is large compared to the open-open residue at E_λ then we may expect that the $n \times n$ open-open block of N will have all its elements to be small. Then rewriting the inverse in Eq. (6.22)

$$\frac{1}{1 - i\sqrt{k}\mathbf{R}\sqrt{k}} \equiv \frac{1}{1 - i\left(M + \frac{V}{E_\lambda - E}\right)} \tag{6.23}$$

where $M \equiv \sqrt{k}N\sqrt{k}$ and $V_{cc'} \equiv (\sqrt{k_c}\gamma_{\lambda c})(\sqrt{k_{c'}}\gamma_{\lambda c'})$, and setting $M = 0$ allows us to simplify the central term in Eq. (6.22) exactly. (We will return to the case $M \neq 0$.)

$$\begin{aligned}
& \frac{1}{1 - i\sqrt{k}\mathbf{R}\sqrt{k}}(1 + i\sqrt{k}\mathbf{R}\sqrt{k}) && (6.24)\\
= \;& 1 + \frac{1}{1 - i\sqrt{k}\mathbf{R}\sqrt{k}} 2i\sqrt{k}\mathbf{R}\sqrt{k} && (6.25)\\
= \;& 1 + \frac{1}{1 - \frac{iV}{E_\lambda - E}} 2i\frac{V}{E_\lambda - E} \qquad (\text{with} M = 0) && (6.26)\\
= \;& 1 + \frac{1}{E_\lambda - E - iV} 2iV && (6.27)\\
= \;& 1 + \frac{1}{E_\lambda - E - i(\Gamma_\lambda/2 + i\Delta E)} 2iVk && (6.28)
\end{aligned}$$

where we used

$$\begin{aligned}
V^2 &= \left((\gamma_{\lambda 1}^2 k_1 + \cdots + \gamma_{\lambda n}^2 k_n) + (\gamma_{\lambda(n+1)}^2 \kappa_{n+1} + \cdots)\right) V && (6.29)\\
&\equiv \left(\left(\frac{\Gamma_{\lambda 1}}{2} + \cdots + \frac{\Gamma_{\lambda n}}{2}\right) + i(\gamma_{\lambda(n+1)}^2 \kappa_{n+1} + \cdots)\right) V && (6.30)\\
&\equiv \left(\frac{\Gamma_\lambda}{2} + i\Delta E_\lambda\right) V && (6.31)
\end{aligned}$$

to get the identities

$$[E_\lambda - E - iV]V = [E_\lambda - E - i(\Gamma_\lambda/2 + i\Delta E)]V \tag{6.32}$$

$$\Rightarrow \frac{1}{E_\lambda - E - i(\Gamma_\lambda/2 + i\Delta E)}V \quad = \quad \frac{1}{E_\lambda - E - iV}V \tag{6.33}$$

Also define $(\Gamma_{\lambda c}/2)^{1/2} \equiv \gamma_{\lambda c}\sqrt{k_c}, c = 1, 2, \cdots, n$. This defines the sign of the square-root on the lhs. to be the sign of $\gamma_{\lambda c}$ and allows the convenience of expressing things in terms of the $\Gamma_{\lambda c}$'s and their square-roots, and not having to use the $\gamma_{\lambda c}$'s themselves. Thus we arrive at

$$S_{cc'} = e^{-ik_c a}\left(\delta_{cc'} + \frac{i\Gamma_{\lambda c}^{1/2}\Gamma_{\lambda c'}^{1/2}}{E_\lambda^{(r)} - E - i\Gamma_\lambda/2}\right)e^{-ik_{c'}a} \tag{6.34}$$

where $E_\lambda^{(r)} \equiv E_\lambda + \Delta E_\lambda$, for the $n \times n$ open-open unitary block of S in the neighbourhood of a single isolated resonance after neglecting the contribution of the background matrix M. For us the essential point is that

$$\Gamma_{\lambda c} = 2\,k_c(E)\gamma_{\lambda c}^2, \tag{6.35}$$

that the partial widths $\Gamma_{\lambda c}$ depend on the energy E, through the kinematic factor $k_c(E)$. Mostly this energy dependence is small and irrelevant except where the k_c's and hence $\Gamma_{\lambda c}$'s are varying near 0. These are the partial widths of the open channels near threshold. Hence $|S_{ce}|^2$ $(c \neq e)$ an inelastic probability behaves like $k_e \sim \sqrt{\epsilon}$ when the entrance channel is at threshold. Including the background term $(M \neq 0)$ does not change this. To see this we may perform the inverse in Eq. (6.22) to first order in M and then get an additional contribution of the terms

$$e^{-ika}\left(\frac{2i}{1-\frac{iV}{E_\lambda - E}}M + \frac{1}{1-\frac{iV}{E_\lambda - E}} + \frac{1}{1-\frac{iV}{E_\lambda - E}}iM\frac{1}{1-\frac{iV}{E_\lambda - E}}2iV\right)e^{-ika} \tag{6.36}$$

to the S-matrix. Now, both M and V have a factor of $\sqrt{k_c}$ multiplying their cth columns (and rows) from their definitions and so a matrix element $b_{cc'}$ of the matrix in parentheses in Eq. (6.36) will have a $\sqrt{k_c}$ and $\sqrt{k_{c'}}$ dependence. An inelastic element of $S(c \neq c')$ would now take the form

$$S_{cc'} = e^{-ik_c a}\left(b_{cc'} + \frac{i\Gamma_{\lambda c}^{1/2}\Gamma_{\lambda c'}^{1/2}}{E_\lambda^{(r)} - E - i\Gamma_\lambda/2}\right)e^{-ik_{c'}a}, \tag{6.37}$$

As mentioned our interest is in the case when the entrance channel is at threshold so that this dependence is $\sqrt{k_e}$, making the inelastic probability $|S_{ce}|^2$ still continue to behave as $k_e \sim \sqrt{\epsilon}$.

6.5.2 Overlapping Resonances

Here we require the form of the **S** matrix near an energy E where many of the quasibound states may be simultaneously excited, i.e. the resonances overlap.

Again, neglecting background for the moment, the **S** matrix is simply taken to be a sum over the various resonances.

$$\mathbf{S} = 1 - \sum_{\lambda} \frac{iA_\lambda}{E - E_\lambda^{(r)} + i\Gamma_\lambda/2} \tag{6.38}$$

where A_λ is a $n \times n$ rank 1 matrix with the cc'th component as $\Gamma_{\lambda c}^{1/2}\Gamma_{\lambda c'}^{1/2}$. There is no entirely direct justification of this form, but one can see that there is much which it gets correct.

The A_λ are symmetric, hence **S** is symmetric. Obviously it has the poles in the right places allowing the existence of decaying states with a purely outgoing wave at the resonant energies. A crucial additional assumption that also makes **S** approximately unitary is that the signs of the $\Gamma_{\lambda c}^{1/2}$ are random and uncorrelated both in the index λ as well as c, regardless of how close the energy intervals involved may be. One simple consequence is that we approximately have that

$$A_\lambda A_{\lambda'} = \delta_{\lambda\lambda'}\Gamma_\lambda A_\lambda \tag{6.39}$$

in the sense that the l.h.s. is negligible for $\lambda \neq \lambda'$ in comparison to the value for $\lambda = \lambda'$. With Eq. (6.39) it is easy to verify the approximate unitarity of **S**.

We investigate now the onset of the overlapping regime as E increases. $D(E)$, the level spacing of the resonant $E_\lambda^{(r)}$, is a rapidly decreasing function of its argument. On the other hand, $\Gamma_\lambda = \Gamma_{\lambda 1} + \Gamma_{\lambda 2} + \cdots + \Gamma_{\lambda n}$, and since more channels are open at higher energy, Γ_λ is increasing with the energy of the resonance. The widths must therefore eventually overlap, and $\Gamma_\lambda \gg D\left(E_\lambda^{(r)}\right)$ for the larger members of the sequence of $E_\lambda^{(r)}$'s. In this regard there is a useful estimate due to Bohr and Wheeler [**?**], that for n large

$$\frac{\Gamma_\lambda}{D(E_\lambda^{(r)})} \simeq n \ . \tag{6.40}$$

Appendix C.1 derives this using a phase space argument. Here we point out that this is entirely consistent with the assumption of the random signs, indeed requiring it to be true. Take for example a typical inelastic amplitude

$$\mathbf{S}_{cc'} = -i \sum_{\lambda} \frac{\Gamma_{\lambda c}^{1/2}\Gamma_{\lambda c'}^{1/2}}{E_\lambda^{(r)} - E - i\Gamma_\lambda/2} \qquad (c \neq c') \tag{6.41}$$

First let us note that the Γ_λ being the sum of many random variables (the partial widths $\Gamma_{\lambda c}$) do not fluctuate much. Let Γ denote their typical value over the n overlapping resonances. Also since $\Gamma = nD$ it follows that the typical size of a partial width $\Gamma_{\lambda c}$ is D. Therefore the typical size of the product $\Gamma_{\lambda c}^{1/2}\Gamma_{\lambda c'}^{1/2}$ is D but these random variables fluctuate randomly over the index λ, and moreover the sign is random. Thus for energies in the overlapping domain $S_{cc'}$ is a sum of n complex numbers each of typical size $D/\Gamma = 1/n$, but random in sign. This makes for a sum of order $1/\sqrt{n}$. Clearly this is as required to make the $n \times n$

matrix $\mathbf{S}$ unitary. Note that the above argument fails (as is should) if $c \neq c'$ because then the signs of $\Gamma_{\lambda c}^{1/2}\Gamma_{\lambda c}^{1/2} = \Gamma_\lambda > 0$ are of course not random.

Unlike the case of the isolated resonance, the S-matrix elements here are smoothly varying in E. Addition of a background term $B_{cc'}$

$$\mathbf{S}_{cc'} = B_{cc'} - i\sum_\lambda \frac{\Gamma_{\lambda c}^{1/2}\Gamma_{\lambda c'}^{1/2}}{E_\lambda^{(r)} - E - i\Gamma_\lambda/2}. \tag{6.42}$$

just shifts this smooth variation by a constant. If $B_{cc'}$ is also thought of as arising from a sum over the individual backgrounds then for the same reasons as discussed at the end of the preceding section $|B_{ce}|^2 \sim k_e \sim \sqrt{\epsilon}$ for an entrance channel near threshold. For simplicity we will continue to take $B_{cc'}$ to be 0 and look at the case with background in the appendix.

6.6 Q-matrix and Sticking

From the viewpoint of scattering theory, the sticking of the incident particle to the target is just a long-lived resonance. It is natural then to investigate the time-delay for the collision. Smith[14] introduced the collision lifetime or Q-matrix

$$\mathbf{Q} \equiv i\hbar\mathbf{S}\frac{\partial\mathbf{S}^\dagger}{\partial E} \tag{6.43}$$

which encapsulates such information. We review some of the relevant properties of $\mathbf{Q}$. The rhs of Eq. (**??**) involves the 'open-open' upper left block of $\mathbf{S}$ so that $\mathbf{Q}$ is also an $n \times n$ energy-dependent matrix, having dimensions of time. For 1-dimensional elastic potential scattering $\mathbf{S} = e^{i\phi(e)}$ and $\mathbf{Q}$ reduces to the familiar time delay $i\hbar\frac{\partial\phi(E)}{\partial E}$. If $\vec{v}$ is a vector whose entries are the coefficients of the incoming wave in each channel then $\vec{v}^{\dagger\ \mathrm{r}}\mathbf{Q}(E)\vec{v}$ is the average delay time experienced by such an incoming wave. Because physically the particle is incident on only one channel, $\vec{v}$ consists of all 0's except for a 1 in the eth slot so that the relevant quantity is just the matrix element $\mathbf{Q}_{ee}(E)$. Smith shows that this delay time is the surplus probability of being in a neighborhood of the target (measured relative to the probability if no target were present) divided by the flux arriving in channel e. This matches our intuition that when the delay time is long, there is a higher probability that the particle will be found near the target.

Furthermore, as a Hermitian matrix, $\mathbf{Q}(E)$, can be resolved into its eigenstates $\vec{v}^{(1)} \cdots \vec{v}^{(n)}$ with eigenvalues $q_1 \cdots q_n$. The components of $\vec{v}^{(1)}$ are the incoming coefficients of a quasi-bound state with lifetime q_1 and so on. Then

$$\vec{v}^{\dagger\ \mathrm{r}}\mathbf{Q}(E)\vec{v} = \sum_{j=1}^{n} q_j|\vec{v}^{(j)} \cdot \vec{v}|^2. \tag{6.44}$$

As can be seen from this expression, the average time delay results, in general, from the excitation of multiple quasi-stuck states each with its lifetime q_j and

probability of formation $|\vec{v}^{(j)} \cdot \vec{v}|^2$. However, we will find that using our resonant approximation to the **S** matrix near a resonant energy $E_\lambda^{(r)}$ the time delay will consist of only one term from the sum on the rhs of Eq. (6.44), all the other eigenvalues being identically 0.

Using equation Eq. (**??**),

$$\mathbf{Q}(E) = i\hbar\left(\sum_{\lambda'} \frac{-iA_{\lambda'}}{\left[E - E_{\lambda'}^{(r)} - i\Gamma_{\lambda'}/2\right]^2} - \sum_{\lambda\lambda'} \frac{A_\lambda A_{\lambda'}}{\left[E - E_\lambda^{(r)} + i\Gamma_\lambda/2\right]\left[E - E_{\lambda'}^{(r)} - i\Gamma_{\lambda'}/2\right]^2}\right) \quad (6.45)$$

which using Eq. (6.39) simplifies to

$$= \sum_\lambda \frac{\hbar}{(E - E_\lambda^{(r)})^2 + (\Gamma_\lambda/2)^2} A_\lambda \ , \quad (6.46)$$

a remarkably simple answer. We need $Q_{ee}(E)$, where e is the entrance channel.

$$Q_{ee}(E) = \sum_\lambda \frac{\hbar\Gamma_{\lambda e}}{(E - E_\lambda^{(r)})^2 + (\Gamma_\lambda/2)^2} \quad (6.47)$$

$$= \sum_\lambda \left(\frac{\hbar\Gamma_\lambda}{(E - E_\lambda^{(r)})^2 + (\Gamma_\lambda/2)^2} \times \frac{\Gamma_{\lambda e}}{\Gamma_\lambda}\right) \quad (6.48)$$

where the second equation has the interpretation (for each term) as the life-time of the mode, multiplied by the probability of its formation. Note how for each resonance $E_\lambda^{(r)}$ there is only one term corresponding to the decomposition of Eq. (6.44). The actual measured lifetime is the average of $Q_{ee}(E)$ averaged over the energy spectrum $|g(E)|^2$ of the collision process.

6.6.1 Energy averaging over spectrum

With the target in state $\Omega_e(u)$ where $c = e$ is the entrance channel, the energy of the target is fixed, and the time-dependent solution will look like

$$\psi(x,u,t) = \int dE \left(g(E) \sum_{c=1}^{\infty} \left(\frac{e^{-ik_c(E)x}}{\sqrt{k_e(E)}}\delta_{ce} - \frac{e^{ik_c(E)x}}{\sqrt{k_c(E)}} S(E)_{ce}\right) \Omega_c(u)\right) . \quad (6.49)$$

Recall, E is the total energy of the system. We are interested in the threshold situation where the incident kinetic energy of the incoming particle $\epsilon \to 0$. This can be arranged if $g(E)$ is peaked at E_0 with a spread ΔE such that i) E_0 is barely above E_e^{target} and ii) $\Delta E = \delta\epsilon$ is some small fraction of ϵ, the mean energy of the incoming particle. The second condition ensures that we may speak unambiguously of the incoming particle's mean energy. So,

$$\langle Q_{ee}(E)\rangle \equiv \int dE |g(E)|^2 Q_{ee}(E) \quad (6.50)$$

$$\simeq \frac{1}{\Delta E}\int dE Q_{ee}(E) \quad (6.51)$$

$\langle\rangle$ denotes the average over the ΔE interval. Now $Q_{ee}(E)$ is just a sum of Lorentzians centred at the $E_\lambda^{(r)}$'s with width Γ_λ and Eq. (6.51) is just a measure of their mean value over the ΔE interval.

So long as the ΔE interval around which we are averaging, is broad enough to straddle many of these Lorentzians, the mean height is just

$$\frac{1}{\Delta E} \times \rho(E)\Delta E \times \frac{\hbar\pi\Gamma_{\lambda e}}{\Gamma_\lambda} \tag{6.52}$$

where the second factor is the number of Lorentzians in the ΔE interval and the third factor is the area under the 'λth' Lorentzian. This is true regardless of whether or not they are overlapping. It will be convenient to write Γ_λ as

$$\Gamma_\lambda = n \times 2\bar{k}_\lambda \,\mathrm{var}(\gamma_\lambda) \tag{6.53}$$

where $\mathrm{var}(\gamma_\lambda)$ is the variance of the set of $\gamma_{\lambda c}{}'s$ over the n open channels and $\bar{k}_\lambda$ is a mean or effective wavenumber k_c over the open channels, which for a particular realization λ we take to be defined by Eq. (6.53) itself. Let $\langle\ \rangle$ denote the average over the occurrences of the quantity in the ΔE interval. $\Gamma \equiv \langle\Gamma_\lambda\rangle$, $\bar{k} \equiv \langle\bar{k}_\lambda\rangle$. Then Eq. (6.52) simplifies

$$\langle Q_{ee}(E)\rangle \simeq \hbar\frac{1}{D}\frac{k_e\langle\gamma_{\lambda e}^2\rangle}{n\bar{k}\langle\mathrm{var}(\gamma_\lambda)\rangle} \tag{6.54}$$

$$\simeq \frac{\hbar}{\Gamma}\frac{k_e}{\bar{k}} \tag{6.55}$$

which tends to 0 as $k_e \sim \sqrt{\epsilon}$. The form of Eq. (6.55) and all the steps leading up to it remain valid whether the Lorentzians are overlapping or not, as long as the $\Delta E = \Delta\epsilon$ interval which we are averaging over includes many of them.

6.6.2 On an isolated resonance

If the target is cold enough that the resonances are isolated, then as the incident particle's energy $\epsilon \to 0$, adhering to the condition $\Delta\epsilon < \epsilon$ will eventually result in $\Delta\epsilon$ becoming narrower than the resonance widths. It becomes possible then for $\Delta\epsilon$ to be centered right around a single isolated resonance at $E_\lambda^{(r)}$. In this case $\langle Q_{ee}(E)\rangle$ is found simply by putting $E = E_\lambda^{(r)}$, because the spectrum $|g(E)|^2$ is well approximated by $\delta(E - E_\lambda^{(r)})$. So

$$\langle Q_{ee}(E)\rangle = \frac{\hbar\Gamma_{\lambda e}}{\Gamma_\lambda^2} = \frac{\hbar}{\Gamma_\lambda}\frac{\Gamma_{\lambda e}}{\Gamma_\lambda} = \frac{\hbar}{\Gamma_\lambda}\frac{k_e}{n\bar{k}}\ . \tag{6.56}$$

Even in this case there is the $\sqrt{\epsilon}$ behavior as $\epsilon \to 0$ and there is no sticking.

In the extreme case that there are no other open channels at all ($n = 1$), $\langle Q_{ee}(E)\rangle \simeq \frac{\hbar\Gamma_{\lambda e}}{\Gamma_\lambda^2} = \frac{\hbar}{\Gamma_{\lambda e}}$ because $\Gamma_\lambda = \Gamma_{\lambda e}$. In fact, $e = 1$, and $\langle Q_{ee}(E)\rangle$ diverges, implying in this case that it is possible to have the particle stick. This is an exception to all the cases above but is experimentally not so relevant because we may always expect to find some exothermic channels open for a target with many degrees of freedom.

6.7 Inelastic cross sections and sticking

Another physically motivated measure of the sticking probability may be obtained by studying the total inelastic cross-section of the collision. The idea is that any long lived "sticking" is overwhelmingly likely to result in an inelastic colision process; i.e. that the scattering particle will leave in a different channel than it entered with. Using the original Wigner approach it is possible to show that for our case where we have only one scattering degree of freedom, the inelastic probability for an exothermic and endothermic collision vanishes like k_e. The only possible exception to this is a measure zero chance of a resonance exactly at the threshold energy, E_e^{target}. In the event that there is a resonance $E_\lambda^{(r)}$ close to but above this threshold energy, it is only necessary that E is below $E_\lambda^{(r)}$ (by an energy of at least ΔE, the spread in energy) in order to observe the usual Wigner threshold behavior:

$$P_{\text{inelastic}} \to 0 \quad \text{like} \quad k_e \propto \sqrt{\epsilon} \tag{6.57}$$

for the inelastic probability. However our problem is unusual in the sense that because of the large number of degrees of freedom of the target, we will always find resonances between E_e^{target} and E no matter how small $E - E_e^{\text{target}} = \epsilon$ is. Thus the Wigner regime is not accessible. Still the surprise is that a simple computation reveals the same behavior holds for large n:

$$\begin{aligned}
P_{\text{inelastic}}(E) &= \sum_{c \neq e} P_{c \leftarrow e}(E) && (6.58)\\
&= \sum_{c \neq e} |S_{ce}(E)|^2 && (6.59)\\
&= \sum_{c \neq e} \sum_{\lambda} \sum_{\lambda'} \frac{{\Gamma_{\lambda c}}^{1/2} {\Gamma_{\lambda e}}^{1/2}}{E - E_\lambda^{(r)} - i\Gamma_\lambda/2} \frac{{\Gamma_{\lambda' c}}^{1/2} {\Gamma_{\lambda' e}}^{1/2}}{E - E_\lambda^{(r)} + i\Gamma_\lambda/2} && (6.60)\\
\Rightarrow P_{\text{inelastic}}(E) &= \sum_{\lambda} \frac{\Gamma_\lambda}{(E - E_\lambda^{(r)})^2 + (\Gamma_\lambda/2)^2} \Gamma_{\lambda e} && (6.61)
\end{aligned}$$

where we used the random sign property of the $\Gamma_{\lambda c}^{1/2}$'s and the understanding that $\sum_{c \neq e} \Gamma_{\lambda c} \simeq \sum_{\text{all c}} \Gamma_{\lambda c} = \Gamma_\lambda$. Since the sum $\sum_{c \neq e}$ is over the $n \gg 1$ open channels, omission of a single term can hardly matter. Apart from the factor $\hbar/\Gamma_\lambda$, the rhs of the above equation is identical to the expression for $Q_{ee}(E)$ in Eq. (6.48). Averaging $P_{\text{inelastic}}(E)$ over many resonances $E_\lambda^{(r)}$ (overlapping or not) we may use the same algebraic simplifications as before to show

$$\langle P_{\text{inelastic}} \rangle = \frac{k_e}{\bar{k}} \tag{6.62}$$

As k_e tends to 0, this gives the $\sqrt{\epsilon}$ Wigner behavior showing that there is no sticking.

The above argument fails when there is only one open channel. There are no inelastic channels to speak of. In this case, if the energy E coincides with a resonant energy $E_\lambda^{(r)}$ we will have the exceptional case of sticking, as discussed at the end of the previous section. But as pointed out there, this is primarily of theoretical interest only.

6.8 Channel Decoherence

The only case for which we stick is seen to be the case of when we are sitting right on top of a resonance with the incoming energy so well resolved that we are completely within the resonance width, AND there are no exothermic channels open. Having no such channels open amounts to an infintesimally low energy for a large target. Otherwise, the sticking probability tends to 0 as $\sqrt{\epsilon}$ in every case.

6.8.1 Time dependent picture

From the time independent point of view, the physical reason for the absence of low energy sticking is contained in the factor $\frac{\Gamma_{\lambda e}}{\Gamma_\lambda}$ of Eq. (6.48). This is the formation probability for the compound state. We will explain physically why it is small for $n \gg 1$. The resonance state is a many-body entangled state. If we imagine the decay of this compound state (already prepared by some other means say) each open channel carries away some fraction of the outgoing flux, with no preference for any one particular channel. Running this whole process in reverse it becomes evident that the optimum way to *form* the compound state is to have each channel carry an incoming flux with exactly the right amplitude and phase. This corresponds to however an entangled initial state. With all the incoming flux instead constrained to be in only one channel it becomes clear that we are not exciting the resonance in the optimal way and the buildup of amplitude inside is not so large; i.e., the compound state has a small probability of forming.

The time dependent view is even more revealing. Imagine a wave packet incident on the system. For a single open channel Feshbach resonance, the build-up of amplitude in the interior region can be decomposed as follows. As the leading edge of the wavepacket approaches the region of attraction, most is turned away due to the quantum reflection phenomena. (It is a useful model to think of the quantum reflection as due to a barrier located some distance away from the interaction region.) The wavefunction in the interaction region constructively interferes with new amplitude entering the region. At the same time, the amplitude leaving the region is out of phase with the reflected wave, cancelling it and assisting more amplitude to enter.

Now suppose many channels are open. All the flux entering the interior must of course return, but it does so fragmented into all the other open channels. Only the fraction that makes it back into the entrance channel has the opportunity to interfere (constructively) with the rest of the entering wavepacket. The con-

structive interference is no longer efficient and is in fact almost negligible for $n \gg 1$, thereby ruining the delicate process that was responsible for the buildup of the wave function inside. The orthogonality of the other channels prevents interference in the scattering dimension. If we trace over the target coordinates, leaving only the scattering coordinate, most of the coherence and the constructive interference is lost, and no resonant buildup occurs. Therefore, one way to understand the non-sticking is to say that decoherence is to blame.

6.8.2 Fabry-Perot and Measurement Analogy

Suppose we have a resonant quantum mechanical Fabry-Perot cavity, where the particle has a high probability of being found in between the two reflecting barriers. Now, during the time it takes for the probability to build up in the interior, suppose we continually measure the position of the particle inside. In doing so we decohere the wave function and in fact never find it there at all. Alternatively, imagine simply tilting one barrier (mirror) to make it non-parallel to the first and redirecting the flux into an orthogonal direction, again spoiling the resonance. Measurement entangles other (orthogonal) degrees of freedom with the one of interest, resulting in flux being effectively re-directed into orthogonal states. Thus the states of the target (if potentially excitable) are in effect continually monitoring (measuring) to see if the incoming particle has made it in inside, ironically then preventing it from ever doing so. The buildup process of constructive interference in the interaction region, described in the preceding paragraph, is slower than linear in t. Therefore, the constant measurement of the particle's presence (and resultant prevention of sticking) is an example of the Zeno "paradox" in measurement theory.

6.9 Conclusion

We have presented a general approach to the low energy sticking problem, in the form of R-matrix theory. This theory is well suited for the task, since it highlights the essential features of multichannel scattering at low incident translational energy. We did not need to make a harmonic or other approximate assumptions about the solid target, which is characterized by its long range interaction with the incoming particle and its density of states. "Warm" surfaces are included in the formalism, and do not change the non-sticking conclusion.

Several supporting arguments for the non-sticking conclusion were given. Perhaps most valuable is the physical decoherence picture associated with the conclusion that there is no sticking in the zero translational energy limit.

Reviewing the observations leading up to the non-sticking conclusion, we start with the near 100% sticking in the zero translational energy limit classically (sticking probability 1). We then invoke the phenomenon of quantum reflection (Fig.6.1), which keeps the incident particle far from the surface (sticking probability 0). Third, we note that quantum reflection can be overcome by resonances (Fig. 6.2), and since resonances are ubiquitous in a many body

target, being the Feshbach states by which a partice could stick to the surface, perhaps sticking approaches 1 after all. Fourth, we suggest that decoherence (from the perspective of the incoming channel, with elestic scattering definded as coherent) ruins the resonance effect, reinstating the quantum reflection as the determining effect. Finally, then, there is no sticking, and the short answer as to why is: quantum reflection and many channel decoherence. The ultrashort explanation is simply quantum reflection, but this is dangerous and non-rigorous, as we have tried to show.

All this does not tell us much about how sticking turns on as incident translational energy is raised. This is the subject of the following paper, where a WKB analysis proves very useful. Quantum reflection is a physical phenomenon liked directly to the failure of the WKB approximation.

Chapter 7

Transition from reflection to sticking in ultracold atom-surface scattering

Abstract

In ——- we showed that under very general circumstances, atoms approaching a surface will not stick as its incoming energy approaches zero. This is true of either warm or cold surfaces. Here we explore the transition region from non sticking to sticking as energy is increased. The key to understanding the transition region is the WKB approximation and the nature of its breakdown. Simple rules for understanding the rollover to higher energy, post-threshold behavior, including analytical formulae for some asymptotic forms of the attractive potential are presented. We discuss a practical example of atom-surface pair in various substrate geometries. We also discuss the case of low energy scattering from clusters.

7.1 Introduction

The problem of sticking of atoms to surfaces at very low collision velocities has a long history and has met with some controversy. The issue goes back to the early distorted wave Born approximation results of Lennard-Jones [1], who obtained the threshold law sticking probability going as k in the limit of low velocities. This paper is a companion to paper I [?], wherein we put the problem on a firmer theoretical foundation. We showed (non-perturbatively) that in an ultracold collision a simplistic one-body view of things is essentially correct even if the number of internal degrees of freedom is very large. We concluded that approaching atoms will not stick to surfaces if the approach velocity is low enough, even if the surface is warm. From the methods used, it is clear that the

non-sticking rule would apply to clusters as well as semi-infinite surfaces, and would also apply to projectiles more complex than atoms.

From an experimental perspective atom-surface sticking could impact the area of guiding and trapping atoms in material wires and containers. In those applications it is necessary to predict the velocities needed for quantum reflection, sticking, and the transition regime between them. We do so in this paper.

Above a certain temperature or kinetic energy, but still well below the attractive well depth of the atom surface potential, atoms will stick to surfaces with near 100 percent certainty. The reason for this is simple: Classical trajectory simulations of atom-surface collisions at low collision velocities indicate sticking with near certainty because the acceleration in the attractive regime is followed by a hard collision with the wall. This almost always leads to sufficient energy loss from the particle to the surface that immediate escape is not possible. This is true so long as the approach energy is significantly less than the well depth, which is itself greater than the temperature of the surface. Therefore, the onset of quantum reflection is heralded by a break down in the WKB approximation - an approximation based purely on the (sticking) classical trajectories.

Thus, there must exist a transition region between the non-sticking regime for very low collision velocities, and the sticking regime at higher velocities. The key to understanding the transition region is to understand the validity of classical mechanics (WKB) as applied to the sticking problem. The correctness of the simplistic one-body physics of quantum reflection from the surface, focusses our study on the WKB approximation to the coordinate normal to the surface. The entrance channel wavefunction thus obtained may also be used as input into the Golden Rule to study the threshold behaviour of the inelastic cross-sections. We do this in Section **??**. The nonsticking threshold behavior we established in paper I is interpreted as an extension of the validity of the so-called Wigner threshold behavior. We are also able to make definite predictions about the nature of the post threshold behavior of sticking in terms of inelastic cross-sections. (Section **??**).

7.2 Quantum reflection and WKB

} We consider the typical case of an attractive potential arising out of the cumulative effect of Van der Waals attractions between target and incident atoms. A classical atom would proceed straight into the interaction region showing no sign of reflection, but the quantum mechanical probability of being found inside is suppressed by a factor of k (as $k \to 0$) as compared to the classical probability (Section 7.6.1.1), where k is the wave vector of the incoming atom. This is tantamount to saying that quantum mechanically the amplitude is reflected back without penetrating the interaction region, analogous to the elementary case of reflection from the edge of a step-down potential in one dimension while attempting to go over the edge. A useful way to view this is to attribute the reflection to the failure of the WKB approximation.

To be specific, we keep the geometry of paper I in mind: an atom is incident

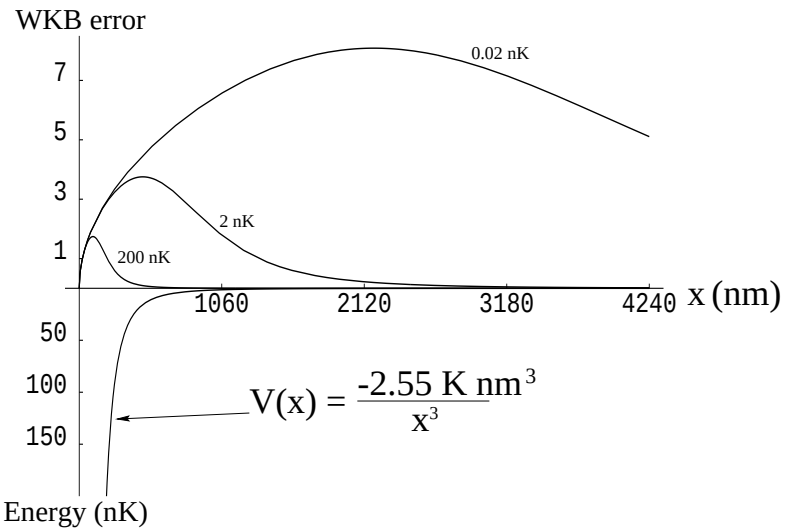

Figure 7.1: The WKB error of Eq. (7.1) for three different values of the incoming energy 200, 2 and 0.02 nK, vs. the distance x nm from the slab (SiN). The long range form of the potential $-c_3/x^3 (c_3 = 220\text{mev}\text{Å}^3)$ is also shown for which the negative 'y-axis' is calibrated in the different units of energy. The sticking probabilities for the three cases are approximately 1, 0.6, 0.1.

from the right ($x > 0$) upon the face of a slab ($x = 0$) that lies to the left of $x = 0$. For a low incoming energy $\epsilon \equiv \hbar^2 k^2/2m$, a left-moving WKB solution begun well inside the interaction region will fail to match onto a purely left-going WKB solution as we integrate out to large distances because the WKB criterion

$$|\lambda'(x)| = \left|\frac{\hbar p'}{p^2}\right| \ll 1 \tag{7.1}$$

for the local accuracy of the wavefunction will in general fail to be valid in some intermediate region. For bounded potentials that turn on abruptly for example at $x = a$, it is obvious that WKB will fail near $x \sim a$. For long-range potentials such as a power law $V(x) = -c_n/x^n$ it is not immediately obvious where this region of WKB failure lies, if it exists at all. It turns out that even in this case it is possible to identify (for small enough ϵ) a distance (dependent on ϵ) at which the potential 'turns on' and where WKB will fail. We will show below that WKB is at its worst ($|\lambda'(x)|$ is maximized) at a distance x where the kinetic and potential energies are approximately equal, i.e where $|V(x)| \sim \epsilon$. The distance away from the slab at which the particle is turned around - or quantum reflected - is precisely this distance. Furthermore, one may heuristically expect that the greater the failure of WKB, the greater the reflection.

Fig. (7.2) shows a plot of the error term in Eq. (7.1) for three different values of the incoming energy of neon on a semi-infinite slab of SiN. The essential

points to notice are:
1) There is a greater error incurred in attempting to apply the WKB (classical mechanics) approximation to colder atoms than to warmer ones. Consequently, we expect that the slower the atom, the more non-classical its behavior. In particular, slow enough atoms will be 'quantum reflected' and will not stick.
2) As the incoming velocity is decreased the atom is reflected at distances progressively further and further away from the slab. This is because the interval in x around which the WKB error is large, may be identified as the region from which the atom is reflected.

A useful qualitative rule of thumb obtained in Section **??** below is that the region of WKB error reaches all the way out to those regions where the potential energy is still roughly the same order of magnitude as the incoming energy (Eq. (7.5)). This means that as $\epsilon \to 0$ the error is still large where the potential energy graph looks essentially flat. In fact as $\epsilon \to 0$ it is easily shown that a plot of the WKB error will show a non-uniform convergence to a polynomial proportional to

$$x^{\frac{n}{2}-1} \qquad \text{for all } n > 0 \tag{7.2}$$

Fig. 7.2 shows the case for $n = 3$.

7.3 WKB failure

fail} Differentiating $p^2/2m + V(x) = \epsilon$ w.r.t. x, we have

$$p' = \frac{-mV'}{p} \tag{7.3}$$

which when used repeatedly to eliminate p' shows that $|p'/p^2|$ in Eq. (7.1) is maximized when

$$\frac{p^2}{3m} = \frac{V'^2}{V''}. \tag{7.4}$$

For $V(x) = -c_n/x^n$, this is exactly when

$$|V(x)| = \epsilon \left(\frac{2(n+1)}{n-2} \right). \tag{7.5}$$

We discover that for $n > 2$ only, we have a point where WKB is at its worst at a distance x where $|V(x)| \sim \epsilon$, and moreover, that this maximum behaves like

$$\max \left| \frac{p'}{p^2} \right| \sim \frac{1}{c_n^{1/n}\, \epsilon^{\frac{1}{2}-\frac{1}{n}}} \sim \frac{1}{c_n^{1/n}\, k^{1-\frac{2}{n}}} \tag{7.6}$$

which for $n > 2$ diverges as $k \to 0$. Note how a *weaker* potential (smaller c_n) is *better* at reflecting a particle at the same energy, but allows the atom to approach closer. Heuristically a sketch of $V(x) = -c_n/x^n$ reveals why: the weaker potential is seen to turn on more abruptly at a point closer to $x = 0$,

promoting an greater breakdown of WKB there. Alternatively a simple scaling argument with Schrodinger's equation reveals the same trend.

The above conclusions are valid only for $n > 2$. For $n \leq 2$ the error term of Eq. (7.1) looks qualitatively different from that in Fig. 7.2. It is small at all distances except near $x = 0$ where it diverges to infinity, as is evident from Eq.(7.2). If the physical parameters are such that this region where WKB fails very close to the slab is never actually manifest in the long-range part of the potential then the 'no-reflection' classical behaviour will be valid all the way up to distances near the slab where the atom will begin to feel the short range forces and loose energy to the internal degrees of freedom. For such a case then with $n < 2$ we believe one will *not* observe quantum reflection.

7.4 Sticking probability

Having established that the reflection is caused by a well-defined localized region, we solve the one-dimensional Schrodinger equation around this region to accurately compute the reflection probability. For an attractive power law potential $V(x) = -c_n/x^n$, the relevant one dimensional equation is

$$\left(\frac{d^2}{dx^2} + \frac{a_n^{n-2}}{x^n} + k^2\right)\phi_e(x) = 0. \tag{7.7}$$

$\phi_e(x)$ is the entrance channel wavefunction. The length scale

$$a_n \equiv (2mc_n/\hbar^2)^{\frac{1}{n-2}}, \tag{7.8}$$

contains all the qualitative information about the reflection. Its relevance is twofold. Firstly, the sticking probability for small k, behaves as

$$P_{\text{sticking}} \sim N_n\, k\, a_n \tag{7.9}$$

where N_n is a pure numeric constant (roughly of order 10 for $n = 3$, and of order 1 for $n = 4, 5$), see Ref. [11]. P_{sticking} may be computed numerically for any k, and Fig. (7.4) shows P_{sticking} vs. ka_n for $n = 3, 4$, and 5. Secondly, the distance at which the particle is turned around is estimated by solving

$$\left(\frac{a_n}{x}\right)^n = (ka_n)^2 \tag{7.10}$$

for x, which is just the requirement that $|V(x)| = \epsilon$. Equation (7.9) together with equation (7.8) makes plain that a smaller c_n is more conducive to making quantum reflection happen, while Eq. (7.10) indicates that the turnaround point is then necessarily closer to the surface. With these effects in mind, we look at some specific cases.

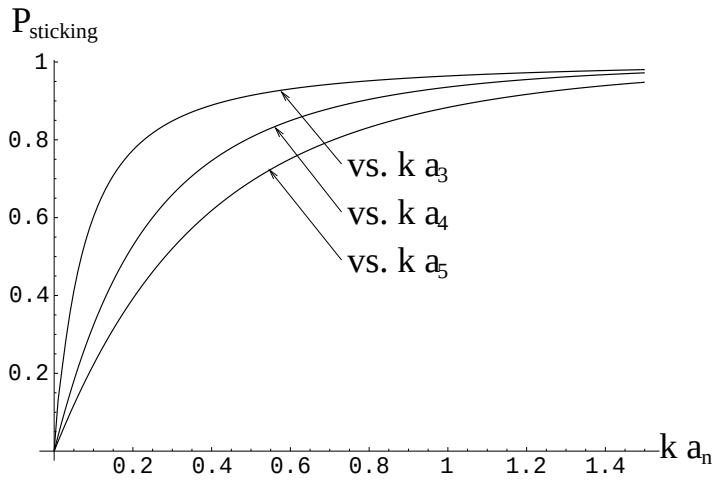

Sticking probabilities for an atom incident on surface providing a long range interaction of the form $V(x) = -c_n/x^n$ for the cases n=3,4,5. Note that the length scale a_n used to compute the dimensionless ka_n coordinate on the 'x-axis' vs. which we plot the sticking probabilities, is different for each n.

7.5 Examples

We examine the case of incidence on a slab which may be treated as semi-infinite, and also the case when it is a thin film. It is useful to first look at these cases pretending there is no Casimir interaction, and assuming that the short range form of the potential is everywhere valid. Afterwards we put in the Casimir interaction. For clarity we will pick a specific example of target and incident atoms for most of our discussions, by specifying the numeric values for the short range potential between the atom and semi-infinite slab, since these are most comprehensively tabulated in reference [**?**]coefficients}.

Fig. **??** shows the sticking probability vs. the temperature of an incoming Ne atom in units of 10^{-9} Kelvin. The slab is silicon-nitride (SiN). The various curves are for the different cases depending on whether we are we are considering a thick or thin slab, and whether the Casimir effect is included or not. We will discuss these cases below, pointing out the relevant length and energy scales involved in deciding to label the slab as semi-infinite or thin. The mapping from the mathematically natural ka_n (with $n = 3$ and $c_3 = 220$ meV Å^3) scale of Fig. 7.4 to the more physical temperature scale of Fig. **??** is made using

$$T \simeq [69.08 \text{ Kelvin}] \left(\frac{m_H}{m_{\text{atom}}}\right)^3 \left(\frac{\text{meV Å}^3}{c_3}\right)^2 (ka_3)^2 \qquad (7.11)$$

where we used $\langle\epsilon\rangle = (3/2)k_BT$ to compute the temperature by setting$\langle\epsilon\rangle$ equal to the incoming energy. m_H = mass of hydrogen atom, and for our example

$m_{\rm Ne} = 20.03\, m_H$.

All the graphs in Fig. **??** have an initial slope of 0.5 indicating the $\sqrt{\epsilon}$ behaviour of the sticking probabilities once the energies are low enough to be in the Quantum Reflection regime. A particular temperature at which there is a transition to the post-threshold sticking regime, we arbitrarily (but intuitively) define as the temperature where the slope becomes 0.4. For the thin film case of 10 nm in our example this temperature is 10 nK.

While the parameters in our example are fairly typical, it is clear that the cubic dependence on mass and quadratic dependence on the c_3 coefficient in Eq.(7.11), will make this temperature range over quite a few orders of magnitude. The c_3's in Ref [**?**]coefficients}, listed in units of meV $-$ Å^3 for a variety of surface atom pairs, range in values from 100 to 3000.

7.5.1 Semi-Infinite Slab (without Casimir)

Even though c_3 coefficients are known both theoretically and experimentally for many surface-atom pairs, for completeness we take a moment to look at a quick way of estimating them. This is provided by the London formula

$$V_{\text{atom-atom}}(r) = \frac{-3}{2}\frac{I_A I_B}{I_A + I_B}\frac{\alpha_A \alpha_B}{r^6} \equiv \frac{-c_6}{r^6}, \tag{7.12}$$

which estimates the Van der Waals interaction between any two atoms. I is the ionization potential and α the polarizability of each atom. Then summing over all the atoms in the semi-infinite slab (thick) we get

$$V_{\text{slab-atom}}(x) = \frac{-\pi c_6 \rho_{\text{atoms}}}{6} \times \frac{1}{x^3} \equiv \frac{-c_3}{x^3} \tag{7.13}$$

where ρ_{atoms} = the density of slab atoms. These estimates are not very accurate, but correctly indicate the physical quantities on which the answer depends. Reference [**?**]coefficients} provides a useful compendium of these coefficients. We have used $c_3 = 220 \pm 4$ meV Å^3 for neon atoms incident on silicon nitride from work of [**?**]value}. This choice of c_3 makes

$$a_3 \simeq 212 \text{ nm} \tag{7.14}$$

Thus the 'semi-infinite slab' curve of Fig. **??** is the $n = 3$ curve of Fig. **??** scaled to temperature units using Eq. (7.11).

7.5.2 Thin Slab (without Casimir)

From far enough away any slab will appear thin. The surface-atom interaction will behave like

$$\frac{-c_3}{x^3} - \frac{-c_3}{(x+d)^3} \simeq \frac{-3dc_3}{x^4} \tag{7.15}$$

for $x \gg d$, where d is the thickness of the slab. The resulting c_4 coefficient equal to $3dc_3$ gives an a_4 coefficient that can be written as

$$a_4 = \sqrt{\frac{2m}{\hbar^2} 3dc_3} = a_3 \left[\frac{3d}{a_3}\right]^{(1/2)}. \tag{7.16}$$

For macroscopic values of $d(\gg a_3)$ then, it is only for vanishingly small incident energies that the finiteness of the slab becomes apparent. For any macroscopic d this will be physically irrelevant. For microscopic $d(\ll a_3)$ however, this window in energy over which the thinness of the slab makes an appreciable difference can be larger and even prevail for all energies. To continue our illustrative example we pick the microscopic value of $d = 10$ nm. This makes $a_4 \simeq 800$nm. The 'thin slab' curve of Figure **??** shows that the sticking probabilities are substantially reduced and the onset of Quantum Reflection occurs at a much higher energy.

As a benchmark case, we also include what will likely be the physically limiting case for a continuous film of $d = 1$ nm. This further reduces the sticking probabilities for a fixed temperature by a factor of $\sqrt{10}$, because the important quantity a_4 is reduced by this much. (Eq.(**??**)). The transition temperature appears to have increased by 3 orders of magnitude versus the semi-infinite case.

7.5.3 Semi-infinite slab (Casimir Regime)

As the incoming energy ϵ tends to 0, we have seen that the turn-around region from which the atom 'quantum reflects' moves progressively further away from the slab. But at large distances, however, it is well known that the interaction potential itself takes on a different form due to Casimir effects. In particular, a semi-infinite dielectric slab (dielectric constant ϵ_s) has an interaction potential with an atom of polarizability α given by

$$V_{\text{slab-atom}}(x) = \frac{-3}{8\pi} \frac{\hbar c \alpha}{x^4} \frac{\epsilon_s - 1}{\epsilon_s + 37/23} \qquad x \to \infty \tag{7.17}$$

$$= \frac{-235(eV - \text{Å})\alpha}{x^4} \frac{\epsilon_s - 1}{\epsilon_s + 37/23} \quad x \to \infty \tag{7.18}$$

Even for sufficiently large x, the form above is not exact but a good approximation found in Ref. [**?**]estimates}. Our purpose here is only to estimate the various numbers to see their relevance. It will suffice to put $\alpha_{Ne} = 0.39\text{Å}^3$ and the last factor involving ϵ_s is replaced by 1 since most solids and liquids have ϵ_s substantially greater than 1. This gives a $c_4^{(C)}$ coefficient of $9 \times 10^4 \text{meV Å}^4$ and hence a resulting $a_4^{(C)} = 93$ nm. The superscript 'C' reminds us it is due to the Casimir interaction which is valid only for large enough x.

To estimate the distance beyond which the Casimir form itself is valid, we use the statement from Ref.[**?**]: 'Within a factor of 2, the van der Waals potential is correct at distances less than $0.12\lambda_{tr}$, while the Casimir potential is correct at distances at longer range.' $\lambda_{tr} = (1,240\,\text{nm})/(\frac{\Delta E}{eV})$ here is the wavelength

associated with the transition between the ground and excited state that gives the atom its polarizability. ΔE is the transition energy measured in eV. Knowing this much we may deduce the qualitative features of the sticking probability curve the arguments being similar to the cases above.

For this Casimir case and the one below, however, there is a caveat to all this. The exact manner in which the potential changes its near range form to its long-range Casimir form can certainly affect the sticking probabilities at the intermediate energy where it makes this transition. Some numerical experimentation choosing arbitrary forms of the potential having the correct short range and long-range behavior, confirms this. Therefore the curves in figure 3 involving Casimir forces are only quantitatively and *not* qualitatively correct.

7.5.4 Thin Slab (Casimir Regime)

Even for a thin slab we expect that the distance at which the Casimir interaction is valid remains the same as for a semi-infinite slab made of the same material. At these distances if $x \gg d$ is also valid, then one may expect the surface atom interaction to behave like

$$\frac{-c_4^{(C)}}{x^4} - \frac{-c_4^{(C)}}{(x+d)^4} \simeq \frac{-4dc_4^{(C)}}{x^5} \tag{7.19}$$

The length scale

$$a_5^{(C)} = a_4^{(C)} \left[\frac{4d}{a_4^{(C)}} \right]^{1/3} \tag{7.20}$$

associated with this $c_5 = 4dc_4^{(C)}$ coefficient makes $a_5^{(C)} = 717\text{nm}$. Figure **??** shows a slight decrease in the sticking probabilities, the effect being evidently less here than in the case of the thick slab.

7.5.5 Hydrogen on 'thick' Helium

Rather atypical, but extremely favourable parameters ($c_3 = 18$ meV Å^3) are found in the case of Hydrogen atoms incident on bulk liquid Helium. Evidence for quantum reflection was experimentally seen in this system. [12] A comparison with the parameters used in our example of Ne on SiN:

$$m_{\text{Ne}}/m_H = 20.03 \text{ and } c_3^{(\text{Ne-SiN})}/c_3^{(\text{H-He})} = 220/18. \tag{7.21}$$

With the use of Eq. (**??**equation}), we see that the sticking probabilities for this case are in fact the same curves as in Figure **??** except shifted to the right in temperature by about 6.1 orders of magnitude. This puts it exactly in the milli-Kelvin regime where sticking probabilities of about 0.01 to 0.03 were observed as temperatures ranged from about 0.3 mK to 5 mK. [12] However, the sticking probabilities predicted by the 'semi-infinite slab$^{(C)}$' curve of Fig.

?? are about a factor 2.5 too large, but we feel there is good reason for this. We already mentioned the qualitative manner in which the Casimir forces were included but it seems that a greater error is caused for another reason. The length scale $a_3 = 17$ nm for H-He is so small that the WKB error is close in (see Fig. 7.2) where the interaction potential is not exactly of the form $\sim 1/x^3$. Practically speaking this means that the region over which we must integrate Eq.(??equation}) must include points close to the slab to get some convergence and thus we are violating the assumption that the potential is $\sim 1/x^3$ there. This problem would not plague the Ne-SiN case too much, because the length scale there is substantially bigger. For H-He we must include some short-range information to get an improvement. Still it is the long-range forces that are mostly responsible. Ref [?, ?] and others have modeled this close range behaviour and obtained better agreement; the improvement coming from explicit consideration of the bound states supported by the close range potential. These appear in the potential matrix elements of perturbation theory.

7.6 Relation to threshold behavior

We now wish to take a broader view of the quantum reflection behaviour at threshold ($k \to 0$), and the sticking that sets in as the energy is increased - a Post Threshold behavior. In particular we want to make connection to, and extend the well-known threshold behaviors of inelastic rates which were first stated most generally by Wigner in Ref [?]. For example, Wigner showed that the exothermic excitation rates for collisions between two bodies with bound internal degrees of freedom tend to a constant value as their relative translational energy tends to 0, provided there is no resonance at the 0 translational energy threshold. Equivalently, the exothermic inelastic cross-section diverges as $1/v$, a fact known in the still older literature as the '$1/v$ law'. v is the relative velocity of the collision. Notice especially the proviso in the statement above, that there be no resonance at the threshold energy; suggesting that the many resonances between 0 and ϵ provided by a many body target could make the law inoperative. But the entire thrust of Part 1 was to establish quite generally that this many-resonance regime was precisely the one for which the old '$1/v$ law' is reinstated.

Here we re-examine the Wigner behaviour from a different point of view using our understanding of quantum reflection. In addition to furthering an intuitive understanding of the Wigner behaviour, viewing things in this way will lead naturally to predicting a generic post threshold behavior (e.g. the 1/v law is replaced by a $1/v^2$ law) and an understanding of when the sticking sets back in as ϵ is increased.

The reader will have noted that we have shifted our attention to a three dimensional geometry of incidence on a localized cluster instead of the one dimensional case of incidence on a slab. So long as the target dimensions are dwarfed by the incidence wavelength we will find that both problems are effectively one dimensional due to the fact that it is only the s-wave which can penetrate the

interaction region. For clarity we will deal with both cases separately.

7.6.1 Threshold and Post-Threshold Inelastic Cross-sections

The starting point is the template provided by the golden rule

$$d\sigma_{e\to c} \propto \frac{1}{k}\rho(E_c)\left|\int_{\text{all } \vec{r}} d^3r\ \phi^{(-)}_{c,\vec{k}_c}(\vec{r})U_{ce}(\vec{r})\phi^{(+)}_{e,\vec{k}}(\vec{r})\right|^2 \tag{7.22}$$

for the differential cross-section for inelastic transitions from internal state $\Omega_e(u)$ to $\Omega_c(u)$ where $\vec{k}$ and $\vec{k}_c$ are the incoming and outgoing directions of the incident atom. We describe briefly how Eq. (7.22) is arrived at.

For each internal state $\Omega_c(u)$ $(c = 1, 2, \cdots n)$ that we may imagine freezing the target in (u incorporates all the target degrees of freedom), there is some effective potential felt by the incoming atom. These potentials are just the diagonal elements of the complete interaction potential $U(x, u)$ in the $\Omega_c(u)$ basis, which if present all by themselves (off-diagonal elements 0) could only cause an elastic collision to occur. It is the off-diagonal elements that may be thought of as causing the inelastic transitions. Treating them as a perturbation on the elastic scattering wavefunctions we use the Golden Rule to obtain Eq. (7.22). $\rho(E)$ is the energy density of states of the free atom. $\phi^{(+)}_{e,\vec{k}}(\vec{r})$ is the entrance channel wavefunction and $\phi^{(-)}_{c,\vec{k}_c}(\vec{r})$ is the final channel wavefunction. They are both exact elastic scattering wavefunctions in the potentials $U_{ee}(\vec{r})$ and $U_{cc}(\vec{r})$ respectively. The factor of $1/k$ divides the Golden Rule rate by the flux to get the probability.

Now all the k dependence of $d\sigma_{e\to c}$ and hence $\sigma_{e\to c}$ is due to
1) the factor $1/k$ and
2) The sensitive k-dependence of the amplitude of the entrance channel wavefunction inside the interaction region over which the overlap integral of Eq. (7.22) takes place. This is simply because the incoming amplitude is more reflected away by the potential as $k \to 0$ resulting in the interior amplitude being suppressed by a factor of k as compared to what one would expect classically.

7.6.1.1 Incidence on a Slab

For this one-dimensional situation we speak of an inelastic probability instead of a cross-section, but otherwise Eq. (7.22) remains entirely valid here also with the obvious modifications.

For $k \to 0$, when WKB is invalid, we established quite generally [?]paper1} that the entrance channel wavefunction $\phi_e(x)$ when normalized to have a fixed incoming flux, had its amplitude inside the interaction region behaving like

$$\phi_e(x_{\text{inside}}) \sim k \qquad \text{Threshold} \tag{7.23}$$

Now the change from quantum reflection at threshold to sticking at post threshold (see Fig.2) begins to a occur at those energies at which the WKB wavefunctions - which show no quantum reflection - may be increasingly trusted. At these energies where WKB is valid we may simply use the well-known WKB amplitude factor $1/\sqrt{k(x)}$, to conclude that

$$\phi_e(x_{\text{inside}}) \sim \sqrt{k} \qquad \text{Post-Threshold.} \tag{7.24}$$

The probability density of being found inside then behaves like k^2 at threshold (quantum reflection) and like k at post threshold (no quantum reflection) respectively.

It is quite natural that the probability density inside the interaction region is smaller compared to the outside by a factor of k, even when there is no quantum reflection. This is simply a kinematical effect: where the particle is moving faster, it is less likely to be found by a factor inversely proportional to its velocity there. Classically what is unexpected is that for small enough k near threshold, the probabilities inside are *further* suppressed by a factor of k. Quantum reflection of the amplitude from the region around $|V(x)| = \epsilon$ (section **??**), goes hand in hand with the quantum suppression of the amplitude within this region. So finally including this k-dependence of the amplitude of $\phi_e(x)$ found in equations (7.23) and (7.24) we get

$$\begin{aligned} P_{\ e\to c} &\propto k & \text{Threshold} \\ P_{\ e\to c} &\propto const. & \text{Post-Threshold} \end{aligned} \tag{7.25}$$

7.6.1.2 Incidence on a cluster

Since for large wavelengths only the s-wave interacts with the cluster it is clear that the problem may be reduced in the usual manner to a one dimensional problem again. Therefore for a unit *s-wave flux* the inelastic probabilities will behave as before as in equations (**??**), but what is really relevant is a unit *plain wave* flux which provides a s-wave flux of π/k^2. i.e. Even though the problem is one-dimensional in the radial co-ordinate, the required normalization for the incoming flux is not fixed to be a constant as before, but is now required to grow as $\sim 1/k^2$, in order to correctly account for the increasing (as $k \to 0$) range of impact parameters that all 'count as' s-wave. Thus we have simply to multiply the one-dimensional probabilities of equations (**??**) by this factor of $1/k^2$, and conclude that the inelastic cross-sections for this cluster geometry behave like

$$\begin{aligned} \sigma_{\ e\to c} &\propto \frac{1}{k} & \text{Threshold} \\ \sigma_{\ e\to c} &\propto \frac{1}{k^2} & \text{Post-Threshold} \end{aligned} \tag{7.26}$$

The Threshold result of Eq. (7.26) is just the Wigner '1/v law' we spoke of in section 7.6. But now we can say more. As the incoming wavelength λ increases, we first witness for large enough λ a quadratic dependence to the exothermic

cross-section ($\sigma \propto \lambda^2$). It is only at still larger wavelengths that this dependence eventually changes over to a linear one ($\sigma \propto \lambda$). This happens when the sticking yields to the quantum reflection. This energy is mostly determined by the long range form of the potential, and has nothing to do with the bound state energies or any other details involving the interaction potential.

7.7 Conclusion

Examining the WKB error term provided a quick and easy way to estimate the threshold temperatures required to observe quantum reflection. It became transparent that only power laws dying faster than $-1/x^2$ were capable of acting as quantum reflectors. The validity of WKB at higher temperatures heralded a post-threshold behavior in which the atom sticks. Even for other geometries such as incidence on a localised three dimensional cluster, a WKB analysis together with the Fermi Golden Rule provided a simple understanding of this threshold and post-threshold behavior in terms of inelastic processes being shut off due to a reflection of the incoming amplitude. The extremely long incoming wavelength is invariably impedance mismatched (for potentials shorter ranged than $1/r^2$) by the abrupt change of wavelength in the interaction region, and is therefore reflected. It should be clear that even a repulsive interaction will obviously provide such a mismatch so that the Wigner behavior, or quantum reflection, is quite general; though of course most dramatic if the potential is attractive as we have been considering throughout.

This effect of quantum reflection/suppression, which is ultimately responsible for the threshold behaviour, is dynamical in that it is caused by the presence of the interaction potential. We feel that the original derivation by Wigner that focuses on the $k \to 0$ behaviour of the free space wave functions tends to obscure this physical origin of threshold behaviour. The golden rule approach makes it more explicit and especially paves the way for predicting the Post-Threshold behaviour.

7.8 Acknowledgments

A.M. is most grateful to Michael Haggerty for his kind help and advice and for always being available to discuss things with. A.M. thanks Alex Barnett for pointing him to the references on the Casimir interactions.

This work was supported by the National Science Foundation through a grant for the Institute for Theoretical Atomic and Molecular Physics at Harvard University and Smithsonian Astrophysical Observatory:National Science Foundation Award Number CHE-0073544.

This work was also supported by the National Science Foundation by grants PHY-0071311 and PHY-9876927.

Appendix A

Probability

A.1 Marginal Times Conditional Factorization

In simulating a multivariate distribution $P(x,y)$ it is often of advantage to rewrite it in the "conditional times marginal" form as

$$\begin{aligned} P(x,y) &= \frac{P(x,y)}{\int dx\ P(x,y)} \int dx\ P(x,y) \\ &\equiv P(x|y)P(y) \end{aligned} \tag{A.1.1}$$

where $P(y) \equiv \int dx\ P(x,y)$ is the unconditional, or marginal, y distribution and $P(x|y)$ is the conditional probability of x given y. If the integral is analytically or otherwise tractable, then this rewrite enables the simulation to proceed in two stages. We first draw y from the distribution $P(y)$ and then draw x from the distribution $P(x|y)$ where the y in $P(x|y)$ is now merely a parameter of the distribution $P(x|y)$. Note that Eq. (A.1.1) has all its distributions normalized. Since $P(x,y)$ was assumed normalized, $P(x|y)$ is then automotically normalized w.r.t. x, and $P(y)$ is automatically normalized w.r.t. y. However, it does not follow from

$$P(x,y) \propto f(x,y)g(y), \tag{A.1.2}$$

that $P(x|y) \propto f(x,y)$ and $P(y) \propto g(y)$ unless the normalization integral $\int dx\ f(x,y)$ happens to be independent of y. In general, $\int dx\ f(x,y)$ will depend on y, in which case it is simple to check that

$$P(x|y) = \frac{f(x,y)}{\int dx\ f(x,y)} \propto f(x,y), \tag{A.1.3}$$

and

$$P(y) \propto g(y) \int dx\ f(x,y) \tag{A.1.4}$$

are the correct identifications for the "conditional times marginal" decomposition of Eq. (A.1.1). The y dependence in the denominator of Eq. (A.1.3) is

just a normalization constant in $P(x|y)$ which is a distribution in x. Since the metropolis algorithm pays no heed to such normalization factors, they may be dropped.

A.1.1 Expectation Values

The conditional expectation values $\mu(y)$ and the variance conditional variance $\sigma^2(y)$ of the observable $F(x,y)$

$$\mu(y) \equiv \int dx\, F(x,y)P(x|y) \tag{A.1.5}$$

and

$$\sigma^2(y) \equiv \int dx\, F^2(x,y)P(x|y) - \mu^2(y),$$

embody the first and second moments of the constrained observable $F(x,y)|y$ (F given y). Given these and the marginal probability distribution $P(y)$ of the conditioning parameter, we can find the unconstrained moments of $F(x,y)$ and therefore the unconstrained mean and variance of $F(x,y)$.

A.1.2 First Moment

Since the unconditional mean

$$\mu \equiv \int dxdy\, F(x,y)P(x,y) = \int dy\, \left(\int dx\, F(x,y)P(x|y) \right) P(y), \tag{A.1.6}$$

we have using Eq. (A.1.5) that

$$\mu = \int dy\, \mu(y)P(y).$$

The equality in Eq. (A.1.6) is simply due to the identiy $P(x,y) = P(x|y)P(y)$. Introducing the notation

$$\langle F(x,y) \rangle_x \equiv \int dx\, F(x,y)P(x|y)$$

and

$$\langle M(y) \rangle_y \equiv \int dy\, M(y)P(y)$$

allows this to be written succintly as

$$\mu = \langle \mu(y) \rangle_y$$

which has the obvious interpretation: The unconditional mean is the conditioned mean averaged over the conditioning parameter.

A.1.3 Second Moment

The second moment

$$\begin{aligned}\langle F^2\rangle \equiv \int dxdy\, F^2(x,y)P(x,y) &= \int dy \left(\int dx\, F^2(x,y)P(x|y)\right) P(y) \\ &= \int dy \left(\mu^2(y) + \sigma^2(y)\right) P(y) \\ &= \langle \mu^2(y)\rangle_y + \langle \sigma^2(y)\rangle_y.\end{aligned}$$

Therefore the unconditional variance is obtained as

$$\begin{aligned}\sigma^2 &\equiv \langle F^2\rangle - \langle F\rangle^2 \\ &= \langle \mu^2(y)\rangle_y + \langle \sigma^2(y)\rangle_y - \left(\langle \mu(y)\rangle_y\right)^2 \\ &= \langle \sigma^2(y)\rangle_y + \mathrm{var}[\mu(y)]. \qquad \text{(A.1.7)}\end{aligned}$$

The unconditioned variance is the conditioned variance averaged over the conditioning parameter *plus* the variance of the conditioned mean.

Appendix B

Rotating Frame and Generalized Angular Momentum

B.1 Rotating Frame and a Uniform $\vec{B}$ Field

Consider N interacting particles (mass m_i, charge e_i) with coordinates $\vec{r}_1 \equiv (x_1, y_1, z_1), \vec{r}_2, \cdots$ moving in the presence of a constant magnetic field $\vec{B} = B\hat{z}$ and an electrostatic potential $\phi(\vec{r})$. In addition to feeling the acceleration $e_i\vec{\nabla}\phi(\vec{r}_i)/m_i$ and the acceleration due to forces from all the other particles, the ith particle also feels the velocity dependent Lorentz acceleration

$$\vec{v}_i \times \frac{e_i B}{m_i c}\hat{z}.$$

Provided e_i/m_i is the same for all the particles, this velocity dependent acceleration has precisely the form of a coriolis force

$$2\vec{v}_i \times (\frac{\omega_c}{2})\hat{q}_3$$

acting on the ith particle in a frame that rotates with angular velocity $(\omega_c/2)$ w.r.t. the axes $\hat{q}_1, \hat{q}_2, \hat{q}_3$ of an imagined "inertial frame". Thus by pretending that our true laboratory $\vec{r}$–frame is a non inertial one, we can "explain" the existence of the coriolis-type Lorentz force. See Fig. (B.1). Here $\omega_c \equiv e_i B/(m_i c)$ is the cyclotron frequency independent of i. By keeping up this pretense, however, we would also expect each particle to feel a centrifugal potential energy field of

$$-\frac{1}{2}m_i\left(\frac{\omega_c}{2}\right)^2\rho^2, \tag{B.1.1}$$

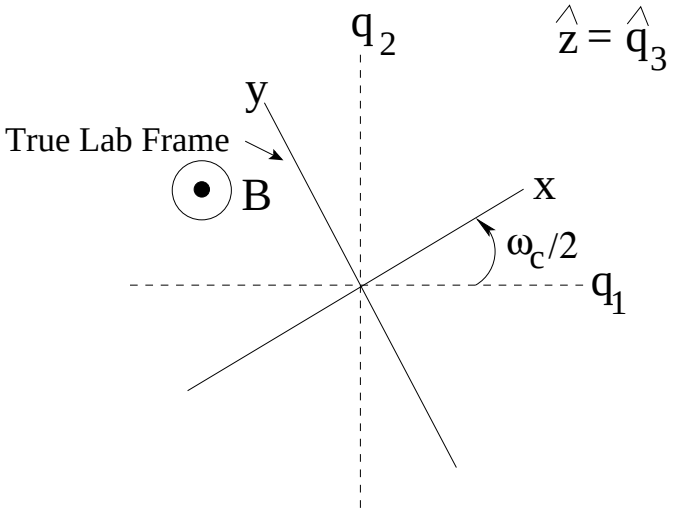

Figure B.1: Rotating frame

in the $\vec{r}$-frame, ($\rho^2 = x^2 + y^2$ is the cylindrical radius) even though this was not something we sought to explain. Fortunately, the *lack* of this extra piece too can be explained simply by supposing that the dynamics in our imagined $\vec{q}$-frame contains the cylindrically symmetric term of Eq. (B.1.1) with the oppsite sign. Thus the motion in our imagined $\vec{q}$-frame takes place in an external potential energy field of

$$e_i\phi\left(\vec{r}_t(\vec{q})\right) + \frac{1}{2}m_i\left(\frac{\omega_c}{2}\right)^2\rho^2, \tag{B.1.2}$$

or an electrostatic potential field

$$\phi\left(\vec{r_t}(\vec{q})\right) + \frac{1}{2}\frac{m_i}{e_i}\left(\frac{\omega_c}{2}\right)^2\rho^2. \tag{B.1.3}$$

Note $\rho^2 = x^2+y^2 = q_1^2+q_2^2$. In general the first term in Eqs. (B.1.2) and (B.1.3) is time dependent because $\vec{r}_t(\vec{q})$ is itself a time dependent change of coordinates. However if $\phi(\vec{r})$ is cylindrically symmetric and provided e_i/m_i is the same for all the particles, Eq. (B.1.3) simplifies to just the time-independent potential

$$\phi(\rho, z) + \frac{1}{2}\frac{m}{e}\left(\frac{\omega_c}{2}\right)^2\rho^2$$

felt universally by each particle. Thus we arrive at the following proposition.
Proposition

The dynamics of interacting charged particles (each with the same charge to mass ratio e/m) moving in a cylindrically symmetric external electric potential $\phi(\rho, z)$ and magnetic field $B\hat{z}$ is simplified when viewed w.r.t. the axes of a frame that has an angular velocity $(-\omega_c/2)\hat{z}$ w.r.t the initial frame. This new time

dependent change of coordinates has the advantage that the dynamics w.r.t. them involves no velocity dependent forces and only an external electrostatic field

$$\begin{aligned} & \phi(\rho,z)+\frac{1}{2}\frac{m}{e}\left(\frac{\omega_c}{2}\right)^2\rho^2 \\ = \quad & \phi(\rho,z)+\frac{1}{2}\frac{eB^2}{mc^2}\left(\frac{\rho}{2}\right)^2. \end{aligned}$$

The essential point to notice is the harmonic cylindrical confinement resulting due to the B field no matter how weak.

B.2 Conservation of generalized angular momentum

B.2.1 e_i/m_i all equal

Let (ρ_i,ϕ_i,z_i) be the cylindrical coordinates of the ith particle in the original $\vec{r}$-frame of Fig. (B.1) in which we feel the magnetic field. Then in the $\vec{q}$-frame the angular velocity of the ith particle is

$$\dot{\phi}_i+\frac{\omega_c}{2},$$

so that the total $\hat{z}$ angular momentum (all mechanical) in the $\vec{q}$-frame is given by the expression

$$L_z=\sum_{i=1}^{N}m_i\rho_i^2\left(\dot{\phi}_i+\frac{\omega_c}{2}\right).$$

Now $\phi(\rho,z)+\frac{1}{2}\frac{m}{e}\left(\frac{\omega_c}{2}\right)^2\rho^2$, the external electrostatic potential felt by each particle in the $\vec{q}$- frame, is cylindrically symmetric. Consequently, L_z is obviously a time-independent conserved quantity. In the original $\vec{r}$-frame however, it does not have the interpretation of being simply the total mechanical angular momentum. Rather,

$$L_z=\sum_{i=1}^{N}m_i\rho_i^2\left(\dot{\phi}_i+\frac{\omega_c}{2}\right)\equiv L_z^{(\mathrm{mech})}+I_z\frac{\omega_c}{2} \tag{B.2.4}$$

contains an extra term which may be thought of as the latent angular momentum in the electromagnetic field due to the very presence of charges in a magnetic field. With time, this latent field angular momentum converts to mechanical angular momentum and then back again to field angular momentum as the moment of intertia I_z fluctuates; only the sum of the two is conserved. In fact, at any given time of our choosing it can all be completely released and converted to mechanical angular momentum by suddenly switching off the magnetic field very quickly. The mechanism by which this is achieved is the induced circular Faraday E field

$$E_\phi=-\frac{1}{c}\frac{\partial B}{\partial t}\frac{\rho}{2}\hat{\phi}$$

which boosts the mechanical angular momentum by

$$\sum_{i=1}^{N} \vec{\rho}_i \times \delta\vec{p}_i = \sum_{i=1}^{N} \vec{\rho}_i \times \left(e_i \frac{-1}{c} dB \frac{\rho_i}{2} \hat{\phi} \right)$$

in a time dt, during which there is a change dB in B. When integrated $\int_B^0 dB$ this simplifies to

$$\sum_{i=1}^{N} m_i \rho_i^2 \frac{\omega_c}{2}$$

as claimed.

B.2.2 e_i/m_i not all equal

The conservation of the generalized angular momentum L_z in Eq. (B.2.4) is in fact much more general than our demonstration above suggests. All the particles not having the same charge to mass ratio immediately precludes the use of our $\vec{q}$-frame in which L_z is interpretable as simple mechanical angular momentum. Still, the cylindrical symmetry in the original frame implies a conserved quantity which we will show to be

$$L_z = \sum_{i=1}^{N} m_i \rho_i^2 \left(\dot{\phi}_i + \frac{\omega_{c_i}}{2} \right) = L_z^{(\text{mech})} + \sum_{i=1}^{N} m_i \rho_i^2 \frac{\omega_{c_i}}{2} \tag{B.2.5}$$

in Sec. (B.2.3). Here the cyclotron frequency $\omega_{c_i} \equiv e_i B/(m_i c)$ for each particle may be different. Notice that this allows the possibility of particles with both +ve and -ve charge so that ω_{c_i} is +ve and -ve respectively. If ω_{c_i} is of a fixed sign for all i, then conservation of L_z in Eq. (B.2.5) implies that none of the ρ_i can get arbitrarily large. Thus we have shown confinement in a slightly different way than in Sec. (B.1). However, if for example ω_{c_1} and ω_{c_2} have different signs, then the corresponding ρ_1 and ρ_2 can $\to \infty$ while still keeping the sum of the first two terms in $\sum_{i=1}^{N} m_i \rho_i^2 \frac{\omega_{c_i}}{2}$ fixed. Physically, this just reflects the fact that two oppositely charged particles when bound together are capable of completely flying out of the trap since when paired together they are insensitive to the magnetic field.

B.2.3 Noether's theorem

The dynamics of a system of N particles (arbitrary charge and mass) moving in a magnetic field $\vec{B}(\vec{r})$ and electrostatic potential $\phi(\vec{r})$ is described by the Hamiltonian

$$H(\vec{r}_1 \cdots \vec{r}_N, \vec{s}_1 \cdots \vec{s}_N) = \sum_{i=1}^{N} \left\{ \frac{\left(\vec{s}_i - \frac{e_i \vec{A}(\vec{r}_i)}{c} \right)^2}{2m_i} + e_i \phi(\vec{r}_i) \right\} + \sum_{i>j}^{N} V(\vec{r}_i, \vec{r}_j). \tag{B.2.6}$$

That is, the equations of motion for the variables

$$\vec{s}_i \equiv \vec{p}_i + \frac{e_i \vec{A}(\vec{r}_i)}{c}, \tag{B.2.7}$$

and

$$\vec{r}_i \equiv \vec{r}_i$$

flow from the Hamiltonian of Eq. (B.2.6). $\vec{s}_i$ the so called canonical momentum of the ith particle is its mechanical momentum plus the latent linear momentum in the electromagnetic field due to the position of the charge in the magnetic field. $\vec{A}(\vec{r})$ is chosen so that $\vec{B}(\vec{r}) = \nabla \times \vec{A}(\vec{r})$, which for a constant magnetic field, may be chosen to be cylindrically symmetric,

$$\begin{aligned} \vec{A}(\vec{r}) &= \frac{B}{2}\rho_i \hat{\phi}(\vec{r}), \\ &= \frac{B}{2}(-y\hat{x} + x\hat{y}) \end{aligned}$$

making

$$\vec{s}_i \equiv m\vec{v}_i + \frac{e_i B}{2c}\rho_i \hat{\phi}(\vec{r}). \tag{B.2.8}$$

If $\phi(\vec{r})$ is also cylindrically symmetric, the entire Hamiltonian is cylindrically symmetric so that H is invariant to the phase space flow induced by the vector field

$$\vec{u} = (\hat{z} \times \vec{r}_1, \cdots \hat{z} \times \vec{r}_N, \hat{z} \times \vec{s}_1 \cdots \hat{z} \times \vec{s}_N), \tag{B.2.9}$$

since this just implements a rotation of the state around the $\hat{z}$ axis of physical space. The infinitesimal generator $\vec{u}$ in Eq. (B.2.9) rotates $\vec{s}$ along with $\vec{r}$. We could equally well have rotated $\vec{p}$ instead of $\vec{s}$ since with our choice of $\vec{A}$ the difference between $\vec{s}$ and $\vec{p}$ is just proportional to $\hat{\phi}(\vec{r})$ which itself gets rotated when $\vec{r}$ is rotated. Noether's theorem then implies the conservation of the quantity

$$\sum_{i=1}^{N} \vec{s}_i \cdot (\hat{z} \times \vec{r}_i).$$

Using Eq. (B.2.8) and $\hat{z} \times \vec{\rho}_i = \rho_i \hat{\phi}$ this simplifies to

$$\sum_{i=1}^{N} \rho_i p_{t_i} + m_i \rho_i^2 \frac{\omega_{c_i}}{2}$$

which is Eq. (B.2.5) as claimed. $p_{t_i} \equiv \vec{p}_i \cdot \hat{\phi}(\vec{r}_i)$ is the tangential component of momentum.

B.2.4 Elementary Verification

Having discovered the conservation of L_z its time independence may be verified yet another way by elementary means. The time derivative of L_z is

$$\sum_{i=1}^{N} \frac{d}{dt}(\rho_i p_{t_i}) + \rho_i \dot{\rho}_i \frac{e_i B}{c} = 0. \tag{B.2.10}$$

Let us explain why it is zero. Since the torque around the $\hat{z}$ axis acting on the ith particle due to the B field is

$$\begin{aligned} & \vec{\rho}_i \times (\vec{v}_i \times \frac{e_i B}{c} \hat{z}) \\ = \quad & \vec{\rho}_i \times (\dot{\rho}_i \frac{e_i B}{c} \hat{\phi} + \#\hat{\rho}) \\ = \quad & \rho_i \dot{\rho}_i \frac{e_i B}{c} (-\hat{z}), \end{aligned}$$

we see that the sum over i of the second term in Eq .(B.2.10) is nothing but the negative of the total external torque on the system of particles due to the B-field. Now $\frac{d}{dt}(\rho_i p_{t_i})$ is the total torque around the $\hat{z}$-axis acting on the ith particle which comprises of an "internal" torque arising from the forces due to all the other particles, and "external" torque arising from the force due to the $B-$field. Since the sum of the "internal" torques will always cancel, $\sum_{i=1}^{N} \frac{d}{dt}(\rho_i p_{t_i})$ simplifies to just the "external" torque on all the particles due to the B-field. Hence the sum in Eq. (B.2.10) is 0.

B.3 Change of Variables: $\vec{r}_1 \cdots \vec{r}_N, \vec{p}_1 \cdots \vec{p}_N$ to $\vec{r}_1 \cdots \vec{r}_N, \vec{s}_1 \cdots \vec{s}_N$

From Eq.(B.2.8)

$$\begin{aligned} ds_{x_i} &= dp_{x_i} + \frac{e_i B}{2c}(-dy_i) \\ ds_{y_i} &= dp_{y_i} + \frac{e_i B}{2c}(dx_i), \end{aligned}$$

$$\begin{aligned} \Longrightarrow \quad (ds_{x_i} \wedge dx_i) \wedge dy_i &= dp_{x_i} \wedge dx_i \wedge dy_i && \text{bec. } dy_i \wedge dy_i = 0 \\ \Longrightarrow \quad (ds_{x_i} \wedge dx_i \wedge dy_i) \wedge ds_{y_i} &= dp_{x_i} \wedge dx_i \wedge dy_i \wedge dp_{y_i} && \text{bec. } dx_i \wedge dx_i = 0. \end{aligned}$$

It follows that the $6N$ volume element is the same in both coordinate systems implying that the Jacobian for the change of coordinates is 1. Obviously this does *not* imply that the change of variables is itself a canonical map, since the Jacobian being 1 is a sufficient condition only in a two dimensional phase space.

Appendix C

C.1 $\Gamma \simeq nD$

With the large number of degrees of freedom involved and assuming thorough phase space mixing associated with the resonance we may reasonably describe the compound state wavefunction by a classical ensemble of points (x, p_x, u, p_u) in the combined phase space of the joint system given by the normalized distribution

$$\frac{1}{\rho_C(E)}\delta(E - H(x, p_x, u, p_u)). \tag{C.1.1}$$

It is understood in the above that the system is restricted to be in the region $x < a$. This makes all accessible states of energy E with $x < a$ equally likely. Then the rate of escape $\Gamma/\hbar$ through the hypersurface $x = a$ of the members of this ensemble is

$$\frac{\Gamma}{\hbar} = \frac{1}{\rho_C(E)} \int_{x=a} du dp_u \int_{p_x \in [0,\infty]} dp_x \frac{p_x}{m} \delta(E - H(x, p_x, u, p_u)). \tag{C.1.2}$$

p_x/m is just the velocity in phase space of a point at $x = a$ in the $\hat{x}$ direction. At $x = a$ we have supposed no interaction. Hence the Hamiltonian separates in Eq. (C.1.2). Therefore

$$\frac{\Gamma}{\hbar} = \frac{1}{\rho_C(E)} \int du dp_u \int_0^\infty d\left(\frac{p_x^2}{2m}\right) \delta\left(E - \left(\frac{p_x^2}{2m} + H^{\text{target}}(u, p_u)\right)\right) \tag{C.1.3}$$

$$= \frac{1}{\rho_C} \int_{H^{\text{target}}(u,p_u)<E} du dp_u \tag{C.1.4}$$

$$= \frac{1}{\rho_C}\Omega_C \simeq \frac{1}{2\pi\hbar\rho_Q}\Omega_Q = \frac{1}{2\pi\hbar} nD. \tag{C.1.5}$$

Therefore $\frac{\Gamma}{D} \simeq n$. ρ_Q (ρ_C) is the quantum (classical) density of states (phase space volume) of the joint system at energy E. Ω_Q (Ω_C) is the quantum (classical) total number of states (total phase space volume) of only the target below

energy E. We have used the correspondence between the Classical and Quantum density of states. $1/\rho_Q$ is identified with D, and the number of states of the target having energy less that E is just n, the number of open channels.

C.2 Inelastic probability with background

We show here that the inelastic probabilities remain essentially unaffected in magnitude with the presence of a background term in the S-matrix. In the isolated case the addition of $b_{cc'}$ to an inelastic element $S_{cc'}$ simply changes the Lorentzian profile of $|S_{cc'}|^2$. In the more important overlapping case, the energy variation of $S_{cc'}$ is smooth in any case without background and

$$|\mathbf{S}_{cc'}|^2 = \left| B_{cc'} - i \sum_{\lambda} \frac{\Gamma_{\lambda c}^{1/2} \Gamma_{\lambda c'}^{1/2}}{E_\lambda^{(r)} - E - i\Gamma_\lambda/2} \right|^2 . \tag{C.2.6}$$

$$= |B_{cc'}|^2 + \sum_{\lambda} \frac{\Gamma_{\lambda c} \Gamma_{\lambda c'}}{\left(E_\lambda^{(r)} - E\right)^2 + {\Gamma_\lambda}^2/4} \tag{C.2.7}$$

where we have used the random sign property of the products $\Gamma_{\lambda c}^{1/2} {\Gamma_{\lambda c}}^{1/2}$ to neglect the 2nd cross-term in comparison to the last one where again the same property is used to simplify the double sum to a single one. Summing over all the inelastic channels then leads to the same result of Eq. (6.61) with an added term of $\sum_{c \neq e} |B_{cc'}|^2$ which itself is proportional to k_e as discussed at the end of Section 6.5.2.

Bibliography

[1] J. E. Lennard-Jones *et. al.*, *Proc. R. Soc.* London, Ser. A **156** 6, (1936); Ser. A **156** 36, (1936).

[2] T.W. Hijmans, J.T.M. Walraven, and G.V. Shlyapnikov, *Phys. Rev.* B **45** , 2561 (1992).

[3] W. Brenig, *Z. Phys.* B **36**, 227 (1980).

[4] D.P. Clougherty and W. Kohn, *Phys. Rev.* B, **46** 4921 (1992).

[5] E. R. Bittner, *J. Chem. Phys.* **100**, 5314 (1993).

[6] P. S. Julienne and F. H. Mies, *J. Opt. Soc. Am.* **B 6**, 2257 (1989).

[7] P. S. Julienne, A.M. Smith, and K. Burnett, Adv. At. Mol. Op. Phys. **30**, 141 (1992).

[8] L.D. Landau and E.M. Lifshitz, *Quantum Mechanics (Non-relativistic Theory)* (Pergamon Press, Oxford (UK) 1981).

[9] C.J. Joachain, *Quantum Collision Theory* (North-Holland, Amsterdam 1975).

[10] G.F. Gribakin and V. V. Flambaum, *Phys. Rev.* A **48** 546 (1993).

[11] R. Côte, E. J. Heller, and A. Dalgarno, "Quantum suppression of cold atom collisions" *Phys. Rev. A* **53**, 234-41 (1996).

[12] I. A. Yu, J. Doyle, J. C. Sandberg, C. L. Cesar, D. Kleppner, and T. J. Greytak, *Phys. Rev. Lett* **71**, 1589 (1993).

[13] J. Doyle, J. C. Sandberg, I. A. Yu, C. L. Cesar, D. Kleppner, and T. J. Greytak, *Phys. Rev. Lett* **67** 603 (1991); C. Carraro and M.W. Cole, *Phys. Rev.* B **45** , 12931 (1992); T.W. Hijmans, J.T.M. Walraven, and G.V. Shlyapnikov, *Phys. Rev.* B **45** , 2561 (1992).

[14] F. T. Smith, *Phys. Rev.* **118**, 349 (1960).

[15] A.M. Lane and R.G. Thomas *Phys. Rev.* **56** (5),416-450 (1939). see pages following 302

[16] T. Ericson, *Phys. Rev. Lett* **5**, 430 (1960).

[17] N. Bohr and J. Wheeler, *Phys. Rev.* **30** (2), 257-353 (April 1958). see page 426 Sec. III